UTILIZING NANOTECHNOLOGY TO IMPROVE THE ACTIVATION OF CD8 T CELLS FOR CANCER IMMUNOTHERAPY

by

Alyssa K. Kosmides

A dissertation submitted to Johns Hopkins University in conformity with the requirements for the degree of Doctor of Philosophy.

Baltimore, Maryland

March 15, 2018

Abstract

The immune system can be manipulated to recognize and eliminate cancerous cells. Many of these manipulations aim to increase the proliferation and activation of tumor-targeting cytotoxic CD8+ T cells through direct stimulation or attenuation of immuno-inhibitory checkpoint pathways. Here, I use nanotechnology to develop platforms that can enhance and/or target immuno-stimulatory properties by controlling the kinetics, costimulation, and nanoscale delivery of immunotherapies.

I first developed a nanoparticle that converts inhibitory signals in the tumor microenvironment to T cell stimulatory signals. By tethering checkpoint blockade and co-stimulatory molecules to a single platform, I made particles that physically link tumor cells and T cells while inhibiting checkpoint activity and activating T cells. These particles delayed or eliminated tumor growth in several murine models at doses 10-100x less than soluble inhibitory and co-stimulatory molecules and resulted in a systemic memory immune response while localizing the nanoparticles to the tumor microenvironment.

Next, I developed a modified type of artificial antigen presenting cell (aAPC) that boosts CD8+ T cell activation for adoptive cell transfer. T cell signaling components were separated onto distinct superparamagnetic nanoparticles and activation was induced by clustering the particles with a magnetic field. This platform streamlined the application of various combinations of co-stimulatory molecules together with a single antigen-specific receptor to increase the expansion of antigen-specific T cells and extend their persistence *in vivo*.

Finally, I developed more effective biodegradable aAPC by modifying the particle material and through combination with checkpoint blockade. Biodegradable aAPC synergized with anti-PD-1 checkpoint blockade to delay the growth of established murine melanoma. A new type of polymeric aAPC also activated antigen-specific CD8+ T cells at doses 100x less than previous particle formulations.

Thesis Committee

Jonathan P. Schneck, M.D. Ph.D. (*primary adviser, reader)*

Professor, Department of Pathology

Johns Hopkins University School of Medicine

Jordan J. Green, Ph.D.

Associate Professor, Department of Biomedical Engineering

Johns Hopkins University School of Medicine

Andrea Cox, M.D. Ph.D.

Professor, Department of Medicine

Johns Hopkins University School of Medicine

Michael Edidin, Ph.D. (*reader*)

Professor Emeritus, Department of Biology

Johns Hopkins University

Acknowledgements

I would like to thank Dr. Jonathan Schneck for being a supportive adviser. I met with him shortly after taking the medical school immunology course and explained that I knew very little immunology but that I found it fascinating and was eager to learn more. He welcomed me into the lab and gave me the freedom to pursue many different projects while learning a new subject. Over the course of the next five years, he maintained that open-minded and honest mentoring style which gave me plenty of opportunities to succeed, fail, and learn from my own mistakes.

I also need to thank Joanie Bieler and Karlo Perica, the lab "mom" and my original mentor, respectively. Without Joanie's comprehensive knowledge and five star baked goods, I would have never made it as long as I did. Karlo, my graduate student mentor, taught me more than I thought possible in the ten short months we overlapped before he graduated from the lab with his PhD. And of course, all of the other members of the Schneck lab, especially Ami Bessell and John Hickey, who helped with both science and sanity throughout the years and inspired me as they brought new children into the world while working hard towards graduate degrees.

I need to thank my thesis committee and close collaborators for all of their attentive time and valuable feedback – Drs. Jordan Green, Michael Edidin, Andrea Cox, as well as fellow graduate student Randall Meyer. I am thankful to have had guidance from such a diverse group of intelligent people.

Finally, I need to thank my family and friends. My fiancé, Joe Galaro, never stopped encouraging me even while also struggling through the ups and downs of his own PhD. I am thankful for my parents, four siblings, grandparents, aunts, uncles, and

cousins who continued to support me even when they were confused why I was “still” in school, and all of the old and new friendships that I kept and made in Baltimore that I know will last a lifetime.

Table of Contents

Abstract ..... **ii**

Acknowledgements ..... **v**

Table of Contents ..... **vii**

List of Figures ..... **xi**

Chapter 1. Summary of the Dissertation **1**

Chapter 2. The Cancer-Immunity Cycle **3**

2.1 T cell activation 3

2.2 Blockades allow cancer progression 5

Chapter 3. Immunoengineering Approaches for T Cell Modulation **8**

3.1 Properties to consider when designing a platform 8

3.1.1 Ligand choice and arrangement 8

3.1.2 Particle size 11

3.1.3 Particle shape 12

3.2 Particle-based approaches 13

3.2.1 Artificial antigen presenting cells 14

3.2.2 Drug-carrier particles 18

3.2.3 Non-T cell interacting particles 22

3.2 Protein engineering 25

3.2.1 Engineered cytokines 26

3.2.2 Antibody Engineering 29

3.3 Combination immunotherapies 33

Chapter 4. Dual Targeting Nanoparticle Stimulates the Immune System to Inhibit Tumor Growth **38**

4.1 Introduction 38

4.2 Methods 40

4.2.1 Mice....40
4.2.2 Reagents and cell lines....41
4.2.3 Immunoswitch particle synthesis and characterization....41
4.2.4 *In vitro* CD8+ T cell activation model....42
4.2.5 B16 *in vivo* tumor growth experiments....43
4.2.6 B16-SIY tumor infiltrating lymphocyte analysis....44
4.2.7 T cell receptor sequencing analysis....45
4.2.8 MC38-OVA *in vivo* tumor models....46
4.2.9 Immunoswitch biodistribution....47
4.2.10 Conjugation assay....48
4.2.11 *In vivo* killing assay....49
4.2.11 Statistics....50
4.3 Results....51
4.3.1 Immunoswitch particles activate T cells *in vitro*....51
4.3.2 Enhanced T cell-tumor cell conjugation....56
4.3.3 Immunoswitch particles inhibit tumor growth *in vivo*....58
4.3.4 Endogenous T cell activation....62
4.3.5 Changes in the T cell receptor repertoire....66
4.3.6 Immunoswitch biodistribution....68
4.3.7 Efficacy in multiple cancer models....70
4.3.8 Efficacy by intravenous immunoswitch injection....72
4.3.9 Intratumoral treatment results in a systemic memory response....73
4.4 Discussion and conclusions....74
Chapter 5. Separating T cell Targeting Components onto Magnetically-Clustered Nanoparticles Boosts Activation....79
5.1 Introduction....79
5.2 Methods....82
5.2.1 Mice....82

5.2.2 Reagents and Cell Lines 82
5.2.3 Particle synthesis and characterization 83
5.2.4 CD8+ T cell aAPC stimulation 86
5.2.5 Specific lysis assay 87
5.2.6 Particle clustering analysis 87
5.2.7 Matlab clustering analysis 88
5.2.8 Fold-enrichment studies 89
5.2.9 Endogenous CD8+ T cell cytokine functionality 89
5.2.10 *In vivo* adoptive transfer studies 89
5.3 Results 90
5.3.1 Separate particle platform activates CD8 cells 90
5.3.2 Dependence of particle size 93
5.3.3 Dependence of signal co-clustering 96
5.3.4 Increased expansion of antigen-specific endogenous CD8 cells 99
5.3.5 High throughput co-stimulatory molecule customization 103
5.3.6 Co-stimulatory molecule selection impacts memory formation *in vivo* 106
5.4 Discussion and conclusions 107
Chapter 6. Improving the Efficacy of Biodegradable Artificial Antigen Presenting Cell Platforms. 112
6.1 Introduction 112
6.2 Methods 115
6.2.1 Artificial antigen presenting cell synthesis and characterization 115
6.2.2 Anti-PD1 monoclonal antibody synthesis 117
6.2.3 *In vitro* artificial antigen presenting cell T cell stimulation 117
6.2.4 *In vitro* anti-PD-1 mAb functionality assay 118
6.2.5 *In vitro* anti-PD-1 mAb and aAPC assay 120
6.2.6 *In vivo* particle and cell biodistribution study 120
6.2.7 *In vivo* tumor treatment study 121
6.2.8 *In vivo* CD8+ T cell harvest and analysis 123

6.3 Results 124
6.3.1 PLGA-based aAPC synthesis and characterization 124
6.3.2 aAPC stimulate peptide-specific CD8+ T cells 127
6.3.3 Anti-PD-1 mAb and aAPC activate cognate CD8 cells *in vitro* 128
6.3.4 PLGA aAPC biodistribution 131
6.3.5 Combination therapy delays tumor growth and extend survival 132
6.3.6 Combination therapy increases T cell functionality 135
6.3.7 PLGA/PBAE hybrid aAPC outperforms traditional PLGA 138
6.4 Discussion and conclusions 143
Chapter 7. Conclusions 148
7.1 Summary of work 148
7.2 Future directions 150
Bibliography 153
Curriculum Vitae 177

List of Figures

Figure 4-1. Immunoswitch particles combine anti-4-1BB and anti-PD-L1 antibodies on a nanoparticle platform. 52

Figure 4-2. Immunoswitch particles link PD-L1 checkpoint blockade with 4-1BB co-stimulation....53

Figure 4-3. In vitro model results in upregulated inhibitory molecules on CD8 and B16 cells. 55

Figure 4-4. Soluble anti-4-1BB and anti-PD-L1 mAb increase T cell activation when co-incubated with target cells. 55

Figure 4-5. Immunoswitch particles increase effector-target cell conjugation....58

Figure 4-6. Immunoswitch particles inhibits tumor growth in vivo 60

Figure 4-7. Immunoswitch particles delay tumor growth in the absence of adoptively transferred cells....61

Figure 4-8. Tumor specific CD8+ T cells are present in the periphery at the same levels in treated and non-treated mice 63

Figure 4-9. A significant portion of the anti-tumor response in the presence and absence of immunoswitch treatment is Kb-SIY specific. 64

Figure 4-10. Tumor-specific CD8+ tumor-infiltrating lymphocytes of immunoswitch treated mice have increased functionality. 65

Figure 4-11. Immunoswitch treatment alters the CD8+ T cell repertoire....67

Figure 4-12. Immunoswitch particles remain at injection site longer than soluble antibody 69

Figure 4-13. Immunoswitch particles reverse tumor growth and extend survival in multiple tumor models and injection routes 71

Figure 4-14. Intratumoral immunoswitch treatment results in a systemic memory immune response....74

Figure 5-1. Standard curves relate absorbance to particle concentration of nanoparticles 85

Figure 5-2. CD8+ T cells are activated by nanoparticles separately expressing signal 1 and signal 2 when particles are clustered within a magnetic field 91

Figure 5-3. Traditional aAPC activate a more robust T cell response at larger particle sizes 94

Figure 5-4. Separate particle platform requires particles on the nanometer size scale for efficient CD8+ T cell stimulation 95

Figure 5-5. Number of nanoparticle clusters per cell is affected by particle size 95
Figure 5-6. Polystyrene and iron-dextran nanoparticles have similar protein densities 96
Figure 5-7. Signal 1 and signal 2 only nanoparticles must be co-clustered on the cell surface for efficient CD8+ T cell activation 97
Figure 5-8. Separate particle platform results in greater expansion of functional cognate CD8+ T cells ... 100
Figure 5-9. Percent recovery of cognate T cells is equivalent with aAPC and separate particle platform .. 101
Figure 5-10. Separate particle platform improves T cell expansion against various antigens 102
Figure 5-11. Separate particle platform results in greater or equal T cell cytokine secretion 103
Figure 5-12. Separate particle platform allows for manipulation of co-stimulatory signal 2 composition . 104
Figure 5-13. Separate particle platform enables customization of co-stimulation 105
Figure 5-14. Separate particle platform activates optimal CD8+ T cells for adoptive cell transfer 107
Figure 6-1. aAPC characterization and functional assessment 126
Figure 6-2. aAPC and anti-PD-1 mAb show greater CD8+ T cell activation in combination 129
Figure 6-3. Co-administration of aAPC with CD8+ T cells impacts aAPC biodistribution 131
Figure 6-4. Anti-PD1 mAb and aAPC synergize to mediate anti-tumor activity in vivo 134
Figure 6-5. Anti-PD1 mAb and aAPC combination therapy decreases PD-1 expression and increases expansion of tumor-specific CD8+ T cells 137
Figure 6-6. PLGA/PBAE and PLGA particle characterization 140
Figure 6-7. PLGA/PBAE hybrid particles activate cognate CD8+ T cells 141
Figure 6-8. PLGA/PBAE bind cognate cells at a higher level than PLGA aAPC 142
Figure 6-9. PLGA/PBAE aAPC inhibit tumor growth 143

Chapter 1. Summary of the Dissertation

The organization of the dissertation is as follows:

Chapter 2 includes background information on the interaction between cancer and the immune system, especially in regards to T cells. It explains how the immune system may be targeted to induce cancer recognition.

Chapter 3 is a literature review on current immunoengineering approaches to modulate the anti-tumor T cell response. It focuses on cell-based and synthetic particles, protein engineering, and combination immunotherapies. Chapters 2 and 3 are largely based on an invited book chapter I am co-authoring with fellow graduate student John Hickey, *Engineered platforms for T cell modulation*, to be published in the International Review of Cell and Molecular Biology, book 342.

Chapter 4 describes a new genus of dual-targeting nanoparticles, termed immunoswitch particles, that delay and reverse melanoma and colon cancer growth in murine models. It includes *in vitro* and *in vivo* data that demonstrate the efficacy and mechanism of action of these tumor- and T cell-targeting nanoparticles. This study was published in *ACS Nano*[1] and is reprinted here with additional data and minor modifications.

Chapter 5 describes a new CD8+ T cell stimulation platform that enhances *in vitro* T cell activation. This platform builds on previous work from the lab and demonstrates how separating signaling components onto separate nanoparticles and subsequently clustering them within a magnetic field enhances activation. This platform

also presents a more streamlined and high throughput approach to customize co-stimulatory signals for activation. This study is not yet published.

Chapter 6 describes ways that biodegradable artificial antigen presenting cells (aAPC) can be improved by altering the aAPC material and by combination immunotherapy. I first show that anti-PD-1 monoclonal antibody checkpoint blockade and poly(lactic-co-glycolic acid) (PLGA)-based aAPC synergize to delay melanoma growth in murine models. This study was published in *Biomaterials*[2] and is reprinted here with minor modifications. Second, I describe preliminary work on a hybrid-polymer aAPC that increases T cell activation up to 100-fold. This data is not yet published.

Chapter 7 is a summary of the other chapters and outlines potential future work in the field.

Chapter 2. The Cancer-Immunity Cycle

The immune system is a complex organization of many different cell types that protect the human body from infection, disease, and foreign material. A breach of the body's physical barriers provokes an influx of innate and adaptive immune cells that can detect and eliminate infection, along with a surge of small molecule cytokines and chemokines that shape the local inflammatory response. The precision, effectiveness, and speed of the immune system is remarkable.

In addition to recognizing bacteria and viruses, the immune system can also recognize less obvious "non-self" material. Cancer develops from progressing mutations that give cells an increased capacity for proliferation, survival, and metastasis. These mutations may be expressed by cancerous cells and recognized as foreign and subsequently attacked by the immune system. However, cancer grows when it has developed mechanisms to evade immune recognition and attack. Cancer immunotherapeutics are a class of clinical therapies that aim to eliminate these defenses and stimulate an anti-cancer immune response, notably a T cell based cellular immune response. Here, I review the basic requirements for T cell activation and how cancer can be recognized or evade recognition by the immune system.

2.1 T cell activation

Minimally, T cells require two signals for activation—signal 1, specific peptide presented in the context of the major histocompatibility complex (MHC), and signal 2, a co-stimulatory signal such as B7.[3] The peptide-MHC complex presented by an antigen presenting cell interacts with the T cell via its T cell receptor (TCR) and is what confers

the specificity of T cell activation. Signal two provides co-stimulation and is required for the activation of naïve T cells. The interaction of B7 on an antigen presenting cell with CD28 on the T cell is thought of as the prototypical co-stimulation, although many different co-stimulatory molecules exist that modulate the T cell expansion, phenotype, and functionality.[4–13]

Before activation, TCR are pre-clustered in small 35-70 nm islands with 7-30 TCRs per island.[14] Upon recognition of cognate antigen, these nanoclusters begin to merge and form what is known as the immune synapse.[15] The lateral organization of the microscale immune synapse is defined by supramolecular activation clusters, or SMACs. TCR and CD28 co-localize within the central SMAC (cSMAC), with a TCR-rich core surrounded by a CD28-rich periphery.[16] Larger adhesion molecules, such as LFA-1, localize within the peripheral SMAC (pSMAC).[17] This nanoscale co-localization of TCR and CD28 is necessary for activation, as separating signal 1 and signal 2 activation by several microns inhibits T cell activation.[18]

There are two major subsets of T cells—CD4+ and CD8+ T cells, otherwise known as T helper cells and cytotoxic T cells, respectively. Upon activation, CD4+ T cells differentiate into different subtypes and can carry out multiple functions, from activating B lymphocytes to suppressing the immune reaction.[19,20] The major subtypes include Th1 and Th2, type 1 and 2 T helper cells,[19] Th17 cells which play roles in allergy and autoimmunity,[21] and Treg cells[22] which play important roles in immune response homeostasis. Cytotoxic CD8+ T cells secrete cytokines and kill target cells upon activation.[23] This subtype is responsible for selectively eliminating virally infected cells.

Upon activation, T cells clonally divide, secrete cytokines, and most importantly, maintain a memory response that provides long-term protection.

In most cases, the immune system is a powerful defense against infection and disease. However, dysfunctions or deficiencies in any part of the system can reduce its effectiveness or even create disease itself. Cancer's ability to evade immune recognition, chronic infection, and autoimmune diseases are all examples of pathologies that defy standard immune responses.

2.2 Blockades allow cancer progression

Cancer arises from the culmination of a series of mutations that lead to a break in normal cell-regulating functions, including enhanced proliferation or a lack of normal apoptotic processes. This can lead to the expression of mutated neo-antigens,[24,25] differentiation antigens, or viral antigens that can be recognized as foreign by the immune system.[26] These antigens are presented on major histocompatibility class I molecules (MHC-I) by resident dendritic cells (DCs) and subsequently activate tumor-antigen specific CD8+ T cells. While a T cell response can sometimes be mounted against these tumor-antigens, mechanisms of central and peripheral tolerance and immunosuppressive actions of the tumor micro-environment often hinder an effective immune response.[27]

The interplay between cancer and the immune system can be viewed as a potentially self-propagating cycle, termed the Cancer-Immunity Cycle, which has been elegantly reviewed by Chen and colleagues.[28] To achieve effective anti-tumor immunity, antigens released upon cancer cell death are processed and presented by antigen presenting cells to activate cognate T cells. These T cells may then recognize and kill the tumor cells, leading to a positive feedback loop for immune activation. Cancer expands

when there is a blockade in a step of this cycle that shields the tumor from immune recognition or attack.

In many cases, tumor antigens do not differ sufficiently from self-antigens to be recognized as foreign by the immune system. This is evidenced by the fact that tumors with higher frequencies of neo-antigens, tumor-specific antigens derived from tumor mutations, correlate with better prognosis following immunotherapy.[24,29–31] Even the response to tumors with many tumor antigens may be limited by an immunosuppressive tumor microenvironment. There are three major pathways by which tumor cells evade immune attack—reduced MHC expression of tumor antigens, secretion of immunosuppressive factors, and the upregulation of negative costimulatory pathways within the tumor microenvironment.[32] Downregulation of MHC expression can protect tumor cell recognition by T cells and is sometimes a method of tumor immune escape.[33] Tumor or stromal cells also can secrete soluble factors, including TGF-β, IL-10, and PGE_2, or express inhibitory checkpoint molecules that suppress immune function. Tumor cells that upregulate immunosuppressive TIM family proteins or the checkpoint molecule programmed death ligand 1 (PD-L1) are correlated with poor prognosis.[34,35]

Immunoengineering therapies target these various pathways to establish a more robust anti-tumor immune response. Many of these therapies target CD8+ T cell activation since CD8+ T cells can directly lyse tumor cells. Therapies may involve stimulating a T cell response that was previously inhibited due to tolerance or immunosuppression, blocking immunosuppressive checkpoint molecules upregulated by cancerous cells, or a combination approach to activate stimulatory pathways while simultaneously blocking inhibitory pathways. Incorporating engineering concepts into the

development of immunotherapies can enhance biomimicry or fine-tune biodistribution and targeted delivery. The next chapter reviews important concepts in engineering immunotherapies and previous work done in the field.

Chapter 3. Immunoengineering Approaches for T Cell Modulation

The dynamics of the immune synapse make T cell activation sensitive to many micro- and nano-scale properties of aAPC activators. The organization and composition of signaling molecules, as well as substrate size, shape, and stiffness of activating particles, interact to affect T cell activation and further to shape the phenotype of the activated cells. Immunoengineering seeks to systematically vary these factors to achieve optimal T cell activation and cancer suppression.

3.1 Properties to consider when designing a platform

3.1.1 Ligand choice and arrangement

T cell activation is modulated through different co-stimulatory and co-inhibitory pathways. When engineering a therapeutic, one first has to determine which specific signaling pathways to activate or inhibit. In addition to pathway choice, ligand nano- and micro-scale arrangement, density, strength, and duration can play a significant role.

T cells require a signal 1 for activation. This can be provided through stimulating the cognate TCR for a particular antigen or through CD3, an invariant molecule which is constitutively associated with the TCR and is responsible for its intracellular signaling.[36] pMHC stimulation of TCR is antigen-specific, while activation through CD3, with an anti-CD3 monoclonal antibody (mAb) for example, activates all T cells regardless of specificity.[3]

While signal 1 is minimally required for activation to occur, the T cell response to that signal alone results in an anergic, under-responsive state. Full activation after receiving signal 1 is modulated by dozens of co-stimulatory and co-inhibitory molecules.[37] CD28 is the pro-typical co-stimulatory molecule, although several other co-stimulatory molecules exist that modify T cell proliferation and phenotype. For example, 4-1BB co-stimulation has been shown to preferentially activate CD8+ T cells over CD4+ T cells,[38] preferentially activate memory CD8+ T cell populations,[8] increase T cell maintenance of CD28 expression,[7] and increase CD8+ T cell secretion of IL-2.[9] Stimulation through the co-stimulatory molecules OX40 and CD27 expressed by T cells has also been shown to enhance activation.[5,6] Altering the combinations and ratios of different co-stimulatory molecules without varying the total number of co-stimulatory molecules can also have tremendous impacts on activation.[6,10]

Besides co-stimulators, T-cell activity is inhibited through several different pathways. These pathways are involved with maintaining homeostasis and establishing a self-regulated immune response following pathogen removal.[39] However, these inhibitory pathways can be utilized by cancer cells to evade and inhibit an anti-tumor response. Programmed death 1 (PD-1) and CTLA-4 expressed by T cells are two checkpoint molecules commonly targeted by immunotherapies.[40,41] Monoclonal antibodies blocking these checkpoint pathways as well as other immuno-inhibitory molecules such as IDO can rescue exhausted T cells.[42] Blocking inhibitory pathways along with activating co-stimulatory pathways can also further augment the T cell response in cancer[43,44] and in chronic infection.[45]

The nano- and micro-scale arrangement of signaling ligands plays an important role in modulating the T cell response to engineered platforms. At the microscale, a focal co-clustering of signal 1 and signal 2 molecules is necessary to initiate activation. When anti-CD3 mAb is patterned on a planar substrate in focal spots, T cells proliferate and secrete cytokines.[46] However, T cell activation is reduced when the same anti-CD3 mAb is tethered in an annular pattern that precludes centralized TCR clustering.[46] Signal 2 must also be co-clustered with signal 1 during stimulation. Separating anti-CD3 and anti-CD28 by a distance of several microns inhibits IL-2 cytokine production.[18]

TCR intermolecular distance must be sufficiently small, on the nano-scale, to induce activation. When anti-CD3 is patterned on planar substrates at defined densities, only surfaces displaying anti-CD3 with intermolecular distances smaller than approximately 60 nm induce optimal activation.[47,48] Interestingly, the minimum intermolecular distance for CD4+ T cell-specific activation with MHC II is close to 115 nm,[49] indicating that ligand organization on aAPC may need to be optimized based on the T cell subset that is targeted.

While TCR and CD28 organization have been most extensively studied, some data indicates that signaling through other co-stimulatory and co-inhibitory pathways may also be sensitive to nanoscale arrangement. T cell inhibition through PD-1 signaling has been shown to depend on the formation of microclusters within the immune synapse.[50,51] When the extracellular domain of PD-1 was extended to preclude its co-localization within the immune synapse, the molecule was not inhibitory. 4-1BB has also been shown to localize within the immune synapse along with CD28 during co-

stimulation.[52] Thus, it is evident that in addition to ligand selection, the micro- and nano-scale arrangement of these various signaling molecules can have tremendous impacts.

3.1.2 Particle size

Engineered particle size is important to many aspects of T cell modulation at both the cellular and systemic level. At the cellular level, the size of the particle affects how it will interact with a T cell by changing the curvature and avidity. For particle therapeutics that will be used *in vivo*, the role of size on biodistribution and circulation time also comes into play, as larger particles are less biocompatible and have reduced drainage to lymphatics and tumor sites. When developing a new platform, it is important to understand how size may affect efficacy and whether it is important to be optimized for *in vivo* applications.

At the cellular level, it is generally thought that particles that most closely mimic endogenous interactions are most effective. Micro-scale particles that most closely mimic the size of endogenous antigen presenting cells are thus most effective in stimulating a response.[53] A majority of T cell activation particles that have been developed so far are about 4-5 μm, comparable to the size of a T cell.[10,54,55]

While microscale particles are most effective at stimulating a T cell response at the cellular level, they become less feasible for *in vivo* applications when systemic biodistribution plays a role. As particle size increases, lymphatic drainage is limited from an injection site and clearance by certain phagocytic cells increases.[56–58] At the systemic level, nanoparticles display improved trafficking properties, slower clearance and enhanced localization to T cells, compared to microparticles .

More recent technologies have demonstrated how sub-micron scale particles can be used to elicit a T cell response. These approaches generally aim to increase the contact area between the T cell and nanoparticle by altering the distribution of particles on the cell surface or local curvature of the nanoparticle. Sub-100 nm particles have been shown to activate T cells at sufficiently high surface densities of stimulatory ligands.[59] In contrast to altering the distribution of ligands on the surface of the nanoparticle, external forces can be used to affect particle distribution on the T cell surface. Superparamagnetic iron-dextran nanoparticles have increased stimulatory capability when clustered on the surface of a T cell to enable micro-scale clustering of signaling molecules.[60]

3.1.3 Particle shape

When synthesizing synthetic platforms for T cell modulation, particle shape can have surprising impacts on their interaction with T cells and macrophages as well as their biodistribution. Spherical and ellipsoidal particles have differing interfacial geometries despite similar length scales and can thus be optimized for T cell interactions. By using shape to vary biodistribution, the half-life and cell and organ targets can be modified.

Particle shape affects biodistribution in part by modifying phagocytosis by the reticuloendothelial system (RES). In contrast to spherical particles, ellipsoidal particles reduce nonspecific RES phagocytosis, an important consideration for extending the half-life of therapeutics to be injected *in vivo*.[56,61–63] In fact, phagocytosis is more dominantly affected by shape rather than size in the range of approximately 1-10 μm.[61] However interestingly, receptor-mediated endocytosis of non-spherical particles is enhanced.[64] Thus, elongating particles for applications where targeted internalization is preferred, such as drug delivery, may also take advantage of longer circulation times.

In addition to affecting biodistribution and half-life, particle geometry plays an important role at the T cell-particle interface. While most T cell-interacting particles, such as artificial antigen presenting cells (aAPC), are spherical in nature, this shape does not recapitulate biological T cell-APC interactions. Spherical particles maximize the curvature and thus minimize the surface area of contact between the T cell and particle. This is especially detrimental as ligand avidity decreases as particle size also decreases to the nanoscale, despite biocompatibility incentives to move to smaller size scales. Ellipsoidal microparticle aAPC were shown to preferentially interact with T cells along their long axis and significantly increase T cell activation *in vitro* and *in vivo*.[65] Nano-aAPC also result in a similar increase in T cell activation with ellipsoidal versus spherical particles while also taking advantage of the increased biocompatibility and superior biodistribution based on particle size.[66]

3.2 Particle-based approaches

One approach to initiating or re-activating an anti-tumor T cell response is to mimic portions of endogenous T cell activation using an engineered platform. Scientists and engineers have developed biocompatible platforms that mimic antigen presentation, orchestrate the delivery of immune-stimulatory drugs, or prompt a new type of immune interaction. These platforms have been built upon a wide variety of biocompatible platforms, from cultured cell lines to biodegradable polymers. Here, I review these particle-based approaches for activating T cells by dividing them into three main categories—artificial antigen presenting cells, drug-delivery platforms, and particles that interact with other immune subtypes with the goal of T cell activation.

3.2.1 Artificial antigen presenting cells

Artificial antigen presenting cells are micro or nano sized platforms designed to mimic endogenous antigen presenting cells for T cell activation. Their major role lies in adoptive cell therapy (ACT)–*ex vivo* activation of autologous lymphocytes with aAPCs expressing tumor-specific peptide-MHC (pMHC), followed by re-infusion of the expanded cells into the patient.[67] Large numbers of expanded lymphocytes, up to 10^{11}, are needed to treat a single patient with ACT.[68] Such robust activation requires the development of optimized aAPC that are both effective and economical. Additionally, research has shown the importance of not just quantity, but more importantly, quality of the resultant cells for a long-lived effector population post-transfer.[69] Thus, extensive work has been done to develop optimal aAPC for this purpose.

aAPC are three dimensional cellular or synthetic platforms that minimally present the two necessary signals for T cell activation—peptide MHC, signal 1, and B7-1/B7-2 or anti-CD28 monoclonal antibody (mAb), signal 2.[70] Many of the earliest aAPC were built upon APC-like cultured cell lines engineered to express signal 1 and signal 2, most notably K562[6,71–73] and the murine NIH/3T3 fibroblast line.[74–76] Despite their early successes, acellular aAPC have become the favored platform due to several benefits over their cellular counterparts. Acellular platforms allow for the ability to control molecule expression, geometry, rigidity, and shape, as well as eliminate unwanted cytokine and cell surface molecule expression. Synthetic platforms can also decrease costs by creating a more easily manufactured all-in-one off-the-shelf therapy.

When engineered on a synthetic platform, aAPC can be created with defined sizes. Most commonly, they are spheres several microns in diameter, meant to closely

mimic the general scale of an endogenous antigen presenting cell.[10,77–80] Large, micron-scale particles reduce the curvature at the T cell-aAPC interface compared to smaller particles and allow for a higher avidity interaction. The aAPC can thus interact with multiple TCR and induce robust activation. The importance of this multivalent interaction has been demonstrated experimentally by stimulating T cells with planar and three-dimensional platforms with differing signal densities. Spherical microparticles with reduced densities of MHC signal 1 cannot activate T cells to the same extent as particles with a high density despite increasing particle dose[79,81], and higher densities of stimulatory molecules correlate with lower effective concentration and prolonged activation.[82]

Despite their success in activating T cells at the cell-particle level, microscale particles have poor biodistribution properties and are thus less than optimal for *in vivo* applications. Microparticles cannot take advantage of the enhanced permeability and retention effect to localize aAPC at the tumor site[83] and do not effectively drain to lymph nodes where effective immune stimulation takes place.[84,85] Thus, more recent work has explored ways to optimize aAPC on more biocompatible nano-scale platforms.

The spherical shape of aAPC is popular largely because of the ease of synthesis using standard chemical synthesis procedures, such as emulsion techniques for PLGA.[86,87] However, spheres minimize the contact area at the T cell-aAPC interface despite the importance of multivalent pMHC-TCR interactions. Recent work has demonstrated how altering aAPC geometry can improve the stimulatory capabilities of both micro- and nano- aAPC. Importantly, modifications to aAPC shape have also helped to bring nano-aAPC into the playing field.

Ellipsoidal synthetic aAPC can be developed by physically stretching spherical-shaped PLGA particles following single emulsion techniques.[65] These oblong particles can be synthesized with aspect ratios over six and be conjugated with equivalent protein densities to spherical particles, allowing for controlled comparison to their spherical counterparts. It was shown that increasing micro-aAPC aspect ratio (i.e. degree of stretching) positively correlates with CD8+ T cell proliferation and maximally induces a 20-fold stronger T cell response. Interestingly, proliferation did not increase linearly with increased particle stretching but rather resulted in more significant gains at specific aspect ratio intervals. This geometry-driven change in T cell proliferation was shown to be correlated with changes to the T cell-aAPC interface. Ellipsoidal aAPC conjugated to more T cells and individual contact areas were larger than spherical interactions, indicating that increased avidity and interactions with multiple TCR may drive their improved efficacy.

This geometry effect has also been shown to be maintained on the nanoscale.[66] Nano-aAPC with spherical diameters on the order of approximately 200 nm induce a five-fold stronger T cell response when they are ellipsoidal in shape. As shown with other systems,[56,61,62] ellipsoidal aAPC resisted uptake by RES cells and had longer circulation times *in vivo*. Nearly 80% of spherical nano-aAPC were uptaken by macrophages, in contrast to less than 15% of ellipsoidal aAPC, demonstrating improved biodistribution of ellipsoidal particles. This increased ability to stimulate T cells and longer circulation times led to significantly increased T cell proliferation *in vivo*.

In contrast to manipulating the geometry of the base particle, magnetic fields have also been utilized to alter how nano-aAPC are perceived by and interact with T cells.

Superparamagnetic spherical iron-dextran aAPC with a diameter of 100 nm do not normally activate a robust T cell response. However, when an external magnetic field is applied, the nano-aAPC cluster on the T cell surface, changing the perceived shape and size of the aAPC by the T cell, and likewise increase proliferation.[59,60] This method enables nano-aAPC to activate rare endogenous T cell populations, such as would be necessary for adoptive cell transfer.

In parallel to studies on how physical properties of the aAPC, such as geometry and size, affect T cell activation, others have demonstrated the significant impacts of ligand choice. Traditionally, aAPC are conjugated with the two necessary signals for T cell activation—anti-CD3 mAb or a specific pMHC, signal 1, and B7 or anti-CD28 mAb, signal 2. Often, a pMHC will be chosen so that T cell activation is limited to be against a specific target antigen, although interesting work has demonstrated how phenotypic markers can be used post-nonspecific activation to select a specific T cell subset.[88] A great deal of work in antigen discovery and immunogenicity has been conducted for the selection of a specific pMHC targets for different applications, but these details are outside of the scope of this chapter.

Despite the fact that signaling through CD28 is the main co-stimulatory signal provided by synthetic aAPCs, the composition of co-stimulatory signals greatly impacts T cell activation. There are dozens of different types of co-stimulatory signal 2 molecules, and altering the combinations and ratios of these signals can impact proliferation, phenotype, and survival *in vivo*. These T cell co-stimulatory molecules include pathways such as CD70-CD27, CD40-CD40L, 4-1BB-4-1BBL, OX40L-OX40, and others expressed on the antigen presenting cell and T cell, respectively.[37]

Studies have shown that co-stimulation through 4-1BB during the rapid expansion protocol for adoptive cell transfer improves the expansion and effector function of tumor-specific T cells.[89] 4-1BB co-stimulation has also been associated with the preferential expansion of memory T cells which are often desired for *in vivo* transfer applications.[90] Combining multiple co-stimulatory signals on the same aAPC also can have significant impacts on T cell functionality. A study combining CD28, 4-1BB, and CD27 signaling on K562 aAPC demonstrated that certain combinations of the co-stimulatory molecules can increase proliferation over 10-fold.[6] Even when the total amount of co-stimulation is equivalent, simply changing the ratio of signal 2 ligands can impact the resultant T cells. In one study, micron sized polystyrene aAPC conjugated with different ratios of anti-CD28 and anti-4-1BB mAb impacted antigen-specific proliferation as much as five-fold.[10] Other co-stimulatory molecules, such as activation through OX40[91] and CD40L[92,93] which been shown to have stimulatory effects on T cells, could also be incorporated in next generation aAPC.

In addition to the choice of signal 1 and signal 2, aAPC can be conjugated with other molecules to enhance their efficacy. CD47 is a molecule ubiquitously expressed by normal cells that protects self-cells against phagocytosis.[94] aAPC that also express CD47 have been shown to also be protected from phagocytosis and induce greater stimulation of T cells *in vivo*.[95]

3.2.2 Drug-carrier particles

T cells receive many different signals that shape their activation. These signals include interaction of T cell surface molecules with stimulatory or inhibitory ligands presented on the surface of antigen presenting cells and tumor cells, as well as signaling

by soluble cytokines and chemokines through cell surface receptors. Synthetic particles that allow for the engineering of shape, biodegradation properties, and conjugation or encapsulation with drugs that affect these various pathways provide a mechanism to dictate drug release distribution and kinetics.

During endogenous T cell stimulation, T cells receive soluble "signal 3" molecules that drive proliferation and cytotoxicity.[96] These soluble mediators are secreted in a localized paracrine or autocrine fashion that increases their local concentration and limits exposure to the desired cells. Because these signals are often broadly immune activating, local delivery ensures that only the target cells are affected. This important aspect of local immune stimulation is lost when immune-activating drugs are administered in a systemic fashion. To more closely mimic the endogenous process and enable maximum T cell expansion, nanoparticles have been used to selectively deliver stimulatory signals in a paracrine manner to T cells of interest. Biodegradable polymers are often the material of choice due to the ability to manipulate their degradation and intracellular delivery properties.

Various methods have been used to target these drug-delivery particles to specific immune subsets. One approach is to combine drug delivery with an aAPC to take advantage of both aAPC-based extracellular stimulation as well as localized drug delivery. In one study, biodegradable aAPC were engineered to encapsulate soluble IL-2, a T cell growth factor, and released IL-2 locally while stimulating T cells via signal 1 and signal 2 expressed on its surface.[54,97] These particles increased T cell proliferation 10-fold compared to non-encapsulating aAPC with bulk IL-2.

Similarly, nanoparticles conjugated with T cell signaling molecules have been used to simply target the nanoparticles to T cells with the goal of intracellular drug delivery. Gelatin nanoparticles approximately 200 nm in diameter conjugated with anti-CD3 mAb have been shown to be selectively internalized by T cells.[98] Over 80% of T cell leukemia cells were observed to uptake the particles, demonstrating the potential for nanoparticles to be used to target the delivery of intracellular signals. More recently, this approach has demonstrated success in transfecting T cells with genetic material. Anti-CD3 mAb-coated biodegradable nanoparticles approximately 150 nm in diameter were engineered to encapsulate a DNA plasmid encoding for a specific chimeric antigen receptor (CAR).[99] The particles showed specific transfection of T cells with approximately 5% of non-T cells showing uptake following intravenous administration. Remarkably, systemic administration of these nanoparticles resulted in the same degree of anti-leukemia activity as compared to adoptive cell transfer of *ex vivo* transfected CAR T cells. Thus, the nanoparticle approach was able to significantly reduce the cost and time requirements of lymphodepletion and *ex vivo* T cell manipulation. More specific targeting of T cell subsets is also possible, as anti-CD4 mAb conjugated lipid nanoparticles have been shown to selectively target CD4+ T cells *in vitro* and *in vivo*.[100] These nanoparticles selectively delivered a CD45 siRNA and induced gene silencing up to 20% in CD4+ T cells five days post intravenous administration.

Localized drug delivery to T cells can also be achieved through combination with adoptive cell therapy. For example, nanoparticles can be covalently linked to T cells expanded *in vitro* prior to re-infusion. In one study, drug-releasing nanoparticles were covalently linked to the surface of tumor-targeting T cells prior to adoptive cell

transfer.[101] When synthesized to release an inhibitor of immune-inhibitory signals, nanoparticle-functionalized T cells achieved greater expansion at the tumor site compared to systemic administration of the drug, achieving a 14 day survival advantage. Importantly, this study also demonstrated that the nanoparticles were translocated into the immune synapse during T cell activation. To further modulate not just the cell-proximity of drug release but also its temporal profile, T cell-bound nanoparticles have been developed that release drug only upon T cell stimulation.[102] When CD8+ T cells become activated they release lytic granules, and this property has recently been used to trigger nanoparticle degradation. These nanoparticles, when bound to HIV-specific CD8+ T cells, were shown to enable the delivery of an immunotherapeutic to a site of high viral replication.

A majority of T cell targeting nanoparticles for local drug delivery to date have targeted CD4, CD3, or TCR expression. However, it is important to appropriately select the targeting molecule for the most effective response. Whether or not a targeting molecule is internalized can significantly affect the T cell response to nanoparticle-mediated drug delivery. A study that investigated targeting nanoparticles that released a TGF-β inhibitor to T cell internalizing versus non-internalizing receptors showed differing responses, and this effect changed if T cells were conjugated with nanoparticles prior to adoptive cell transfer or targeted directly by intravenous particle administration.[103]

When widespread circulation of a drug is important, smaller particles or molecules are often preferred due to their superior biodistribution. However, in some cases, limiting the circulation of a drug may be desired such as with non-specific immune

activators meant to target T cells infiltrating a tumor. Systemic administration of stimulatory molecules such as IL-2 and anti-4-1BB mAb are associated with various off-target toxicities due to widespread immune activation.[104,105] Thus, a different approach to drug delivery is to anchor drugs to particles and inject them locally to the site of interest for the purpose of prolonging drug retention. Studies have shown that anchoring IL-2 and anti-4-1BB mAb to the surface of liposomes approximately 160 nm in diameter significantly reduces off-target toxicities when injected intratumorally.[106,107] Even when injected intratumorally, the soluble antibody and cytokine were detectable at high levels 18 hours post injection and resulted in significant weight loss in treated mice. In contrast, the nanoparticle-anchored drugs limited drug exposure to the tumor site and were shown to treat murine melanoma.

3.2.3 Non-T cell interacting particles

Activating a T cell response through the conjugation of stimulatory molecules on the surface of synthetic particles is a straightforward and direct way to modulate T cells by mimicking endogenous antigen presenting cells. However, T cell signaling involves many complex interactions with membrane-bound and soluble factors. Synthetic particles can be engineered to affect which cell types T cells interact with, alter a cell interaction that is already present, or alter the phenotype and activity of other immune cells that modulate T cell activity.

Dendritic cells (DCs) play a central role in orchestrating both the innate and adaptive immune response.[108] In an optimal response, dendritic cells express peptide fragments of invading pathogens to T cells and express co-stimulatory molecules that enable their efficient activation. However, in the instance of cancer or chronic infection,

this process does not always occur appropriately. One method to initiate a more robust T cell response is thus to enhance antigen or co-stimulus presentation by DCs which can then mediate the T cell response.

Activation of DCs and other antigen presenting cells, like T cell activation, is sensitive to the environment. A stimulatory environment with appropriate kinetics is crucial to induce activation rather than tolerance. In order to control the stimulatory conditions, DCs can be extracted from a patient and the signals for activation can be fully controlled *ex vivo*. Cell-based DC vaccines, such Sipuleucel-T,[109,110] involve this *ex vivo* activation of DCs against a tumor antigen followed by their re-infusion into the patient where they can circulate throughout the body and activate an anti-tumor immune response. However, this approach is time-consuming and expensive as it involves manipulating cells outside of the human body and often has to be completed at non-local sites. Nanoparticles have gained interest in the field of vaccine delivery due to their ability to be engineered to manipulate the biodistribution and kinetics of vaccine delivery *in vivo*.[111] Biomaterials can also potentially be used to target vaccination to specific DC subsets which has an effect on vaccine efficacy.[112]

Various studies have explored using nanoparticles to effectively delivery antigen to DCs directly *in vivo*. In the design of nanoparticle-based vaccination, particle size plays an important role in lymph node trafficking. 25 nm pluronic copolymer-coated nanoparticles injected intradermally were shown to travel to draining lymph nodes through interstitial flow and remain there for at least 120 hours where they could activate a humoral and cellular immune response against a model antigen.[113] In contrast, particles just four times as large—100 nm—were approximately 10% as efficient and were

undetectable in draining lymph nodes within 24 hours. In another study using polystyrene particles ranging in size from 20 nm to 2 μm, 40 nm particles most efficiently trafficked to lymph nodes and activated resident DCs.[114] Similar to spherical nanoparticles, nanodiscs have been used for vaccine delivery. Small vaccine-carrying lipoprotein nanodiscs approximately 10 nm in diameter were shown to be more effective than soluble vaccines.[115] These nanodiscs were coupled with antigen peptides and adjuvant and were shown to elicit up to a 47-fold greater frequency of tumor-specific T cells than soluble vaccines. By utilizing a nanodisc carrier, antigen and adjuvant accumulated more in lymph nodes than soluble injected vaccines where there is a high density of dendritic cells. Most successful particle-based vaccines are engineered with sub-100 nm particles. Particles larger than approximately 200 nm require cellular transport by DCs in the skin to travel to the lymph node.[58]

Various other similar techniques have been utilized that take advantage of nanoparticle trafficking to secondary lymphoid organs by altering size, biomaterial, or incorporating specific receptors. Nanoparticle "backpacks" have been developed that deliver vaccines to lymph node DCs by binding DC receptors, such as CD40 or DEC-205, or by binding endogenous albumin.[116–120] In addition to modulating the biodistribution of the vaccine, approaches have been developed to alter how the delivered peptide is presented by the DC. During normal activation, intracellular antigens are presented on MHC-I and activate a cell-mediated CD8+ T cell response, whereas endocytosed antigens are presented on MHC-II and activate a humoral CD4+ T cell mediated response. To induce presentation by DC on MHC-I, nanoparticle-based

vaccines have been developed that are capable of escaping the endosome upon internalization.[121]

In addition to particles that interact only with T cells (i.e. aAPCs) and particles that interact only with antigen presenting cells (i.e. particle-based vaccines), particles can bind multiple cell types simultaneously to induce new interactions or change existing ones. In these instances, a nanoparticle platform is used to increase avidity for the targeted antigens or alter biodistribution. For example, 50 nm particles have been used to redirect a T cell response against a specific tumor antigen, similar in approach to bispecific T cell engagers.[122] These nanoparticles, termed antigen-specific T cell redirectors (ATR), were conjugated with an antibody against the CD19 tumor antigen and non-tumor peptide-MHC. When MHC-bound ATR were loaded with a human flu peptide, human flu-specific T cells were able to be redirected to kill CD19+ tumor cells.

3.2 Protein engineering

At the smallest scale, proteins and small molecules can be engineered to target specific signals involved with T cell activation. This may involve developing a high affinity antibody to activate or block one or more immune stimulatory or inhibitory pathways, synthesizing modified cytokines that can more effectively bind their targets, or utilizing antibodies to target the delivery of a drug or cytokine to a specific anatomical site. In this section, I review these many different approaches and how engineering principles have been applied to their design. I will focus on how these engineered molecules have been used as monotherapies, although many are combined with synthetic particles or scaffolds for further modulation of their delivery.

3.2.1 Engineered cytokines

During T cell activation, T cells receive soluble pro-inflammatory or anti-inflammatory "signal 3" signals. These signals help to drive cell proliferation, differentiation, and chemotaxis among other functions. Administration of pro-inflammatory cytokines important for immune activation, most commonly the T cell growth factor IL-2, can activate a robust anti-tumor immune response, but systemic injection is complicated by life-threatening toxicities.[123,124] The clinical use of cytokines is also hindered by their rapid clearance from the bloodstream, leading to a typical serum half-life on the order of minutes. Longer-acting engineered cytokines that can selectively activate immune subsets and antibodies that can direct their localization have thus infiltrated the field of immunoengineering.

In the field of cytokine engineering, scientists and engineers have developed cytokines with altered binding to immune cell subsets to create a more clinically-favorable therapeutic. IL-2 signaling occurs through a dimeric or trimeric receptor complex, consisting of IL-2Rα, IL-2Rβ, and IL-2Rγ. Different immune subsets modulate their sensitivity to IL-2 signaling by modulating their expression of these three subunits. Naïve T cells only express the moderate affinity IL-2Rβ and IL-2Rγ subunits, whereas memory T cells and regulatory T cells also express the high affinity IL-2Rα and are thus more sensitive to IL-2 signaling.[125] Importantly, pulmonary edema, a major toxicity upon systemic IL-2 administration, has been shown to be mainly IL-2Rα-dependent.[126] An engineered IL-2Rα-independent "superkine" was shown to shift the cellular response upon *in vivo* treatment compared to wild-type IL-2.[127] This IL-2 superkine was engineered to have increased binding for the IL-2Rβ subunit and thus activated cells in an

IL-2Rα-independent fashion. The IL-2 superkine significantly increased the expansion of CD8+ T cells *in vivo* while having no changed effect on regulatory T cell expansion. By shifting the cellular response, it was also shown to significantly reduce pulmonary edema and increase the anti-tumor effect in several murine models. Further modifications of this engineered IL-2 cytokine have demonstrated how modulating binding activity to the other sub-units can further control the cellular response.

Superagonists against other immunomodulatory cytokines have also been developed. For example, IL-15 is a cytokine that contributes to T cell and NK cell development, proliferation, and activation.[128] Endogenously, IL-15 is bound to IL-15Rα and expressed on the cell surface of antigen presenting cells to T cells and NK cells displaying IL-2Rβγc. This cell surface expression by IL-2Rβγc induces a necessary conformational change that enhances binding to IL-2Rβγc. Thus, the administration of soluble IL-15 has only a moderate effect on T cell expansion. Early IL-15 superagonists were engineered by binding IL-15 to a recombinant IL-15Rα prior to transfer, and was shown to selectively induce robust expansion of memory CD8+ T cells and natural killer cells.[129] More recently, IL-15 superagonists have been engineered that have four- to five-fold higher binding to IL-2Rβγc than endogenous IL-15,[130] and superagonists linked to Fc binding domains to enhance serum half-life.[131]

High-affinity superagonist cytokines can modulate the cells that respond to treatment and increase the efficacy compared to endogenous cytokines but often do not solve the problem of systemic toxicities. In this regard, cytokines have been bound to tumor-targeting antibodies to increase their localization to the tumor microenvironment. Cytokine-antibody fusion proteins have been developed in over a dozen types of variants.

In the simplest terms, cytokines can be linked via the N- or C- terminus of an antibody to affect the spatial relationship between cytokine delivery and antibody binding.[132] Additional modifications of the constant region can also modulate how the fusion protein interacts with Fcγ receptors, initiates the complement cascade, or alters molecular weight and biodistribution.[133] In addition to targeting cytokines to the tumor microenvironment, the physical constraint of a tumor-targeting antibody with a T or other immune cell targeting cytokine can present synergies by additional mechanisms. For example, immunocytokines that target tumor-expressed antigens have been shown to increase effector-target cell conjugation between tumor cells and T cells or natural killer cells much like a bispecific antibody.[132] Other families of immunocytokines that link cytokines with tumor-associated extracellular matrix components are thought to mediate an anti-tumor effect primarily through localizing the cytokine delivery.[134]

Immunocytokines have been developed that incorporate various different tumor-associated antigens, from PD-L1 or CD20. However, a majority of those previously developed have utilized IL-2, IL-12, IL-15, or TNF.[132] For example, authors have shown superior anti-tumor activity of an IL-15 superagonist-rituximab fusion protein compared to rituximab alone.[135,136] By linking the cytokine with a tumor-targeting antibody, the fusion proteins were capable of taking advantages of both—specific binding to CD20 on tumor cells, stimulation through the IL-2Rβγ$_c$ on immune cells, and binding to Fcγ receptors on macrophages and natural killer cells. Other immunocytokines that deliver anti-inflammatory cytokines for organ-specific autoimmune disease,[137] target cytokine delivery to necrotic areas of tumors through incorporation of anti-DNA antibodies,[138] or

combine the blockade of tumor-expressed immune-inhibitory molecules[139] have also been developed.

3.2.2 Antibody Engineering

In addition to cytokine engineering, antibodies are constantly being developed to block or stimulate cell targets, alter cell-mediated cytotoxicity and biodistribution, or selectively deliver drugs to a site of disease. Monoclonal antibodies are able to selectively bind an antigen that may be uniquely expressed or upregulated on tumor cells and possess longer half-lives than small molecules.[140] Their precision thus makes them a common method to target individual pathways with fewer off-target toxicities. However, beyond selecting a molecular target, applying engineering principles to their design can improve their biodistribution, alter their interaction with immune cells, turn them into a "backpack" to deliver a drug or nanoparticle to a disease site, or manipulate an antibody to target multiple cell types simultaneously. Here, I will not review the process of monoclonal antibody production or selection of target antigen, but rather will explore how these antibodies have been further manipulated to customize their *in vivo* effects.

Antibodies can be separated into three major categories—those whose major mechanism of action is through the blockade or stimulation of the targeted pathway, those used to deliver a drug payload, and those whose structure has been engineered to bind multiple different cell types simultaneously to redirect functionality. Endogenously, antibodies often bind infected cells or foreign pathogens. The exposed constant region of these antibodies can then mediate antibody-dependent cellular cytotoxicity or complement-dependent cytotoxicity. Thus most fundamentally, antibody engineering often involves the modification of the Fc region to modulate how the bound antibodies

will interact with the immune system.[141] When antibody-mediated cell death is desired, such as when antibodies target molecules on infected or tumor cells, isotypes such as human IgG1 are often incorporated that initiate these processes.[142,143] In other cases, an antibody may be developed to block or stimulate a certain pathway on a healthy cell-type, such as the programmed death 1 (PD-1) inhibitory molecule on T cells. When cell death would be detrimental, the antibody is engineered to have an IgG2 or IgG4 isotype that has limited interaction with Fc receptors.[144] In all cases, antibodies are humanized by replacing the constant region and sometimes parts of the variable region with the human sequence.[145]

T cells have a complex interaction with cancerous cells. While cancerous cells may express mutated neo-antigens that are recognized by the immune system, they also often upregulate immunosuppressant molecules that inhibit efficient T cell stimulation and lack expression of co-stimulatory molecules.[37] Many monoclonal antibodies have been developed that block these inhibitory pathways on T cells or tumor cells or stimulate signaling pathways on T cells directly to jumpstart the cancer immunity cycle. Clinical administration of soluble antagonist antibodies against the inhibitory checkpoint molecules PD-1[41,146] and its ligand, PD-L1,[147] and CTLA-4[40,148,149] have shown tremendous success in recent years. The success of these checkpoint blockades have been correlated with tumor mutation load—tumors with more mutations and more neoantigens are associated with improved clinical benefit.[150,151] Agonistic antibodies have also been developed that stimulate T cell signaling through co-stimulation, such as anti-CD28, anti-4-1BB, and anti-OX40.[5,9,91,152] However, because of the structured arrangement of the

signaling molecules during T cell activation, co-stimulatory molecules are often delivered on particle platforms[6,10] that enable the formation of the immune synapse.

The direct function of an antibody is often to affect a certain pathway. However, antibodies have also been conjugated with various drugs and utilized to deliver payloads to specific T cells or tumor cells. In cancer immunotherapy, many of these antibody-drug conjugates target tumor-expressed antigens, such as Her2, CD19, or CD22, and interesting strategies have been engineered to increase tumor-specificity. For example, a protein was developed that has a peptide sequence that shields the antibody's antigen binding site from binding until it is cleaved within the tumor microenvironment.[153] This method can thus enhance tumor-specificity when the antigen target is not uniquely expressed by cancerous cells. This type of approach could also potentially be used to decrease off-target toxicities of checkpoint inhibitors and co-stimulatory antibodies as these are not limited to the cancerous tissue. Fusion proteins have also been made that deliver multiple payloads simultaneously. For example, a trifunctional fusion protein linked an antibody against a tumor-associated antigen with both 4-1BBL and IL-15.[154] The fusion protein was more efficient than corresponding bifunctional proteins in activating T cells and inducing an anti-tumor response *in vivo*. The approach to lymphoid malignancies is slightly different, where antibodies have been developed to delivery cytotoxic drugs to T cells themselves. An antibody drug conjugate targeting IL-7R expressed on lymphatic cells demonstrated how this method could be used to treat lymphoid malignancies or autoimmune disorders.[155]

One of the most unique antibody based approaches in cancer immunotherapy has been the development of bispecific antibodies. Bispecific antibodies are antibodies that

have been engineered to have two different variable portions, each specific for a different antigen. Their specific structure can come in many forms and each varies in terms of size, spatial relationship between antigen-binding sites, and synthesis protocol and thus may affect half-life and interactions with the corresponding ligands.[156] The physical constraint of the two antibody fragments is often central to their function. Bispecific antibodies are used to physically link two different cell types or dimerize two different molecules on the surface of the same cell. On the larger scale are individual antibodies linked by a chemical linker and a family of bispecific antibodies called Triomab which maintain the full IgG shape by linking two half antibodies, each with one heavy and one light chain.[157] These types of approaches can be easily synthesized by standard protocols to allow for high-throughput manufacturing and have extended half-lives compared to smaller proteins, but maintain expression of the Fc region which may be recognized by Fc receptors and lead to unwanted off-target effects. At the opposite end of the spectrum are bispecific T cell engagers (BiTEs) where the heavy and light chain of two different variable domains are linked by a short serine-glycine linker.[158] These bispecific antibodies reduce Fc receptor recognition, but their small size, approximately 55 kDa, reduces half-life and necessitates constant intravenous infusion.[159]

Likely the most well-known type of bispecific antibodies in the field of cancer immunotherapy are bispecific T cell engagers (BiTEs). BiTEs link an anti-CD3 antibody fragment with an antibody fragment against a tumor-associated antigen.[160] The BiTE can thus physically link tumor cells with T cells while activing T cells to induce tumor cell lysis. Because BiTEs incorporate anti-CD3 rather than a pMHC, they can activate all T cells and thus are associated with dose-limiting toxicities including cytokine storms.[161]

BiTEs have been developed linking T cell stimulation with various tumor-associated antigens such as CD19,[162,163] BCMA,[164] and EphA2.[165] However, like many targeted immunotherapies, they require the selection of a tumor-associated antigen to target and thus antigen escape is a concern. Interestingly, it was recently shown that BiTEs can mediate lysis of bystander tumor cells not expressing the targeted antigen.[166]

T cell-targeting bispecific antibodies have also been developed that link molecules on the same cell. A recent bispecific antibody, synthesized by chemically linking agonistic antibodies against the co-stimulatory receptors CD137 and CD134 on T cells, was more effective at activating an anti-tumor T cell response than either antibody individually.[167] In contrast to monotherapy, the platform uniquely induced preferential expansion of effector T cells. Thus, in addition to redirecting cells, bispecific antibodies can potentially impact T cell activation by physically co-clustering molecules on the surface of the same cell. This approach may be interesting in the targeting other T cell signaling molecules since the activation process is highly sensitive to receptor clustering and spatial localization.

3.3 Combination immunotherapies

Methods of both direct T cell activation and blockade of inhibitory checkpoint pathways have resulted in exciting results in preclinical studies and clinical trials. However, there remains a large population of patients who do not respond to monotherapies. Thus, it has become evident that targeting a single stage of the Cancer-Immunity Cycle is not sufficient and that combination therapies that target multiple complementary pathways will have a greater chance of capturing a large response pool. Because there is a diverse array of inhibitory and stimulatory pathways that affect T cell

activation, monotherapies allow for tumor escape through the upregulation of alternative pathways.

Combination therapies against multiple checkpoint molecules can de-activate multiple different T cell inhibitory pathways. Notably, anti-PD-1 mAbs have been co-administered with anti-CTLA-4 mAb in several clinical trials. Because these two pathways are non-redundant, blocking both can synergize T cell activation. The combination therapy significantly enhances the objective response rate to as high as 60%, but also increases the amount of adverse toxicities associated with widespread immune activation.[40] Importantly, the efficacy of combination checkpoint blockade in comparison to monotherapy is dependent on biomarker expression, such as PD-L1, in a patient's tumor and indicates the importance of using biomarkers to guide therapeutic interventions to reduce costs due to unnecessary combinations.[148] Additional combinations of inhibitory molecule blockades have also demonstrated improved efficacy. Doublets of anti-CTLA-4, anti-PD-L1, and an IDO inhibitor all enhanced the re-activation of tumor infiltrating lymphocytes in a murine melanoma model. These studies demonstrated that the combination therapies were effective by re-activating tumor infiltrating lymphocytes rather than inducing new T cell migration.[42] Thus, in tumors lacking T cell infiltration, combination therapies that also induce migration into the tumor may be more effective.

Combination therapies that link T cell stimulation with checkpoint blockade aim to intervene at the two major ways by which T cell activation is modulated. T cell stimulation can be mediated directly through the administration of co-stimulatory antibodies, or indirectly through a DC-based vaccine. Even when an anti-tumor T cell

population is present, however, activated T cells upregulate inhibitory molecules such as PD-1 and CTLA-4 in a homeostatic fashion. Tumor cells can also upregulate inhibitory ligands such as PD-L1, especially in response to T cell secretion of IFN-γ, which diminish the activity of these cells.

Checkpoint blockade has now been combined with almost every approach to T cell stimulation to maintain activation. In chronic viral infection, co-administration of antagonistic antibodies against PD-L1 and agonistic antibodies against 4-1BB were shown to enhance the expansion of viral-specific CD8+ T cells compared to monotherapy.[45] The combination therapy also impacted the kinetics of the T cell response, indicating that combination therapies may be used to modulate how quickly T cells are expanded against a certain antigen. In cancer immunotherapy, co-administration of anti-PD-1 and anti-4-1BB can enhance an anti-tumor response by modulating T cell phenotype and density of tumor infiltrating lymphocytes.[43,44] Checkpoint blockade has also been shown to increase the efficacy of peptide-pulsed DC vaccination, in this case blocking inhibitory molecules on DCs.[168] Various other approaches have shown synergy between the combination of anti-PD-1 checkpoint blockade and granulocyte macrophage colony-stimulating factor,[169] OX40 and CD27 co-stimulation with anti-PD-L1 checkpoint blockade,[5] and anti-OX40 co-stimulation and vaccination.[91]

Checkpoint blockade has also been combined with therapeutics that enhance tumor immunogenicity. Treatments that induce tumor cell death or increase mutational load, including oncolytic viruses, radiation, or chemotherapy, can enhance antigen presentation and activation to tumor-specific T cells.[170] However, the anti-tumor T cell response is often still limited by the expression of inhibitory molecules by both tumor and

immune cells. Radiation has been shown to synergize with anti-CTLA-4 checkpoint blockade, with local radiation leading to the regression of even distant metastases.[171] However, resistance to this dual treatment was shown to be mediated at least partially by tumor upregulation of PD-L1. In response to this observation, combination therapy comprised of radiation, anti-CTLA-4, and anti-PD-L1 was shown to increase the response rate and minimize tumor immune escape.[172] Checkpoint blockade also can increase the efficacy of oncolytic viruses that preferentially infect and lyses cancerous cells. A study with the oncolytic Newcastle Disease Virus demonstrated that its combination with anti-CTLA-4 could completely eliminate established murine melanoma and even lead to an improved abscopal effect.[173]

While combination therapies often involve the co-administration of multiple therapeutics, another approach to combination therapy is to develop a single therapeutic with multiple mechanisms of action. CD80, the ligand expressed by antigen presenting cells that induces T cell proliferation upon ligation with T cell expressed CD28, has additional binding partners. CD80 has also been shown to bind PD-L1 and plays a role in inducing apoptosis of activated CD8+ T cells.[174,175] This dual interaction has been taken advantage of in a soluble form of CD80 as a therapeutic.[176] This CD80-Fc fusion protein was shown to both neutralize the inhibitory PD-1/PD-L1 interaction while simultaneously stimulating T cells through CD28.

While combining stimulatory and inhibitory molecules in a single all-in-one therapeutic may be desirable from an engineering perspective, the immunological mechanisms behind their success may indicate that sequential delivery may be more effective. In one study, anti-PD-1 administration following anti-OX40 co-stimulation was

effective at delaying tumor growth, but not vise-versa or co-injection—it was necessary for the co-stimulation to first boost the T cell response to a state where checkpoint molecules played a role in inhibiting the response.[177] Thus, sequential delivery or biodegradable particles that can mediate this type of release may be beneficial.

Chapter 4. Dual Targeting Nanoparticle Stimulates the Immune System to Inhibit Tumor Growth[1]

4.1. Introduction

Cancer provokes an immune response to tumor-associated antigens. This can initiate the activation of tumor-specific T cells and result in tumor cell death in a process known as the cancer-immunity cycle.[28] Cancer thrives when there is a blockade in this cycle that allows cancer escape, and current immunotherapeutics aim to take down these barriers.[178]

Many emerging immunotherapies target activation of a tumor-specific T cell response.[68,70,179–181] T cell activation can be initiated by ligating two necessary signals—the T cell receptor with its cognate peptide-MHC, termed signal 1, and a costimulatory molecule, termed signal 2—using cellular or nanoparticle-based platforms. Different molecules can serve as co-stimulatory signals to T cells[37] such as B7-1/B7-2 or 4-1BBL which bind to CD28 and 4-1BB on the T cell, respectively. Signaling through 4-1BB in particular has gained interest in recent years for its ability to induce a more effective anti-tumor immune response than CD28 alone. Ligation of 4-1BB on T cells has been demonstrated to enhance cytotoxicity, prevent activation-induced cell death, and increase expansion and cytokine secretion preferentially in cytotoxic CD8+ T cells.[8,9,38] Despite the ability of 4-1BB activation to initiate and maintain more effective tumor-targeting CD8+ T cells, the tumor microenvironment often upregulates immunosuppressive surface

[1] Sections of this chapter are reprinted (adapted) with permission from "Kosmides, A., Sidhom, J.-W., Fraser, A., Bessell, C.A., and Schneck, J.P. Dual Targeting Nanoparticle Stimulates the Immune System to Inhibit Tumor Growth. *ACS Nano* **2017**, *11*, 5417-5429." Copyright 2017 American Chemical Society.

antigens and cytokines that diminish their cytotoxic effects.[27,32,182–185] Programmed death ligand 1 (PD-L1) is one such cell surface antigen, a checkpoint molecule upregulated on many cancers including melanoma, ovarian cancer, renal cell cancer, and non-small cell lung cancer.[186] Since a large proportion of tumor-infiltrating lymphocytes express PD-L1's receptor, programmed death 1 (PD-1),[180] expression of PD-L1 suppresses tumor-infiltrating lymphocyte effector functions.[187,188]

Monoclonal antibodies (mAb) that block checkpoint molecules such as PD-1, PD-L1, and CTLA-4 delay tumor growth in murine melanoma models,[168,187] and anti-PD-1 and anti-CTLA-4 mAb have been approved by the FDA with overall patient response rates of up to approximately 30%.[41,189–191] While expression of PD-L1 within the tumor microenvironment correlates with outcome, its overall expression cannot predict response indicating that there are other mechanisms at play.[192] Complete response rates in these patients have been as low as 5%[193] and demonstrates the need for additional development.

Recent studies have shown that checkpoint blockade efficacy can be further improved through combination with immunotherapies targeting diverse pathways. For example, a clinical trial combining PD-1 and CTLA-4 blockade nearly doubled survival time compared to anti-PD-1 mAb alone.[148] Additional studies in mice have shown similar results, with superior tumor control in mice treated with PD-1 antagonists in combination with CTLA-4 checkpoint blockade and 4-1BB co-stimulation.[42,43] However, these non-specific approaches require high concentrations of antibody, as high as 100-200 μg/dose in murine models, and a majority of patients experience significant off-target side effects, especially when treated with a combination of antibodies.[148] Improvements in

combinatorial immunotherapeutics are thus imperative to enable their use at safe and effective levels.

Here, we describe our development of a nanoparticle platform for combinatorial immunotherapeutics. These nanoparticles, termed immunoswitch particles, switch off the immunosuppressive PD-L1 pathway on tumor cells while simultaneously switching on the costimulatory 4-1BB pathway on CD8+ T cells. By physically constraining the antibodies on a nanoparticle platform, immunoswitch particles result in synergy between the two immunotherapies and are thus effective at low doses. *In vivo* we found that immunoswitch treatment had significant anti-tumor activity in both murine melanoma and colon cancer models and that the anti-tumor activity was seen with or without a model foreign antigen. The particles increase tumor-specific CD8+ T cell activation as compared to soluble antibody and do not require *a priori* selection of a cognate signal 1, allowing for activation of a robust polyclonal response. We show that immunoswitch particles mediate not only an increase in the number and specificity of tumor-specific CD8+ T cells, but also a change in the endogenous T cell receptor repertoire. This conserved change demonstrates that therapy recruits an altered set of T cell receptors for more effective recognition even when recognizing a defined tumor antigen. Immunoswitch particles represent a signal-switching approach to T cell-mediated cancer immunotherapy that simultaneously targets two stages of the cancer immunity cycle.

4.2. Methods

4.2.1 Mice

2C T cell receptor transgenic mice were maintained as heterozygotes by breeding on a C57/BL6 background. C57BL/6 and Nu/J mice were purchased from Jackson

Laboratories (Bar Harbor, ME, USA). All mice used were 6-8 weeks of age and were maintained according to Johns Hopkins University's Institutional Review Board.

4.2.2 Reagents and cell lines

B16-SIY was a gift from Tom Gajewski (The University of Chicago, IL, USA). B16-F10 and MC38-OVA were a gift from Charles Drake (Johns Hopkins University, MD, USA). RMA-S cells were a gift from Michael Edidin (Johns Hopkins University, MD, USA). Tumor cell lines have been authenticated by cognate T cell cytotoxicity.

Anti-PD-L1 monoclonal antibody clone 10F.9G2, anti-4-1BB clone 3H3, anti-CD3 clone 145.2C11, anti-CD28 clone 37.51, and their respective isotype controls were purchased from BioXCell (West Lebanon, NH). Fluorescently labeled monoclonal antibodies were purchased from BioLegend (San Diego, CA, USA). SIY peptide was purchased from GenScript (Piscataway, NJ).

4.2.3 Immunoswitch particle synthesis and characterization

Anti-biotin coated iron-dextran 50-100 nm particles were purchased from Miltenyi (Miltenyi Biotec; Auburn, CA). Anti-PD-L1 antibody clone 10F.9G2, anti-4-1BB clone 3H3, and their respective isotype controls were biotinylated using EZ-Link sulfo-NHS-biotin (Thermo Fisher Scientific; Waltham, MA) according to the manufacturer’s protocol. Particles and a 2-fold molar excess of the biotinylated antibodies of interest were combined and allowed to conjugate for 24 hours at 4˚C. Unbound antibody was removed by running the particles over an MS column (Miltenyi Biotec, Auburn, CA) and washing according to the manufacturer’s protocol.

Particle size was determined by nanoparticle tracking analysis using a Nanosight LM10. To characterize particle conjugation, a standard curve relating absorbance to

particle concentration was made using a Beckman Coulter AD340 plate reader and Nanosight LM10. Particles were then subsequently measured for absorbance to determine concentration, and all particles were brought to a concentration of 1.4 x 10^{12} particles/ml. The amount of specific antibody per particle was determined by staining the particles with fluorescently-labeled secondary antibodies against the antibody of interest. Excess antibody was removed by running the particles over an MS column (Miltenyi Biotec; Auburn, CA), and antibody concentration was measured by comparing particle fluorescence to a standard curve and correlating with the total bead concentration.

4.2.4 *In vitro* CD8+ T cell activation model

On day -8, primary splenocytes were isolated from naïve 2C transgenic mouse spleens through cell straining. Cells were treated with 4 mL of ACK lysis buffer for 1 minute to lyse red blood cells. CD8+ T cells were isolated by negative selection with the Miltenyi CD8a+ isolation kit IIa following the manufacturer's protocol (Miltenyi, Auburn, CA). Micro anti-CD3/anti-CD28 expander beads were synthesized on 4.5μm M-450 Epoxy Dynabeads (Life Technologies; Grand Island, NY) at a 1:1 molar protein ratio, following manufacturer's protocol. 2C CD8+ T cells were mixed with micro expander beads at a 1:1 ratio and cultured in RPMI supplemented with L-glutamine, non essential amino acids, vitamin solution, sodium pyruvate, β-mercaptoethanol, 10% FBS, ciproflaxin, and a cocktail of T cell growth factors. On day -4, additional T cell growth factors and expander beads were added at a 2:1 bead:cell ratio. On day -2, B16-SIY and B16-F10 cells were cultured in RPMI supplemented with L-glutamine, non essential amino acids, vitamin solution, sodium pyruvate, β-mercaptoethanol, 10% FBS, ciproflaxin, and 20 ng/ml recombinant murine IFN-γ (R&D Systems, Minneapolis, MN).

On day 0, B16-F10 and B16-SIY were harvested and washed three times to remove all IFN-γ, as confirmed by ELISA. 2C cells were also harvested, washed three times, and beads were removed with a magnet. Live CD8+ cells were isolated by density centrifugation using Ficoll-Paque PLUS (GE Healthcare Life Sciences; Pittsburgh, PA). Surface marker expression on both cell types was measured using a BD FacsCalibur flow cytometer and analyzed in FlowJo (TreeStar). For IFN-γ release studies, 2C cells and B16-SIY or B16-F10 cells were mixed at a 1:1 effector target ratio in the presence of particles or soluble antibody. The cells were incubated for 18 hours at 37˚, then supernatants were collected. IFN-γ was measured by ELISA using the ebioscience murine IFN-γ Ready-SET-Go! Kit (San Diego, CA). For cytotoxicity assay, 2C cells and B16-SIY cells were mixed at a 1:1 effector target ratio in the presence of immunoswitch particles and 100 µg/ml anti-Kb (clone 20.8.4) or respective isotype mAb. After four hours, supernatant was harvested and cytotoxicity was measured using a CytoTox-Glo Cytotoxicity Assay (Promega; Madison, WI) according to the manufacturer's protocol. Luminescence was read on a Tropix TR717 Microplate Luminometer.

4.2.5 B16 *in vivo* tumor growth experiments

Immunoswitch and isotype particles were synthesized and characterized as described above. Amount of antibody on the particles was quantified and a solution of equal concentration non-biotinylated antibody was diluted in PBS. Particles and soluble antibody were put to a concentration of 13µg/mL total antibody (6.3µg/mL anti-PD-L1 and 6.3µg/mL anti-4-1BB) and treated mice received 100 µl each.

C57BL/6 mice were injected with $1x10^6$ B16-SIY or $3x10^5$ B16-F10 cells subcutaneously on the right flank on day 0. For adoptive transfer experiments, CD8+

cells were harvested from naïve 2C splenocytes and stimulated with anti-CD3/anti-CD28 expander beads on days 0 and 4 as described above. On day 8, when all mice had palpable tumor, beads were isolated from CD8+ cells and live cells were isolated by density centrifugation using Ficoll-Paque PLUS (GE Healthcare Life Sciences; Pittsburgh, PA). $5x10^5$ 2C CD8+ cells were intravenously injected into all groups (except no treatment group). For all experiments, isotype particles, immunoswitch particles, or soluble antibody were injected intratumorally on days 8, 11, and 15. For intravenous studies, immunoswitch particles or soluble antibody were injected retro-orbitally on days 4, 8, 11, and 15. Beginning on day 4-8, tumors were measured every 2-3 days using digital calipers, and tumor size was computed by multiplying the longest dimension by the length of the perpendicular dimension. Mice were sacrificed when tumor area surpassed 200 mm^2.

4.2.6 B16-SIY tumor infiltrating lymphocyte analysis

Immunoswitch particles were synthesized and characterized as above. C57BL/6 (Jackson Labs; Bar Harbor, ME) mice were injected with $1x10^6$ B16-SIY cells subcutaneously on day 0. Immunoswitch particle treatment was administered intratumorally on days 8 and 11 (n=5/group).

On day 14, tumors were measured and peripheral blood, tumors, spleens, and tumor draining lymph nodes were isolated. Spleens and tumor draining lymph nodes were brought to a single cell suspension using a cell strainer, washed, then re-suspended in PBS. Tumors were coarsely sectioned using scissors then brought to a single cell suspension using a cell strainer. Tumor-infiltrating lymphocytes were isolated by density centrifugation using Ficoll-Paque PLUS (GE Healthcare Life Sciences; Pittsburgh, PA)

then washed three times and resuspended in PBS. Cell counts were taken using a hemocytometer.

For phenotypic analysis, isolated cells were stained with a fluorescently labeled with a live/dead stain (Thermo Fish Scientific; Waltham, MA), CD8 antibody (BioLegend; San Diego, CA), and biotinylated Kb-SIY dimer followed by fluorescently labeled streptavidin. Cells were run on a BD LSR II flow cytometer and analyzed using FlowJo (TreeStar). CD8 cell density was measured by multiplying the CD8 purity measured by flow cytometry by the total cell count, and dividing by the tumor volume (longest dimension squared and multiplied by the perpendicular dimension).
For functional analysis, an equivalent number of tumor-infiltrating lymphocytes from individual mice (n=3/group) were co-incubated with SIY pulsed RMA-S cells and anti-CD107 FITC. After 12 hours, GolgiStop/GolgiPlug (BD Biosciences, San Jose, CA) were added to solution. Six hours later, cells were stained for surface markers, then fixed and permeabilized with BD Cytofix/Cytoperm and stained with fluorescently labeled antibodies against intracellular cytokines according to the manufacturer's protocol. Labeled cells were read on an LSR II and analyzed with FlowJo.

4.2.7 T cell receptor sequencing analysis

In vivo tumor administration and treatment was identical to that in *4.2.6 B16-SIY tumor infiltrating lymphocyte analysis* (n=3/group). On day 14, tumor-infiltrating lymphocytes were isolated as above. Isolated cells were stained with a fluorescently labeled anti-CD8 mAb and live/dead stain (Thermo Fish Scientific; Waltham, MA) and CD8 antibody (BioLegend; San Diego, CA), and each sample was sorted based on

live/CD8+ cells. CD8+ cell samples were sent to Adaptive Biotechnologies for deep sequencing of the T cell receptor beta chain.

To assess V-beta usage analysis compared to a Kb-SIY response, spleens were isolated and pooled from 3 non-tumor bearing C57BL/6 mice. CD8+ T cells were isolated by negative selection as described above, and stimulated for 7 days with Kb-SIY/anti-CD28 nano-aAPC according to our previously published Enrichment + Expansion protocol.[194] On day 7, cells were fluorescently labeled with a live/dead stain, CD8 antibody, and Kb-SIY dimer as described above. Cells were sorted for live/CD8+/Kb-SIY+ and sent to Adaptive Biotechnologies for sequencing.

To assess characteristics of T cell receptor sequence repertoire, tsv files from adaptive were downloaded from their online portal, converted to excel files, and unproductive sequences were removed (only clones with amino acid CDR3 sequences were examined). All clones with the same amino acid sequence were combined and their net frequency was calculated. In order to examine the presence of clones in either immunoswitch or non-treated cohorts, only sequences with a contribution above 0.5% were examined. To examine the conservation of the response between animals in both cohorts, the top 85% of the CD8+ T cells response was examined and conservation of response was determined as the weighted average (by reads) an identical sequence makes up in the two samples being compared.

4.2.8 MC38-OVA *in vivo* tumor models

Immunoswitch particles and isotype particles were synthesized as described above. Amount of antibody on all particles was quantified by the methods described

above, and particles were put at a concentration of 13μg/mL total antibody. Treated mice received 100 μl particles/mouse.

C57BL/6 (Jackson Labs; Bar Harbor, ME) mice were injected with $1x10^6$ MC38-OVA cells subcutaneously on the right flank on day 0 and cages were randomly assigned to one of three groups: 1) no treatment, 2) isotype particles, or 3) immunoswitch particles (n=6 in isotype, n=10/other groups). On days 8, 11, 15, and 18 treated mice received intratumoral injections of immunoswitch or isotype particles and tumors were measured every 2-3 days. For re-inoculation studies, cured or age-matched C57BL/6 mice were injected with $1x10^6$ MC38-OVA cells subcutaneously on the opposite (left) flank on day 28. Beginning on day 8, tumors were measured every 2-3 days using digital calipers, and tumor size was computed by multiplying the longest dimension by the length of the perpendicular dimension. Mice were sacrificed when tumor area surpassed 200 mm^2.

4.2.9 Immunoswitch biodistribution

Immunoswitch particles were synthesized as described above. Immunoswitch particles and a mixture of soluble anti-4-1BB and anti-PD-L1 antibody were labeled with IRDye 680RD protein labeled kits from LI-COR Biosciences (Lincoln, Nebraska) according to the manufacturer's protocol.

Nu/J mice (Jackson Labs; Bar Harbor, ME) were injected with equal protein amounts of either IR-labeled soluble antibody or immunoswitch particles subcutaneously on the right flank (n=3/group). Dorsal, ventral, right, and left images of the mice were taken at 3, 24, 48, and 72 hours post injection. Only right images which show the injection area are shown. All images from any individual mouse had matched thresholding. Images were analyzed in ImageJ by defining a region of interest (ROI)

around the initial injection site which was then duplicated in all images. The mean gray value of each ROI was then measured in ImageJ. The mean grey value for an image of an individual mouse at time *T* was then normalized to the mean grey value at 3 hours using the following equation:

$$Mean\ gray\ value\ (normalized) = \frac{mean\ gray\ value_{t=T}}{mean\ gray\ value_{t=3}}$$

This data was then fit to a one phase exponential decay curve using the GraphPad non-linear regression analysis module (GraphPad Software; La Jolla, CA).

For organ analysis studies, C57BL/6 mice (n=3/group) were injected subcutaneously with B16-SIY cells on day 0. Eight days later, IR-labeled immunoswitch particles were injected intratumorally into half of the tumor-bearing mice. 48 hours after treatment, the tumor, spleen, tumor draining lymph node, and contralateral lymph node of each mouse were dissected and imaged on an IR imager. Images were analyzed in ImageJ by defining a region of interest (ROI) around each lymph node which was then duplicated in all images. Tumor and spleen ROI were defined for each image independently due to their difference in size and shape. The mean gray value of each ROI was then measured in ImageJ and was normalized to the maximum of the sensor.

4.2.10 Conjugation assay

2C CD8+ T cells were isolated from naïve splenoctyes and stimulated on days -8 and -4 with expander beads as previously described. B16-F10 cells were incubated with media supplemented with 20 ng/ml recombinant murine IFN-γ (R&D Systems; Minneapolis, MN) on day -2 for 48 hours.

On day 0, CD8 cells and B16-F10 cells were isolated from beads and IFN-γ respectively, as previously described. CD8 cell membranes were labeled with the PKH26

red fluorescent cell linker kit and B16-F10 cell membranes were labeled with the PKH67 green fluorescent cell linker kit (Sigma-Aldrich; St. Louis, MO) according to the manufacturer's protocol. Effector and target cells were co-incubated at a 1:1 ratio with immunoswitch or isotype particles. After 1 hour, cells were briefly vortexed and fixed. For flow cytometry experiments, cells were fixed in 0.5% paraformaldehyde for 20 min at room temperature. Cells were then read on a BD FacsCalibur. Conjugate formation was measured by first gating on all CD8+ T cells (*i.e.* red cells), and then on those also bound to B16-F10 cells (*i.e.* also expressing green) using FlowJo (TreeStar). Flow cytometry experiments were repeated 3 independent times. For confocal microscopy experiments, cells were fixed in 2% paraformaldehyde for 20 min at room temperature. Cells were then read on a Zeiss LSM510-Meta laser scanning confocal microscope at 100x magnification. Two to three non-overlapping images were taken per experiment, and the experiment was repeated three independent times. Conjugate formation was determined manually by observing red/green overlap/contact using ImageJ. Each image was taken as an independent data point. For both flow cytometry and confocal microscopy studies, conjugation was measured as the percent of CD8 cells forming conjugates with B16-F10 cells divided by the total number of CD8 cells.

4.2.11 *In vivo* killing assay

C57BL/6 mice, five per group, were injected with MC38-OVA tumor and treated with immunoswitch particles as in *4.2.8 MC38-OVA in vivo tumor models*. On day 28 post tumor inoculation, immunoswitch-treated mice were categorized by their response status—"cured" meaning no palpable tumor, or "not cured" meaning palpable tumor. Splenocytes were harvested from naïve C57BL/6 mice and stained with a high or low

level of CellTrace Violet (Thermo Fisher Scientific) according to the manufacturer's protocol. Cells with a high level of CellTrace Violet were pulsed with the OVA peptide and cells with a low level of CellTrace Violet were pulsed with a non-cognate SIY peptide—1 μg of peptide was added per 10^7 cells and incubated for 1 hour at 37˚C. Cell samples were separately washed then mixed at a 1:1 ratio with a total of 10^8 cells/ml. Observation of two separate CellTrace Violet peaks was confirmed by flow cytometry. 100 μl of the cell mixture was injected into each cured, not cured, and naïve mouse by retro-orbital injection.

Twenty-four hours post injection, mice were sacrificed and splenocytes harvested. Lymphocytes were isolated by density centrifugation with Lympholyte Cell Separation Media (Cedarlane; Burlington, Ontario, Canada). Lymphocytes were read on flow cytometry and number of low and high-stained CellTrace Violet cells were quantified.

4.2.11 Statistics

Information on statistical tests are present in all figure legends. One and two-way ANOVA were used when making multiple comparisons. Bonferroni posttests were performed when comparing all groups, and Dunnett's posttests were performed when the hypotheses being tested involved comparison against a single group. One-tailed and two-tailed t-tests were used when comparing two groups, as indicated in figure legends. All datasets were assumed to fit a normal distribution, and all graphs show mean and error bars represent SEM. All *n* values are present within figure legends. *In vivo* tumor treatment studies were repeated in two independent experiments to ensure adequate sample size and reproducibility. Mice with outlier tumor size before the beginning of

treatment were removed from the studies. Randomization was performed by cage in all animal studies. All statistical analysis was performed using GraphPad Prism software.

4.3 Results

4.3.1 Immunoswitch particles activate T cells *in vitro*

Immunoswitch particles link checkpoint blockade with T cell costimulation on a single nanoparticle platform. The particles are synthesized by conjugating 80 nm iron-dextran nanoparticles with a 1:1 molar ratio (**Figure 4-1**) of agonistic antibodies against 4-1BB (a costimulatory receptor found on the effector T cells) and antagonistic antibodies against PD-L1 (found on the cancer cells) (**Figure 4-2A – inset**). The hypothesized mechanism of action of the immunoswitch particles is shown in a schematic in **Figure 4-2A** – the particles target tumor cells expressing PD-L1 and simultaneously block access to PD-1 on T cells. Their costimulatory antibody binds to 4-1BB on CD8+ T cells, targeting them to the tumor cells and thus switching a negative signal into a co-stimulatory signal. The clonotypic T cell receptor on the CD8+ T cell receives cognate signal 1 stimulation from the tumor cell itself.

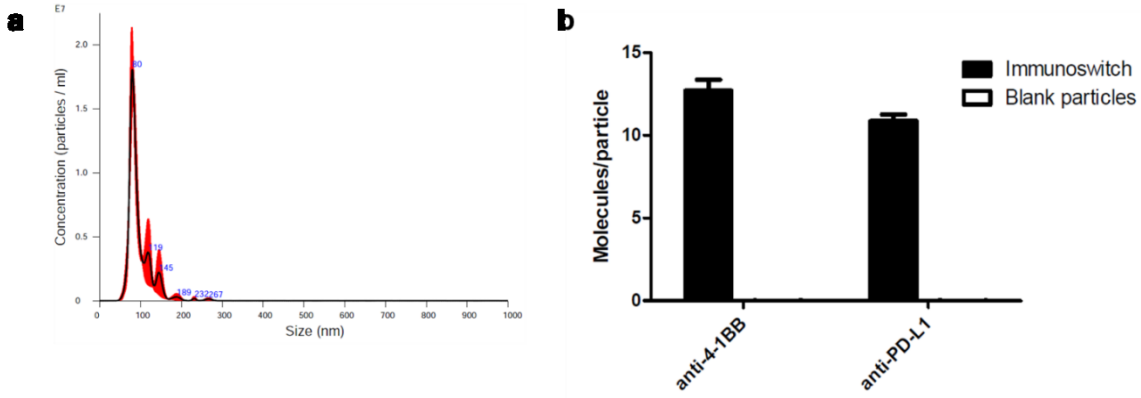

Figure 4-1. *Immunoswitch particles combine anti-4-1BB and anti-PD-L1 antibodies on a nanoparticle platform. (a) Iron-dextran nanoparticle platform is 80nm in diameter. Unconjugated iron-dextran nanoparticle size was measured by nanoparticle tracking analysis. Mean (black) and SEM (red) of 3 separate captures of a single sample is shown. The mode of the dataset is 81.1 +/- 1.6 nm and the mean of the dataset is 96.0 +/- 1.9 nm. (b) Number of anti-4-1BB and anti-PD-L1 molecules per particle, as measured by fluorescently labeled secondary antibody. Mean +/- SEM is shown, averaged across 3 independent experiments. No significant differences in antibody level per each particle type, as measured by two-way ANOVA with Bonferroni posttest.*

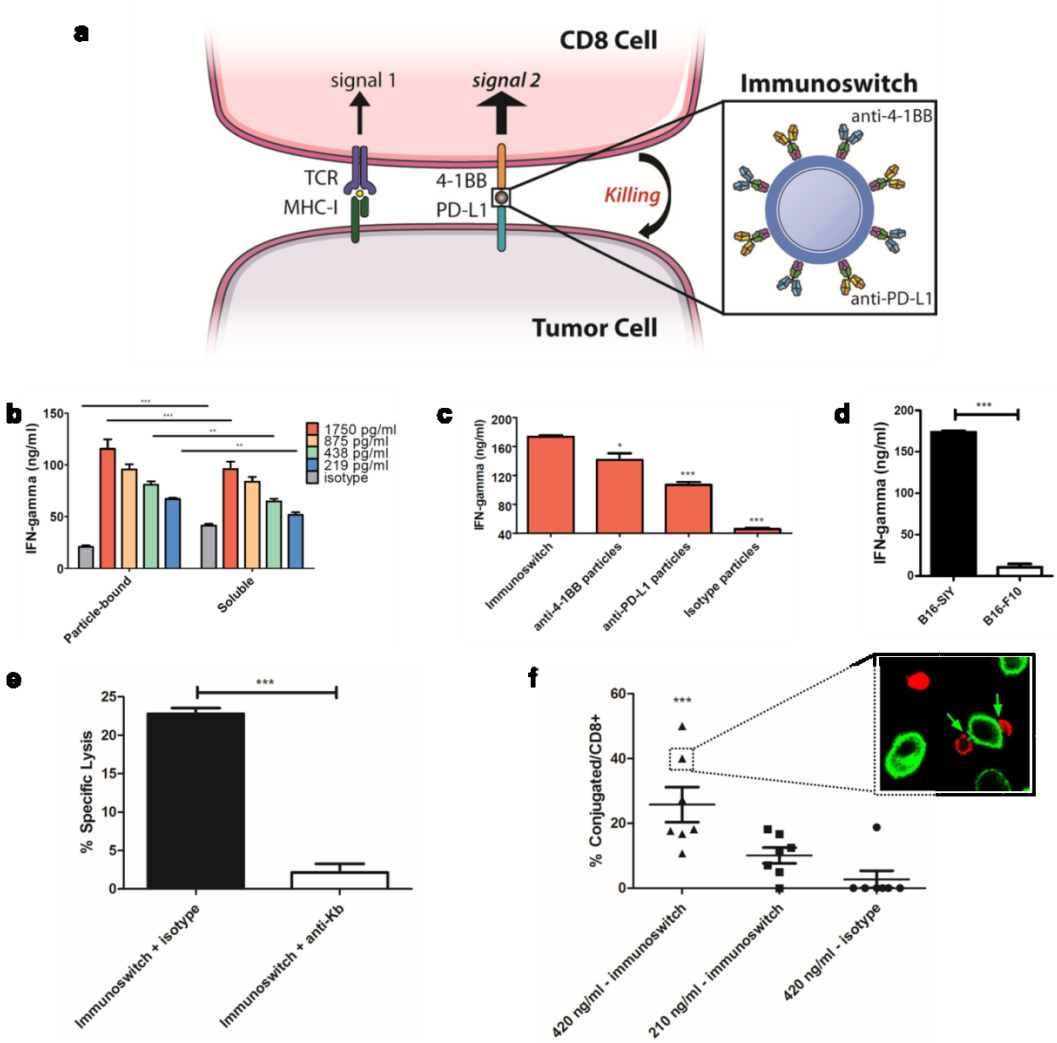

Figure 4-2. *Immunoswitch particles link PD-L1 checkpoint blockade with 4-1BB co-stimulation. (a) Schematic showing immunoswitch particle interaction with CD8+ T cell and cognate target cell. Inset – immunoswitch particles are synthesized by conjugating anti-4-1BB and anti-PD-L1 monoclonal antibodies to the surface of 80 nm particles. (b) IFN-γ secretion from PD-1^{hi} 2C CD8 cells co-incubated with PD-L1^{hi} cognate B16-SIY cells and immunoswitch particles or soluble antibody. Concentrations refer to total antibody in culture. Significance measured by two-way ANOVA with Bonferroni posttest ($p=0.0064$, $F_{1,30}=8.607$ treatment variation; $p<0.0001$, $F_{4,30}=79.76$ concentration variation). (c) IFN-γ secretion from PD-1^{hi} CD8 cells co-incubated with PD-L1^{hi} B16-SIY and 9 μg/ml of the indicated particle type. Significance measured by one-way ANOVA with Dunnett's posttest. Comparisons to immunoswitch particles are shown. (d) IFN-γ secretion from PD-1^{hi} 2C CD8 cells co-incubated with PD-L1^{hi} cognate B16-SIY cells or non-cognate B16-F10 cells and immunoswitch particles. Significant was measured by two-tailed t-test ($p<0.0001$). Mean +/- SEM of 3 samples is shown for (b-d). (e) Percent specific lysis of B16-SIY cells by 2C CD8+ T cells when co-incubated for 4 hours at a 1:1 effector-target ratio in the presence of immunoswitch particles and 100 μg/ml anti-Kb blocking mAb or isotype control. Significance was measured by two-tailed t-test. (f) PD-1^{hi} 2C CD8 cells and PD-L1^{hi} B16-F10 cells were labeled with a red and green membrane dye, respectively. Percent of CD8 cells forming conjugates were counted. Each data point represents an independent image taken across three independent experiments. 50 ng of immunoswitch particles significantly increased conjugation rate over isotype particles as measured by one-way ANOVA ($p=0.0013$) with Dunnett's posttest. Arrows show conjugate formation. Cell and antibody images in (a) are adapted under a Creative Commons License from Servier Medical Art (http://www.servier.com/Powerpoint-image-bank). (***$p<0.001$, **$p<0.01$, *$p<0.05$)*

Immunoswitch particle activity was analyzed in vitro using a model of repetitive antigen stimulation known to mimic the tumor microenvironment.[195] 2C T cell receptor transgenic CD8+ T cells, specific for the SIY peptide presented in the context of the H-2 Kb MHC, were repetitively stimulated with anti-CD3/anti-CD28 expander beads. Murine melanoma cells—either non-cognate B16-F10 cells or cognate B16-SIY cells, a transfected tumor cell line derived from B16-F10 which expresses the cognate Kb-SIY antigen—were treated with 20 ng/ml IFN-γ. These treatments resulted in upregulation of PD-1 and 4-1BB expression on the CD8+ T cells (**Figure 4-3A**) and upregulation of PD-L1, but not PD-L2, on the murine melanoma cells (**Figure 4-3B,C**). Treatment with either soluble anti-4-1BB or anti-PD-L1 mAb increased CD8+ T cell activation in a dose dependent fashion, demonstrating the ability to study immunoswitch nanoparticle activity in this model (**Figure 4-4**).

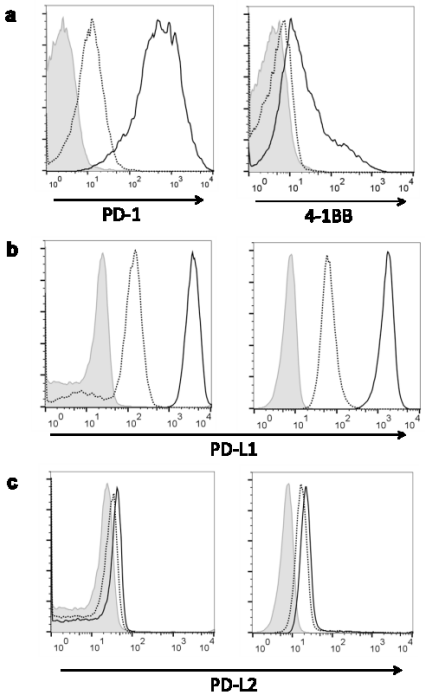

Figure 4-3. *In vitro model results in upregulated inhibitory molecules on CD8 and B16 cells. (a) Flow cytometry plots of PD-1 and 4-1BB expression on CD8 cells on day 0 (dotted) and day 8 after expander bead stimulation on days 0 and 4 (solid), as compared with isotype (grey, filled). B16 cells were cultured in media supplemented with 20 ng/ml IFN-γ for 48 hours, and PD-L1 and PD-L2 expression was assessed by flow cytometry. Flow cytometry plot of PD-L1 (b) and PD-L2 (c) expression by B16-SIY (left) and B16-F10 (right) cells on day 0 (dotted) and 48 hours after IFN-γ treatment (solid), as compared with isotype (grey). B16-SIY and B16-F10 upregulate PD-L1 but not PD-L2 in response to IFN-γ incubation.*

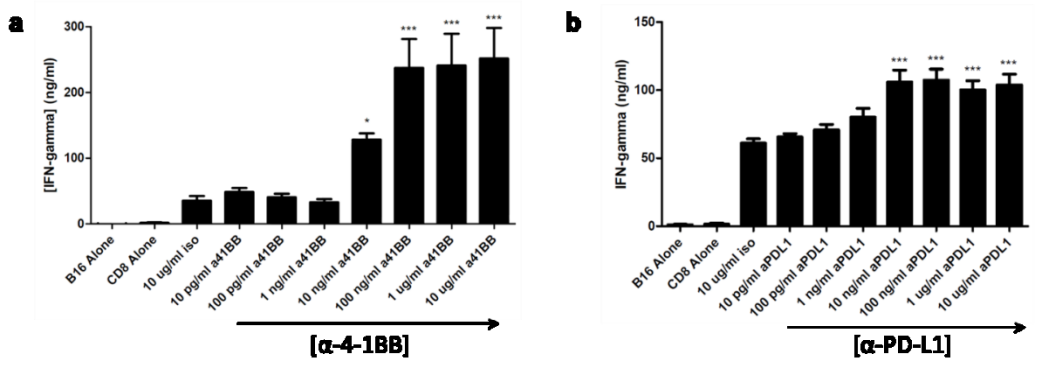

Figure 4-4. *Soluble anti-4-1BB and anti-PD-L1 mAb increase T cell activation when co-incubated with target cells. PD-1^{hi} 2C CD8 cells and PD-L1^{hi} cognate B16-SIY cells were co-incubated at a 1:1 ratio in the presence of titrating amounts of soluble anti-4-1BB (a) or anti-PD-L1 (b) antibody. IFN-γ secretion by CD8 cells was measured by ELISA after 18 hours. Both antibodies induced a significant increase in the level of IFN-γ secretion as compared to isotype at concentrations at and above 10 ng/ml. Mean +/- SEM are shown of three replicates. Significance measured by one-way ANOVA with Dunnett's posttest, comparing each condition to isotype. (*p<0.05, ***p<0.001)*

PD-1^{hi} CD8+ T cells and PD-L1^{hi} B16-SIY cells were co-incubated with immunoswitch particles, and T cell stimulation was measured by IFN-γ secretion. Compared to cultures treated with isotype particles, there was maximally over a 6-fold increase in IFN-γ secretion by immunoswitch particle-treated cultures (**Figure 4-2B**). As expected, cultures treated with soluble anti-4-1BB and anti-PD-L1 also increased IFN-γ secretion, although only a 2 to 3-fold increase over isotype antibody controls. This data shows that the antibodies maintain their functionality even when constrained on nanoparticles and in fact potentially have increased T cell stimulatory activity.

To investigate the requirement for both antibodies on the surface of the nanoparticle, we compared CD8+ T cell activation in response to co-incubation with immunoswitch particles *versus* anti-4-1BB mAb only or anti-PD-L1 mAb only particles. The greatest IFN-γ secretion, maximally 173±3 ng, was measured in immunoswitch particle treated cultures (**Figure 4-2C**). In contrast, only 141±18 ng and 107±8 ng of IFN-γ was produced by cultures treated with anti-4-1BB and anti-PD-L1 only particles, respectively.

4.3.2 Enhanced T cell-tumor cell conjugation

To understand the mechanism of immunoswitch particle activity, we studied their cellular interactions. We sought to investigate both their ability to mediate CD8+ T cell-tumor cell conjugation as well as requirements for cognate peptide-MHC stimulation.

We investigated the requirement for peptide-MHC recognition by comparing 2C CD8+ T cell activation when co-incubated with immunoswitch particles and cognate B16-SIY or non-cognate B16-F10 tumor cells. In the presence of B16-SIY cells, immunoswitch particles resulted in robust IFN-γ secretion (**Figure 4-2D**). There was no IFN-γ secretion in response to immunoswitch particles when 2C CD8+ T cells were

stimulated with B16-F10 tumor cells lacking the cognate antigen. We further investigated the signal 1 dependence of immunoswitch activation by measuring cytotoxicity of cognate tumor cells *in vitro*. 2C CD8+ T cells were co-incubated with cognate B16-SIY cells, immunoswitch particles, and an anti-Kb mAb to block the signal 1 peptide-MHC interaction. At a 1:1 effector-target cell ratio, immunoswitch particles resulted in 22.8% specific lysis of B16-SIY cells (**Figure 4-2E**). This was reduced to only 2.16% when an anti-Kb mAb was included during the co-incubation. Immunoswitch particle stimulation and cytotoxicity is dependent on the CD8+ T cell receiving a cognate signal 1 from the tumor cell itself.

In addition to requiring a cognate tumor cell for CD8+ T cell activation, we also investigated the hypothesis that immunoswitch particles increase effector-target cell conjugation. 2C CD8+ T cells and B16-F10 melanoma cells were labeled with a red and green membrane dye, respectively. Non-cognate B16-F10 cells were chosen to eliminate conjugate formation mediated by the T cell receptor-peptide-MHC interaction. Labeled 2C CD8+ T cells and B16-F10 cells were co-incubated in the presence of immunoswitch or isotype particles. After 1 hour, cells were fixed and conjugate formation was measured by confocal microscopy or flow cytometry. Confocal microscopy showed an increase in effector-target cell conjugation mediated by immunoswitch particles (**Figure 4-2F, Figure 4-5A**). At a 420 ng/ml total antibody dose, immunoswitch particles resulted in significantly higher conjugate formation than isotype particles, nearing 30% of CD8+ T cells conjugated to tumor targets. Isotype particles resulted in minimal conjugate formation, indicating that PD-1/PD-L1 expression plays little to no role in effector-target cell conjugation in this system. These results of confocal

microscopy were validated by a flow cytometry-based conjugation assay. 420 ng/ml of immunoswitch particles resulted in significantly greater effector-target cell conjugation as compared to isotype (**Figure 4-5B**). These results indicate that immunoswitch particles increase conjugation by physically linking effector and target cells in an antigen independent fashion.

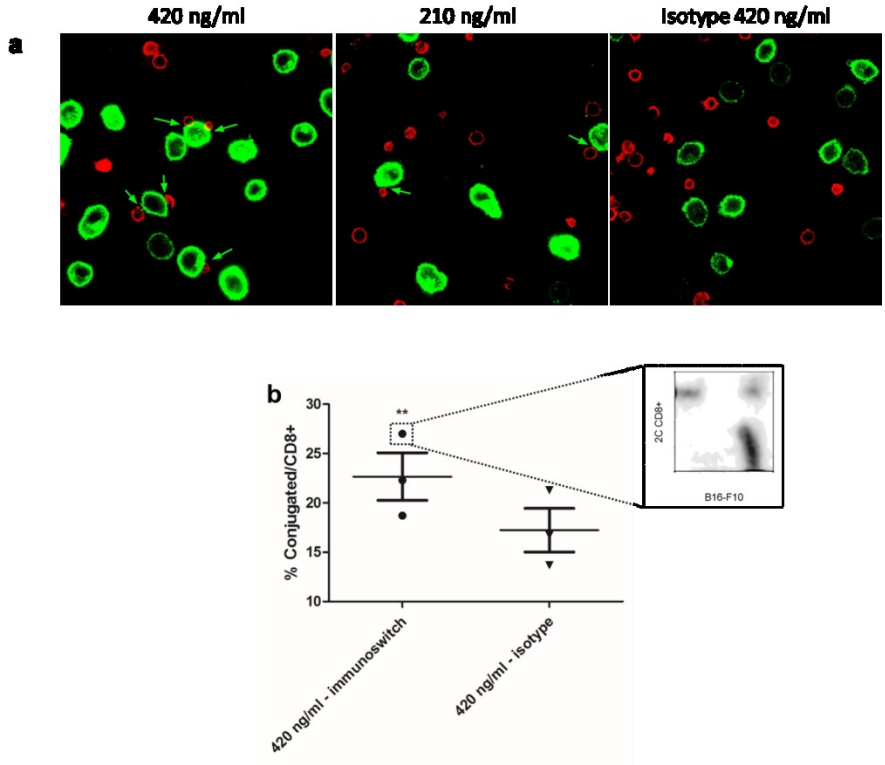

Figure 4-5. *Immunoswitch particles increase effector-target cell conjugation. (a) Representative confocal images of 2C CD8+ T cells (red) and B16-F10 cells (green) in the presence of immunoswitch or isotype particles. Arrows show conjugate formation. (b) Conjugate formation was measured by gating on double red and green positive cells by flow cytometry. Each data point represents an independent experiment. 50 ng of immunoswitch particles significantly increased conjugation rate as measured by two-tailed paired t-test (p=0.0016).*

4.3.3 Immunoswitch particles inhibit tumor growth *in vivo*

We investigated the efficacy of immunoswitch nanoparticle treatment in several *in vivo* models. Our first model, based on our *in vitro* system, was an adoptive transfer of

the repetitively stimulated PD-1^{hi} tumor-specific 2C CD8+ T cells into mice with pre-established B16-SIY melanoma tumors, followed at intervals by immunoswitch particles. Adoptively transferred cells were used as a model of exhausted tumor-specific cells that would likely be present in a patient's tumor microenvironment prior to treatment. C57BL/6 mice were injected with 1x10^6 B16-SIY tumor cells on day 0, and 5x10^5 PD-1^{hi} 2C CD8+ T cells were adoptively transferred on day 8 (**Figure 4-6A, schematic**). T cell recipients were treated with immunoswitch particles on days 8, 11 and 15, or with various controls: 1) PD-1^{hi} 2C CD8+ T cells alone, 2) PD-1^{hi} 2C CD8+ T cells + isotype-conjugated particles, or 3) PD-1^{hi} 2C CD8+ T cells + soluble anti-4-1BB mAb + soluble anti-PD-L1 mAb. All treatment groups received a total of 1.3 ug of antibody per mouse per treatment intratumorally, approximately 10-100-fold less than the amount typically used for systemic treatment.[42,43,45]

Immunoswitch treatment significantly delayed tumor growth compared to all other groups ($p<0.001$). Adoptive cell transfer alone, isotype particles, and soluble antibody did not result in significant slowing of tumor growth compared to no treatment (**Figure 4-6B**). This indicates that the particles themselves do not have any effect due to the intratumoral injection and that conjugating the antibodies to a rigid nanoparticle is necessary for their anti-tumor activity. Additionally, immunoswitch particles were the only treatment to significantly extend survival (**Figure 4-6C**)—mice died later or not at all by day 31. Soluble antibody also extended survival in a small number of mice, although this change was not statistically significant.

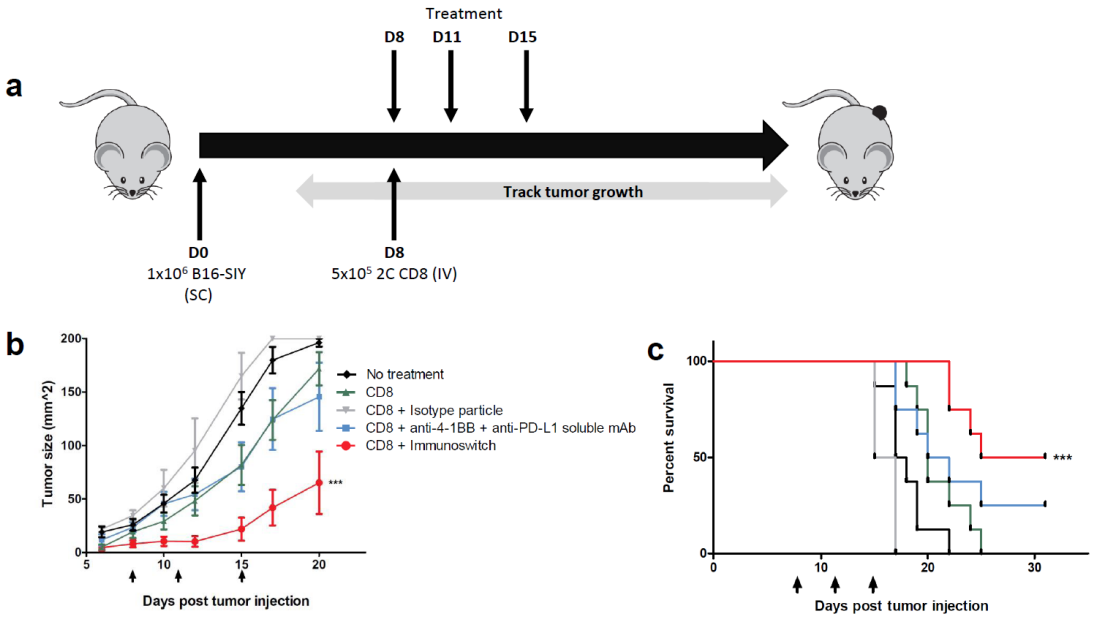

Figure 4-6. *Immunoswitch particles inhibits tumor growth in vivo. (a) Schematic showing our* in vivo *model. C57BL/6 mice (n=4 isotype, n=8 all other groups) were injected with 1x10^6 B16-SIY cells subcutaneously (SC) on day 0. 2C CD8 cells were isolated on day 0, stimulated with anti-CD3/anti-CD28 expander beads on days 0 and 4 as previously described,[25] isolated from the beads and injected intravenously (IV) on day 8. Particle and antibody treatments were given intratumorally (IT) on days 8, 11, and 15. (b) Tumor growth curves show only immunoswitch treatment significantly delayed tumor growth as compared to no treatment and all other controls, past day 15. Black arrows indicate treatment days. Significance measured by two-way ANOVA with Bonferroni posttest ($p<0.001$). (c) Immunoswitch treatment significantly extended survival as compared to no treatment. Significance measured by log-rank test ($p=0.0002$). Combined results from two independent experiments are shown. (***$p<0.001$)*

In our second *in vivo* model, we analyzed immunoswitch particle activity *in vivo* in the absence of adoptively transferred T cells in the pre-established B16-SIY model (**Figure 4-7A**, **schematic**). Controls included no treatment or animals co-injected with a mixture of single-coated anti-4-1BB only and anti-PD-L1 only particles. This second control was included to investigate the importance of effector-target cell conjugation seen *in vitro* on *in vivo* activity. If immobilizing the antibodies on a rigid nanoparticle platform is sufficient for activity, we would expect both immunoswitch particles and separately conjugated nanoparticles to perform equivalently.

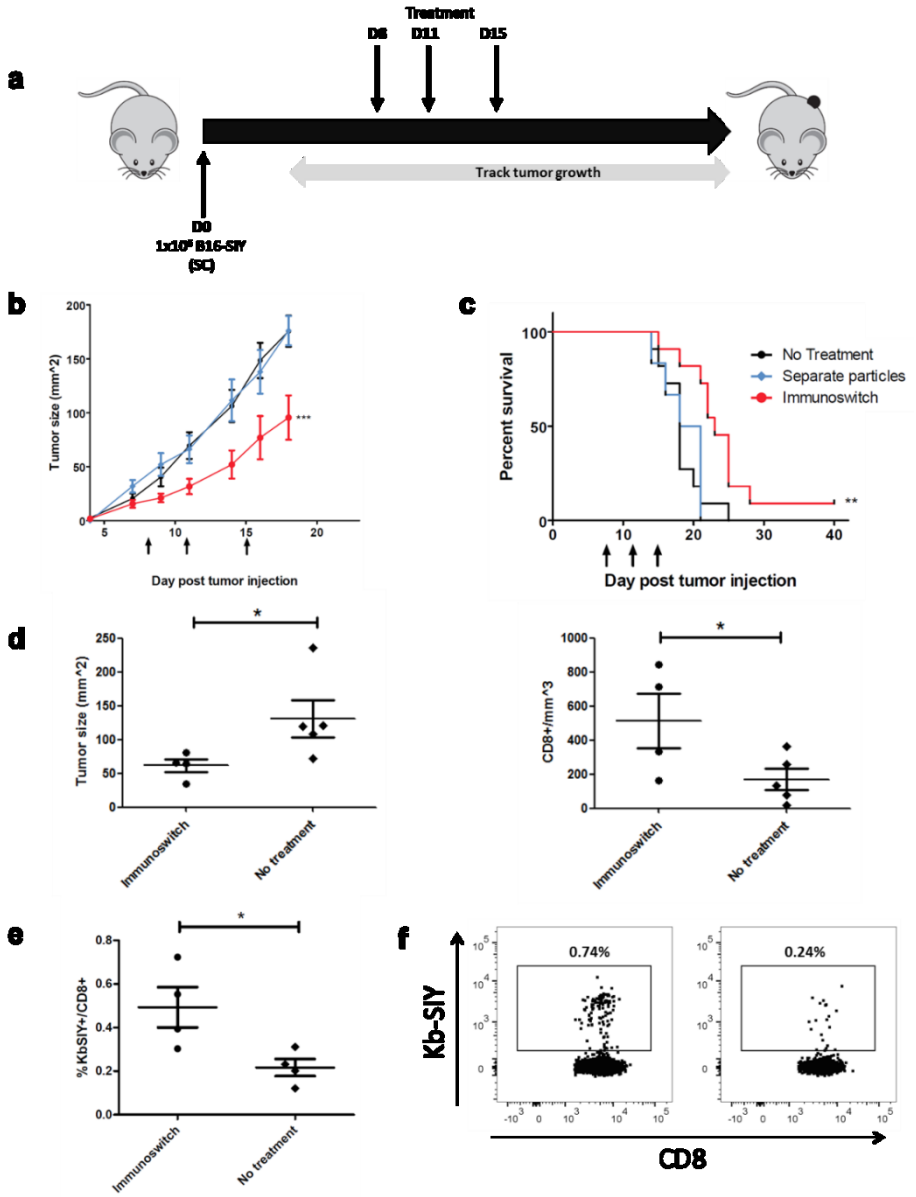

Figure 4-7. *Immunoswitch particles delay tumor growth in the absence of adoptively transferred cells. (a) C57BL/6 mice (n=6 separate particle treatment, n=11/other groups) were injected with B16-SIY cells SC on day 0. Treatment - either immunoswitch particles or a co-injection of anti-4-1BB and anti-PD-L1 particles - was injected IT on days 8, 11, and 15. No adoptive transfer of tumor-specific cells was given. (b) Immunoswitch particles, but not separate anti-4-1BB and anti-PD-L1 mAb particles, delayed tumor growth compared to no treatment at all time points past day 11. Arrows indicate treatment days. Significance was measured by two-way ANOVA with Bonferroni posttest (p=0.007). (c) Only immunoswitch particle treatment significantly extended survival. Significance was measured by log-rank test (p=0.0066). Results from two independent experiments are combined for (a-c). (d) C57BL/6 mice (n=5/group) were injected with B16-SIY cells as above, and half were treated with immunoswitch particles IT on days 8 and 11. On day 14 tumor-infiltrating lymphocytes and tumor draining lymph nodes were harvested and analyzed. The non-treated group had significantly larger tumors (p=0.034) and a lower CD8+ T cell density (p=0.032) within the tumor on day 14. Significance was measured by two-tailed t-test. (e) CD8+ cells within the tumor draining lymph nodes of immunoswitch-treated mice had higher Kb-SIY (expressed by tumor) specificity. Significance was measured by two-tailed t-test (p=0.033). (f) Representative flow plots showing Kb-SIY specificity of CD8+ T cells from tumor draining lymph nodes of immunoswitch (left) or non-treated (right) mice. (***p<0.001, **p<0.01, *p<0.05)*

Only immunoswitch treated animals had delayed tumor growth and extended survival compared to all other groups (**Figure 4-7B,C**). By day 18, non-treated and separate particle-treated mice had an average tumor size of approximately 176 mm^2, whereas immunoswitch particle-treated mice had an average tumor size of nearly half, approximately 95 mm^2. This indicates that immunoswitch particles stimulate the polyclonal endogenous repertoire of CD8+ T cells, and that both antibodies must be presented by the same nanoparticle for *in vivo* activity.

4.3.4 Endogenous T cell activation

To mechanistically study how immunoswitch particles activate an immune response, we analyzed tumor-infiltrating lymphocytes and tumor draining lymph nodes of immunoswitch treated animals. C57BL/6 mice were injected with B16-SIY tumor on day 0. Immunoswitch particles were administered days 8 and 11 and tumors and tumor draining lymph nodes were harvested and analyzed on day 14.

As expected, immunoswitch treated mice had significantly smaller tumors (**Figure 4-7D**). The density of CD8+ T cells within the tumor-infiltrating lymphocytes compartment more than doubled in the immunoswitch treated group compared to no treatment (**Figure 4-7D**), while CD4+ T cell density remained unchanged (data not shown). The impact of immunoswitch treatment on antigen-specific T cells was analyzed by determining the Kb-SIY-specific CD8+ T cell response to the B16-SIY tumors. There were approximately double the percentage of Kb-SIY positive CD8+ T cells within the tumor draining lymph node of immunoswitch treated animals compared to non-treated animals—0.49±0.2% and 0.22±0.1%, respectively (**Figure 4-7E,F**), while no difference

in Kb-SIY positive CD8+ T cells were seen within the spleen, peripheral blood (**Figure 4-8**), or tumor-infiltrating lymphocytes (**Figure 4-9A**).

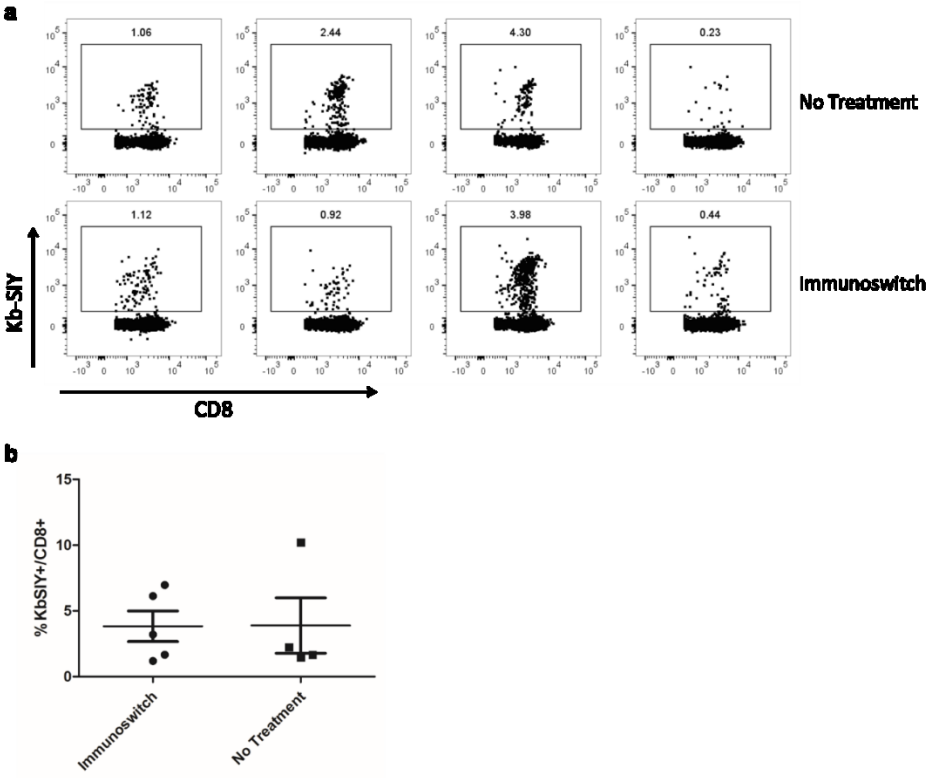

Figure 4-8. *Tumor specific CD8+ T cells are present in the periphery at the same levels in treated and non-treated mice. (a) Flow plots of Kb-SIY staining on CD8+ T cells from the spleens of immunoswitch-treated and non-treated mice. (b) Percent of Kb-SIY+/CD8+ T cells in the peripheral blood of immunoswitch-treated and non-treated mice.*

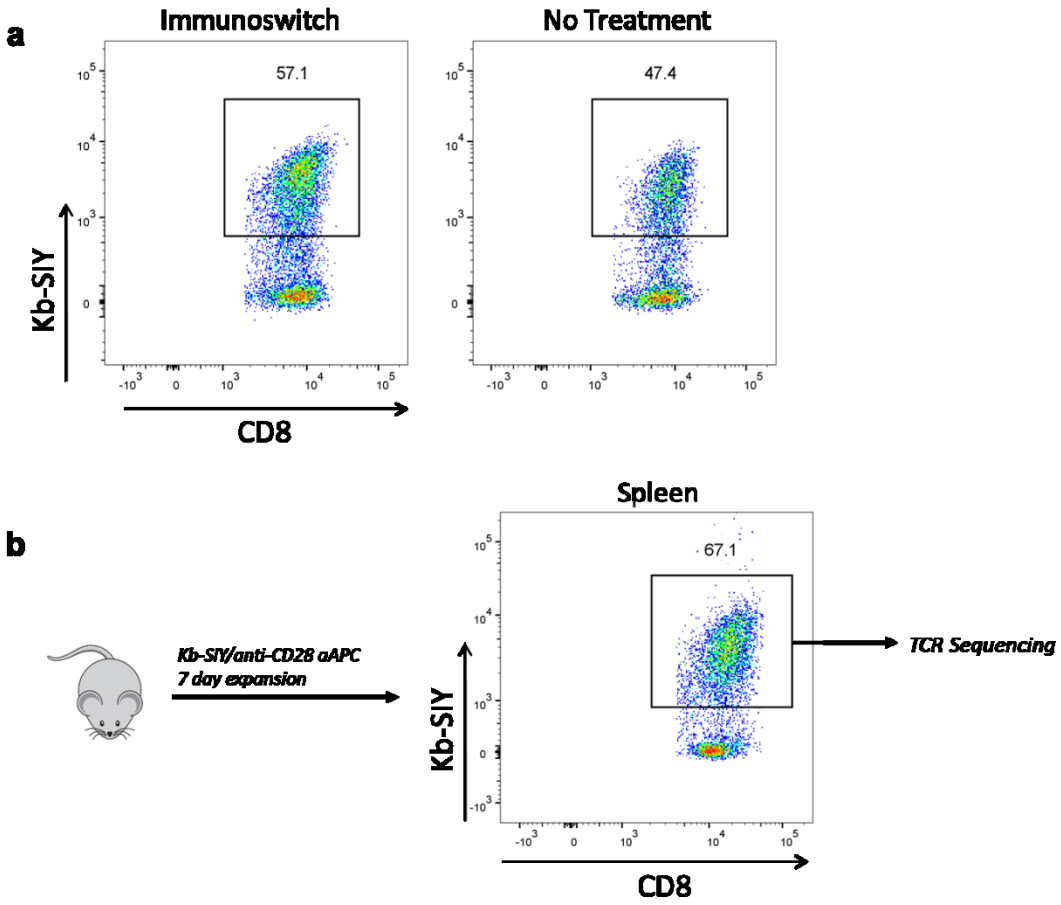

Figure 4-9. *A significant portion of the anti-tumor response in the presence and absence of immunoswitch treatment is Kb-SIY specific. (a) Representative flow plots of Kb-SIY staining on CD8+ T cells from the TILs of immunoswitch-treated and non-treated mice. (b) Expansion protocol used to sequence the Kb-SIY specific CD8+ T cell response. Splenocytes from non-tumor bearing C57BL/6 mice were expanded with Kb-SIY/anti-CD28 aAPC for 7 days. Kb-SIY+ cells were sorted and sequenced after 7 days.*

Since immunoswitch treated mice have significantly delayed tumor growth, we hypothesized that treatment may increase the functionality of tumor infiltrating lymphocytes. To study the functionality of Kb-SIY+ CD8+ tumor-infiltrating lymphocytes following immunoswitch treatment, mice were treated and tumor-infiltrating lymphocytes harvested on day 14 as above. Tumor-infiltrating lymphocytes were re-stimulated *in vitro* with SIY pulsed RMA-S cells and cytokine and CD107 production analyzed.

Immunoswitch treated animals had more than double the percentage of CD8+ tumor-infiltrating lymphocytes expressing CD107, a degranulation marker and indicator of the ability of T cells to lyse target tumor cells (**Figure 4-10A**). CD8+ tumor-infiltrating lymphocytes also produced more IFN-γ compared to tumor-infiltrating lymphocytes from non-treated mice (**Figure 4-10B,C**). This was seen by both an increase in the percent of IFN-γ+ cells (**Figure 4-10B**) and a 38% increase in the mean fluorescence intensity of IFN-γ+ cells, indicating greater per-cell production (**Figure 4-10C**). Together, these data indicate that immunoswitch particles stimulate an anti-tumor CD8+ T cell response by increasing their density, local tumor specificity, and *in vivo* functionality, consistent with findings that anti-4-1BB mAb primarily targets CD8+ T cells.[38]

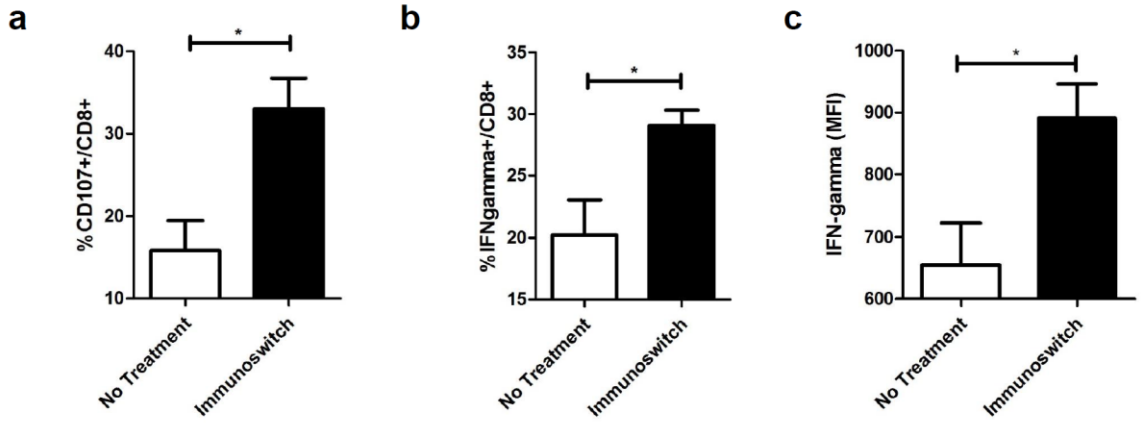

Figure 4-10. *Tumor-specific CD8+ tumor-infiltrating lymphocytes of immunoswitch treated mice have increased functionality. (a) C57BL/6 mice (n=3/group) were injected with B16-SIY cells SC on day 0. Immunoswitch particles were injected IT on days 8 and 11. On day 14 tumor-infiltrating lymphocytes were harvested and re-stimulated with SIY pulsed RMA-S cells. Intracellular cytokine staining indicated an increased frequency of CD107 producing (a) and IFN-γ producing (b) CD8+ T cells following immunoswitch treatment. The mean fluorescence intensity (MFI) of IFN-γ+ cells was increased in treated mice. Significance was measured by one-tailed t-test (*p<0.05).*

4.3.5 Changes in the T cell receptor repertoire

To gain a deeper understanding of the mechanism of action of immunoswitch particles, we analyzed the T cell receptor repertoire of the tumor infiltrating CD8+ T cells. As described above, tumors were harvested on day 14 and tumor-infiltrating CD8+ T cells were sorted and T cell receptors sequenced to determine amino acid sequence of the CDR3 region of the T cell receptor beta chains (T cell receptor V-beta). V-beta usage by the tumor-infiltrating lymphocytes of each treatment group was compared to usage in a naïve C57BL/6 mouse and to a Kb-SIY-specific response obtained by using a previously established CD8+ T cell activation protocol[194] to expand Kb-SIY-specific cells from splenocytes of naïve C57BL/6 mice. After a 7 day stimulation, Kb-SIY+ CD8+ T cells were sorted and sequenced (**Figure 4-9B**). As seen previously by Kb-SIY peptide-MHC staining of the tumor-infiltrating lymphocytes, the primary response of both immunoswitch-treated and tumor-bearing non-treated mice was dominated by V-beta 13 which is characteristic of a Kb-SIY response (

Figure 4-11**A**).

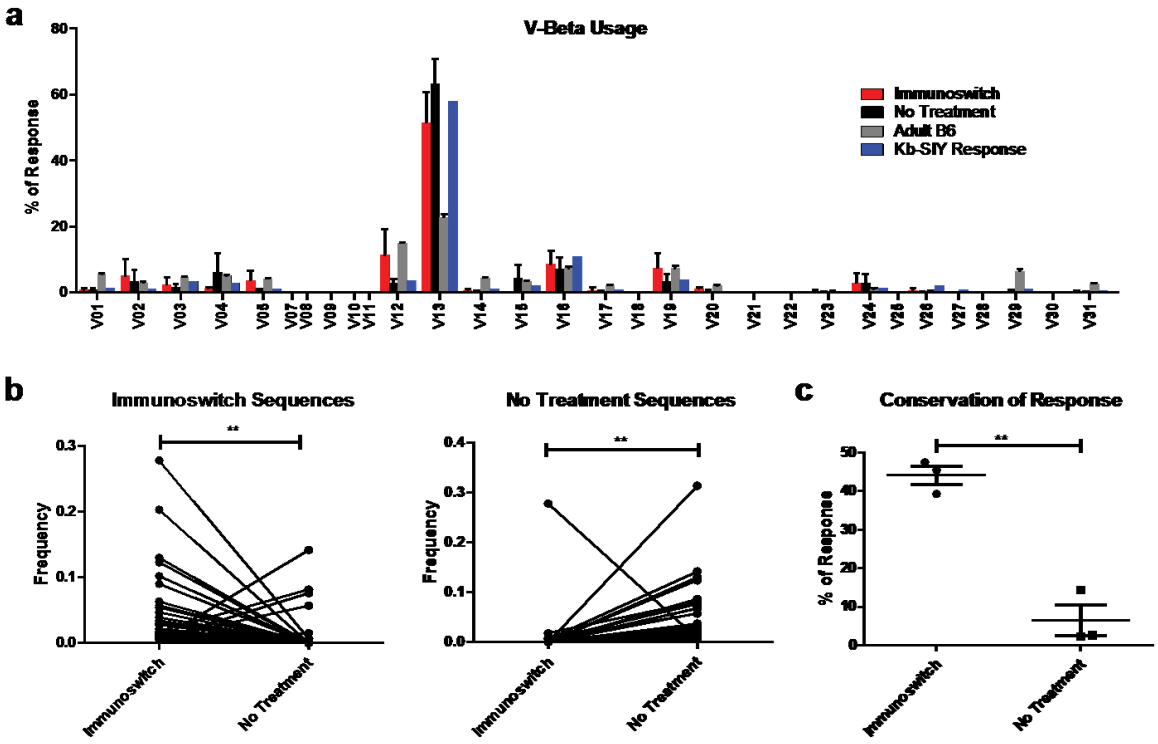

Figure 4-11. *Immunoswitch treatment alters the CD8+ T cell repertoire. (a) T cell receptor V-beta usage in CD8+ tumor-infiltrating lymphocytes from immunoswitch-treated, non-treated, non-tumor bearing adult B6 mice, or a Kb-SIY-specific CD8+ T cell response. C57BL/6 mice (n=3/group) were injected with B16-SIY cells SC on day 0. Immunoswitch particles were injected IT into treated mice on days 8 and 11, and tumor-infiltrating lymphocytes were isolated on day 14. Immunoswitch treated and non-treated mice skew towards T cell receptor V-beta 13, as is seen in a Kb-SIY specific response. (b) T cell receptor clones present in the CD8+ tumor-infiltrating lymphocytes of immunoswitch-treated mice are present at significantly higher frequencies than in the tumor-infiltrating lymphocytes of non-treated mice (left). T cell receptor clones present in the CD8+ tumor-infiltrating lymphocytes of non-treated mice are present at significantly higher frequencies than in the tumor-infiltrating lymphocytes of immunoswitch-treated mice (right). Significance measured by two-tailed paired t test ($p<0.01$). (c) CD8+ T cell receptor clones are conserved to a significantly higher extent in immunoswitch-treated mice. Each point represents the percent of overlapping clonal response between two mice of the same group. Significance measured by two-tailed t test ($p<0.01$).*

Despite the similarity in V-beta usage, the T cell receptor repertoire of these cells was significantly altered by immunoswitch treatment. T cell receptor clones, defined by the amino acid sequence of the CDR3 region, present in the tumor-infiltrating lymphocytes of immunoswitch treated mice appear at significantly lower levels in non-treated mice (

Figure 4-11**B**). Similarly, T cell receptor clones present in non-treated mice are present at significantly lower levels than in immunoswitch treated mice (

Figure 4-11**B**). This indicates that although a majority of the response both in the presence and absence of treatment is specific for the tumor-expressed Kb-SIY model antigen, the clones making up this response are changed by immunoswitch therapy.

Next, we investigated the conservation of this changed CD8+ T cell response after immunoswitch treatment. The clones that make up the majority of the response between pairs of immunoswitch-treated mice overlap by 44.1±4.3% (

Figure 4-11**C**). This contrasts with only 6.43±6.92% of an overlapping response between pairs of non-treated mice. Thus, immunoswitch particle treatment selects for a highly conserved anti-tumor response. This indicates that treatment delays tumor growth by inducing expansion of a specific population of anti-tumor CD8+ T cells with an altered T cell receptor sequence signature.

4.3.6 Immunoswitch biodistribution

In addition to altering the immune response, nanoparticles are larger than soluble antibody and thus have a different biodistribution.[106,196] Therefore, we sought to characterize the pharmacokinetics of immunoswitch particle treatment. We hypothesized that immunoswitch particles would diffuse from the injection site more slowly than soluble antibodies, resulting in a higher average concentration over time.

Immunoswitch particles or an equivalent amount of soluble antibody were labeled with an infrared (IR) dye and injected subcutaneously into nude mice. Mice were imaged using a full body IR imager after 3, 24, 48, and 72 hours to quantify biodistribution. Soluble antibody was cleared from the injection site significantly more rapidly than

immunoswitch particles (**Figure 4-12A,B**). By 24 hours, approximately 72% of immunoswitch particles, but only 26% of soluble antibody remained at the injection site. Within 72 hours, this decreased to 60% of immunoswitch particles and 8% of soluble antibody. A fit of the data to one-phase decay equations showed a half-life of 15.2 hours for soluble antibody compared to 84.5 hours for immunoswitch particles.

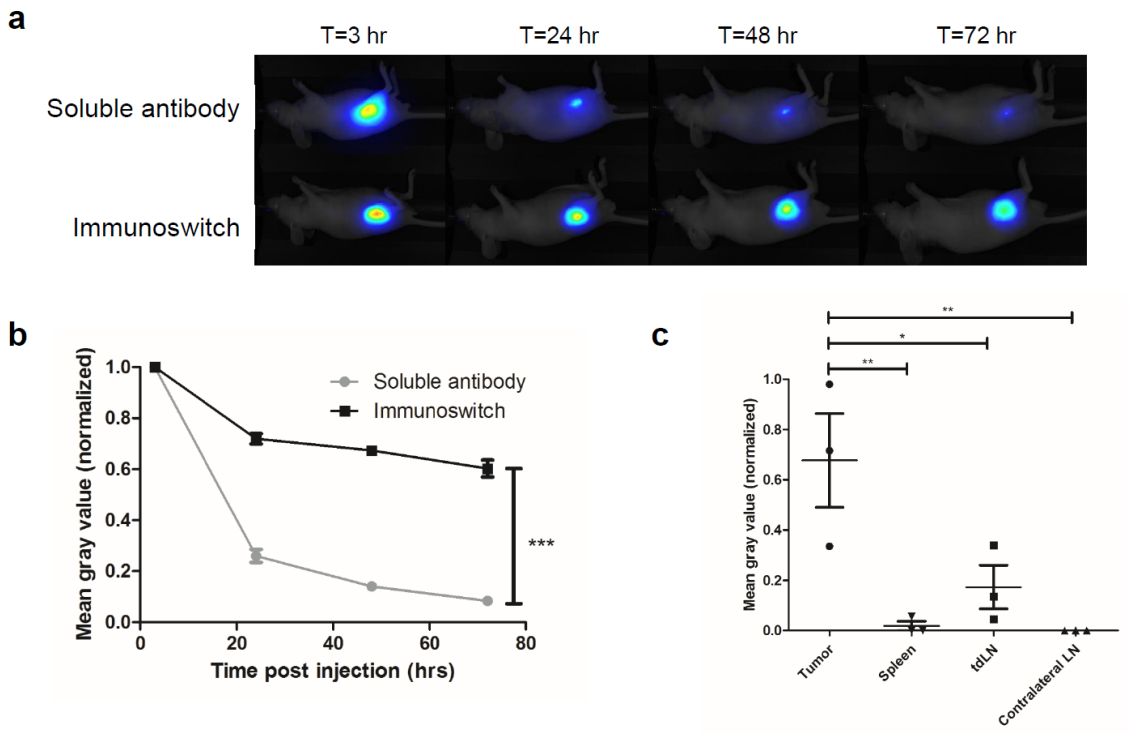

Figure 4-12. *Immunoswitch particles remain at injection site longer than soluble antibody. (a) Nude mice (n=3/group) were injected with IR-labeled soluble antibody or immunoswitch particles at t=0 hours. Mice were imaged with a full body IR imager at t=3, 24, 48, and 72 hours post injection. (b) Change in mean gray value over time in target region of interest. Images from individual mice were normalized to the mean gray value at t=3 hours (see Materials and Methods). An immediate decrease is observed after injection followed by a consistent clearance rate. Clearance from the injection site is greater for soluble antibodies than immunoswitch particles at all time points.* $t_{1/2,soluble}$*=15.2 hours and* $t_{1/2,immunoswitch}$*=84.5 hours when fit to a one phase decay equation. Significance measured by two-way ANOVA with Bonferroni posttest (p<0.0001,* $F_{1,16}$*=995.7 treatment variation). (c) C57BL/6 mice (n=3) were injected with IR-labeled immunoswitch particles 8 days after B16-SIY inoculation. Tumor, spleen, tumor draining lymph node, and contralateral lymph node were harvested 48 hours after treatment. Immunoswitch particles are retained primarily in the tumor and tumor draining lymph node. Values were recorded relative to the sensor's maximum (*i.e. *0-1 scale). Significance measured by two-way ANOVA with Tukey's posttest. (*p<0.05, **p<0.01,***p<0.001)*

Similarly sized nanoparticles have been shown to drain to the proximal tumor draining lymph node following intratumoral injection but not to more distal sites, minimizing systemic toxicity.[196] We therefore examined the organ biodistribution of immunoswitch particles following intratumoral injection. C57BL/6 mice were injected with IR-labeled immunoswitch particles 8 days after B16-SIY tumor inoculation. 48 hours after treatment, the tumor, tumor draining lymph node, contralateral lymph node, and spleen were dissected and imaged by an IR imager. Immunoswitch particles were found in the tumor and tumor draining lymph node (**Figure 4-12C**), consistent with our finding that tumor-specific CD8+ T cells are present at higher levels in the tumor draining lymph node of immunoswitch treated mice. There were little to no detectable levels immunoswitch particles in the contralateral lymph node or spleen. Prolonged retention of the immunoswitch particles at the tumor site and tumor draining lymph node may contribute to their increased efficacy over soluble antibody. This sequestration of immunostimulatory ligands in the tumor site is consistent with the findings of others in the development of nanocarriers for tumor microenvironment immunomodulation.[106,196]

4.3.7 Efficacy in multiple cancer models

We sought to investigate the broader applicability of immunoswitch particles by assessing treatment in additional tumor models, colon cancer and B16-F10, and through different injection routes, IV administration. We first studied their efficacy in MC38-OVA, a murine colon cancer expressing a model foreign antigen, OVA. C57BL/6 mice were injected subcutaneously with MC38-OVA tumors on day 0. Mice were treated with immunoswitch or isotype particles intratumorally on days 8, 11, 15, and 18 and tumors were measured.

Immunoswitch treated mice had significantly delayed tumor growth, averaging 19 mm^2 on day 36, as compared to 158 mm^2 for non-treated mice and 126 mm^2 for isotype particle treated mice (**Figure 4-13A**). 70% of immunoswitch-treated mice survived past day 55 as compared with 10% of non-treated mice (**Figure 4-13B**). These effects were even more pronounced than those seen in the B16-SIY model. In 5 of 10 mice, immunoswitch particle treatment led to complete regression of palpable MC38-OVA tumors. The MC38-OVA cell line also expresses different peptide-MHC from B16-SIY, demonstrating the robustness of immunoswitch treatment in the absence of adoptively transferred cells.

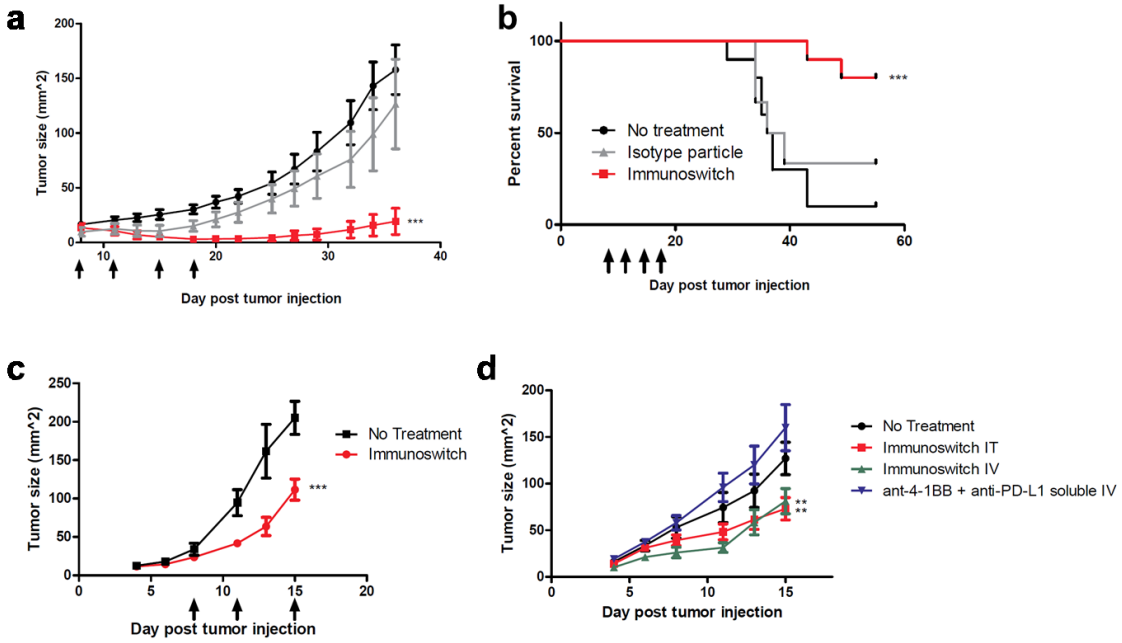

Figure 4-13. *Immunoswitch particles reverse tumor growth and extend survival in multiple tumor models and injection routes. (a) C57BL/6 mice (n=6 in isotype, n=10/other groups) were injected with MC38-OVA murine colon cancer cells SC on day 0. Treated mice received IT injections on days 8, 11, 15, and 18. Only immunoswitch particles significantly delayed and reversed tumor growth as compared with no treatment, past day 22. Significance was measured by two-way ANOVA with Bonferroni posttest (p=0.0003). Arrows indicate treatment days. (b) Only immunoswitch particles significantly extended survival as compared as compared to no treatment, as measured by log-rank test. Combined results from two independent experiments are shown. (c) C57BL/6 mice (n=5/group) were injected with B16-F10 cells SC on day 0. Treated mice received IT injections on days 8, 11, and 15. Immunoswitch treatment delayed tumor growth as compared to no treatment, past day 11. Significance was measured by two-way ANOVA with Bonferroni posttest. Arrows indicate treatment days. (d) C57BL/6 mice (n≥5/group) were injected with B16-SIY cells SC on day 0. IV immunoswitch particles were administered on days 4, 8, 11, and 15 and days 8, 11, and 15*

*by IT. Immunoswitch particles injected either IT or IV delay tumor growth past day 13 compared to no treatment ($p<0.01$). Soluble injected antibody has no effect on tumor growth. Significance was measured by two-way ANOVA with Bonferroni posttest. (**$p<0.01$, ***$p<0.001$)*

The tumor models, B16-SIY and MC38-OVA, both express strong model foreign antigens. Thus, we next sought to investigate the efficacy of immunoswitch particle therapy in a less immunogenic tumor model, B16-F10, which is identical to B16-SIY except that it lacks expression of the Kb-SIY model foreign antigen, to demonstrate broader therapeutic relevance.

C57BL/6 mice were injected subcutaneously with B16-F10 tumors on day 0. Mice were treated with immunoswitch particles intratumorally on days 8, 11, and 15 and tumors were measured. Immunoswitch particle therapy resulted in significantly delayed tumor growth compared to non-treated mice (**Figure 4-13C**). By day 15, the tumor size was nearly halved by immunoswitch treatment—tumors averaged 112 mm^2 for immunoswitch-treated mice compared to 205 mm^2 for non-treated mice. Immunoswitch particle treatment also resulted in significantly extended survival compared to no treatment. This data demonstrates the broader applicability of immunoswitch particle therapy to less immunogenic tumor models.

4.3.8 Efficacy by intravenous immunoswitch injection

We further investigated the route of administration by studying their effect on tumor growth when injected intravenously. C57BL/6 mice were injected subcutaneously with B16-SIY tumors and were treated with immunoswitch particles intravenously on days 4, 8, 11, and 15. Mice treated with immunoswitch particles intravenously were given one additional early dose on day 4, a standard time point used for checkpoint inhibition studies in the B16-SIY model.[42] Intravenous treatment resulted in similar anti-

tumor efficacy to our standard intratumoral treatment (**Figure 4-13D**). In contrast, similar doses of IV administered soluble antibody had no effect on tumor growth as was seen with intratumoral injection of soluble antibodies.

4.3.9 Intratumoral treatment results in a systemic memory response

Finally, we sought to determine if intratumoral immunoswitch treatment results in a systemic memory response. This factor is important for the clinical implications of this localized therapeutic. Because immunoswitch treatment was able to cure over 50% of mice with palpable MC38-OVA tumors, this model allowed us to study how the systemic response differed in cured versus uncured mice, as well as the protection against future tumor inoculation in cured mice.

C57BL/6 mice were inoculated with MC38-OVA tumors on day 0 and treated intratumorally with immunoswitch particles on days 8, 11, 15, and 18. To assess the presence of a systemic immune response, mice were injected retro-orbitally with differentially fluorescently labeled cognate (OVA) or non-cognate (SIY) peptide-pulsed splenocytes on day 28 when tumors were no longer palpable in cured mice. On day 29, mice were sacrificed and splenocytes analyzed. There was a significant increase in the *in vivo* killing of OVA-pulsed cells in mice that were cured following immunoswitch treatment compared to both naïve, non-tumor bearing mice, and mice treated but not cured following immunoswitch treatment (**Figure 4-14A**). Conversely, there was no significant increase of OVA-specific killing in mice treated but not cured from immunoswitch treatment. This data indicates that although immunoswitch particles are administered locally, they initiate a systemic immune response in cured mice.

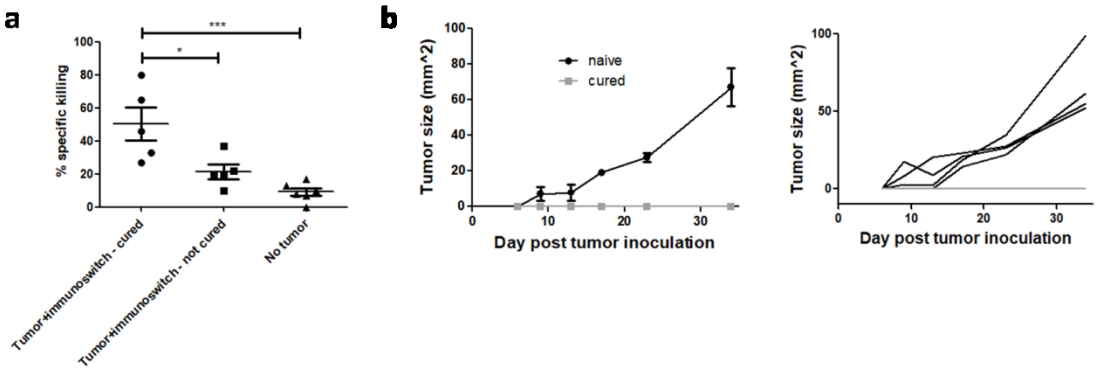

Figure 4-14. *Intratumoral immunoswitch treatment results in a systemic memory immune response. (a) C57BL/6 mice were inoculated with MC38-OVA tumors on day 0 and treated with immunoswitch particles intratumorally. On day 28, cognate (OVA) or non-cognate peptide-pulsed splenocytes were injected retro-orbitally. Splenocytes were harvested and analyzed on day 29 and specific killing of OVA-pulsed cells calculated. Mice cured from immunoswitch treatment had significant killing of OVA-specific cells, over 50%. Significance measured by one-way ANOVA with Tukey's post-test. Data combined from two independent experiments. (b) C57BL/6 mice were inoculated with MC38-OVA tumors on the right flank on day 0 and treated with immunoswitch particles intratumorally. On day 28, cured mice or age-matched controls were re-inoculated with MC38-OVA cells on the opposite flank. All naïve mice grew MC38-OVA tumors, shown by average tumor size (left) and individual tumor sizes (right), whereas no cured mice developed tumors. Tumor growth was significantly inhibited in cured mice (p=0.002) as measured by two-way ANOVA. (*p<0.05, ***p<0.001)*

To assess the presence of a memory response, immunoswitch-cured mice or age-matched controls were inoculated with MC38-OVA tumors on the opposite flank 28 days post-initial tumor inoculation. All naïve age-matched mice developed palpable tumors, whereas no cured mice developed tumors over the course of more than 30 days (**Figure 4-14B**). Thus, local intratumoral immunoswitch treatment is able to induce a systemic memory immune response that protects mice from future tumor re-challenge.

4.4 Discussion and conclusions

Combinatorial immunotherapy for cancer treatment has resulted in promising success in clinical trials. However, the use of non-specific immunomodulators such as checkpoint blockade requires high doses of the drugs and significant off-target side

effects, especially when multiple drugs are used in combination.[148] There is incentive to develop more effective and less toxic treatments. Sequestering immunotherapeutics on a rigid nanoparticle platform alters their biodistribution and may reduce off-target toxicities. In this way, Kwong, et. al. have laid the groundwork in the development of nanoparticles to deliver and present immunostimulatory ligands, such as anti-4-1BB or anti-CD40, to CD8+ T cells and other immune cells.[106,196] However, their nanoparticles were not designed to target two different cell types in the tumor microenvironment. Immunoswitch nanoparticles do this, linking immunomodulators differentially expressed on CD8+ T cells and target cells within the tumor and have significant anti-tumor activity *in vivo*.

We have created an immunoswitch nanoparticle that blocks the immunosuppressive PD-L1 pathway while switching on the 4-1BB costimulatory pathway of tumor-targeting CD8+ T cells on a single injectable platform. These particles utilize spatial constraints to enhance the efficacy of two developing immunotherapies. Immunoswitch particles inhibited tumor growth more effectively than equivalent amounts of soluble anti-PD-L1 and anti-4-1BB mAb. While tethering the antibodies to a rigid particle platform increases avidity for their ligand and may play a role in their efficacy, we identified at least two additional mechanisms that explain immunoswitch-based T cell activation and anti-tumor activity.

Combining both anti-PD-L1 and anti-4-1BB mAb on a single platform physically links the effector and target cells. This was directly shown *in vitro* by confocal microscopy and flow cytometry. The importance of the physical linkage of both antibodies to a single nanoparticle was also seen *in vivo* despite the complexity of the

tumor microenvironment; co-injected separately conjugated particles, bearing either anti-PD-L1 or anti-4-1BB mAb, were ineffective. Additionally, we showed that immunoswitch particles diffuse from the injection site more slowly than their soluble counterpart. This implies a higher local concentration of the bio-active particles integrated over time and consequently a decreased concentration at off-target sites. Although soluble antibody and separately conjugated particles had some *in vitro* activity, stimulating IFN-γ secretion, they had no *in vivo* effect. In contrast, immunoswitch treatment had significant anti-tumor activity *in vivo*. Thus, *in vitro* IFN-γ secretion may not fully explain *in vivo* activity where other factors such as biodistribution and shaping of the endogenous T cell receptor repertoire may play a larger role.

While the immunoswitch particles led to antigen-independent effector-target cell conjugation, target cell recognition and IFN-γ effector cytokine secretion was signal 1 dependent. This was demonstrated *in vitro* when transgenic 2C CD8+ T cells were not stimulated by immunoswitch particles in the presence of non-cognate target cells. However, *a priori* knowledge of the tumor antigen is not necessary since signal 1 is derived from the tumor cell itself. Thus, immunoswitch particles can activate a diverse polyclonal T cell response *in vivo* and reduce the chance of antigenic escape.[197]

Murine melanoma tumor control mediated by immunoswitch particles was observed even in the absence of adoptively transferred tumor-specific CD8+ T cells and when administered systemically by intravenous treatment. We showed that immunoswitch particles exert their effect by increasing the density, specificity, and functionality of endogenous tumor-specific CD8+ T cells. Tumor-infiltrating lymphocytes of immunoswitch treated mice increased IFN-γ production and CD107

expression. In addition, more IFN-γ was made on a per cell basis as seen by an increase in IFN-γ MFI after immunoswitch treatment. There was no difference in tumor-specific CD8+ T cell levels in the spleen or in circulation, indicating that immune activation is concentrated to the tumor site and thus may limit off-target immune-mediated toxicities, as supported by the particle biodistribution. Additionally, this approach may be generally applicable as tumor control was also evident in an MC38-OVA colon cancer model and in a less immunogenic B16-F10 melanoma cancer model lacking a model foreign antigen. Despite local intratumoral treatment, immunoswitch particles demonstrated a systemic memory immune response that protects mice against future re-challenge. However, the data does not prove whether the systemic immune response is a consequence of or the cause of immunoswitch-mediated tumor eradication—i.e. the elimination of the tumor may cause the tumor-specific CD8+ T cells to enter systemic circulation, whereas these tumor-specific cells may be maintained within the tumor microenvironment of non-cured mice. Further experiments are required to tease apart this cause-effect relationship.

Finally, sequencing analysis of the tumor-infiltrating lymphocytes revealed that the immunoswitch-mediated anti-tumor response is mediated by a change in the T cell receptor repertoire. Immunoswitch particle treatment expands a different set of CD8+ T cell T cell receptor clones not present at high levels in non-treated mice. This altered T cell receptor repertoire is highly conserved, indicating that treatment enables the immune system to find the “correct” anti-tumor immune response without switching recognition to a different antigen. While many existing therapies induce alterations in the breadth and

depth of the T cell response,[29,198] we show that immunoswitch particles change the clonal composition of the response against a defined tumor antigen.

Immunoswitch particles are an immunotherapy that utilizes a single, nanoparticle-based injectable therapeutic. By combining multiple targeting moieties on the surface of a single particle, this represents a genre of nanoparticle-based approaches for cancer immunotherapy. The increased effectiveness of immunoswitch particles over soluble antibody can allow for reduced cost and complexity of a multi-faceted therapeutic. The nanoparticle platform also allows for further modifications to optimize biodistribution or deliver signals locally. For example, nanoparticle size or shape can be engineered to reduce clearance or target specific cell types,[58,199] and the core can be designed to release an immune-stimulant such as IL-2.[97] Additionally, we have shown proof of concept of a "signal-switching" approach that links two signaling pathways. This can be extended to other parts of the cancer-immunity cycle, including other inhibitory and/or co-stimulatory pathways, such as Lag-3, CTLA-4, or CD28, in addition to pathways relevant in autoimmunity and other disease states. Thus, immunoswitch particles are a nanoparticle-based combination therapy and build a framework for further mechanistic and translational studies.

Chapter 5. Separating T Cell Targeting Components onto Magnetically-Clustered Nanoparticles Boosts Activation[2]

5.1 Introduction

Decades of research have built a framework for understanding T cell signaling and have led to protocols for the *in vivo* and *in vitro* activation of T cells for basic science studies as well as immunotherapeutic applications. However, it has become evident that current platforms are not optimized for effective T cell stimulation. T cell activation is sensitive to the composition and organization of a large family of signaling molecules, many of which are often absent or difficult to optimize using the current methods of synthetic or modified antigen-presenting cells.

Minimally, T cells require two signals for activation—signal 1, specific peptide-MHC (pMHC), and signal 2, a co-stimulatory signal such as the B7 interaction with CD28. During endogenous T cell activation, signal 1 and 2 co-cluster in the immune synapse, a dynamic microcluster of signaling molecules at the interface of the T cell and antigen presenting cell.[15] This co-clustering is necessary, as micropatterned surfaces that separate signal 1 and signal 2 by several microns eliminate activation.[18]

Although the B7/CD28 interaction is thought of as the "prototypical" signal 2, dozens of different molecules can serve as co-stimulation for CD8+ T cell activation,

[2] Sections of this chapter are reprinted (adapted) with permission from "Kosmides, A., Necochea, K., Hickey, J.W., and Schneck, J.P. Separating T Cell Targeting Components onto Magnetically Clustered Nanoparticles Boosts Activation. *Nano Letters*, Epub ahead of print". Copyright 2018 American Chemical Society.

among them 4-1BB, CD27, and OX40, and each plays a different role in the activation process.[4–8] The specificity and phenotype of activated T cells is sensitive to co-stimulatory molecule composition[6,7,9–13] and affects the ability to stimulate a long-lived memory population able to kill virally infected or tumor cells. Even simply changing the ratio of co-stimulatory molecules or their timing during stimulation alters T cell functionality.[9,10]

One reductionist approach for CD8+ T cell stimulation utilizes artificial antigen presenting cells (aAPCs), three-dimensional platforms that minimally present the two signals necessary for T cell activation—signal 1, specific peptide-MHC (pMHC), and signal 2, such as B7/anti-CD28 monoclonal antibody (mAb).[200,201] In contrast to cell-based methods such as K562-based antigen presentation,[6] cell-free aAPC provide an engineered, more cost-effective off-the-shelf therapeutic. These particles can be used to activate and expand a patient's CD8+ and CD4+ T cells against tumor antigens for adoptive cell therapy (ACT).[68,84,202–205] The signaling molecules are often randomly conjugated to the surface of the aAPC[53,200,201] which leaves little control over the nanoscale organization of the molecules, despite this showing importance empirically.[15,47] When length scales have been more systematically investigated, it has been performed on flat substrates which lack the properties of three-dimensional activation structures.[47,48] Progress in understanding the dynamics of T cell activation requires methods of such analyses on three dimensional platforms that can be systematically manipulated.

Initially, traditional aAPCs were micron sized and thus have radii larger than the necessary degree of co-clustering. This necessitates that all signaling molecules be

conjugated to the surface of the same aAPC. Thus, for each type of co-stimulation condition studied, new aAPC must be synthesized which limits the ability to study large numbers of co-stimulatory conditions and increases time spent on quality controlling and potential for error.[206] Nano-aAPC with length scales closer to that required for signal clustering during T cell activation could allow for more control over signal distribution. Our previous work has demonstrated the ability to increase the effectiveness of nano-aAPC which normally are not capable of activating a robust T cell response.[60] By constructing aAPC on paramagnetic iron-dextran nanoparticles, the aAPC can be clustered on the T cell surface using an external magnetic field to more closely mimic the clustering required for endogenous T cell activation. Because of the small length scales of these nano-aAPC, we hypothesized that we could use this approach to separate the signaling components onto distinct particles.

Here, we develop and validate a reductionist T cell stimulation platform with each type of signaling molecule on separate paramagnetic nanoparticles. Previously, T cell signaling components could not be isolated on distinct particles unless embedded into a solid substrate or nanomatrix.[207] However, with the paramagnetic nanoparticle platform, the separately conjugated particles can be co-clustered on the cell surface in the presence of a magnetic field[60] to mimic the signal microcluster and activate T cells. This new system provides a streamlined approach to T cell activation where a small number of homogenous particles to be easily synthesized and added into culture at different times, ratios, and amounts to customize stimulatory conditions. This platform can also be utilized to study biophysical aspects of T cell activation. We demonstrate that by altering nanoparticle size and composition, the separate particle platform can be used to assess the

optimal degree of clustering between signaling molecules. This platform outperforms traditional methods to expand endogenous CD8+ T cell populations by enabling greater initial enrichment of the cells of interest, and can be used to systematically study the biophysical effects of signal clustering on the cell surface.

5.2 Methods

5.2.1 Mice

PMEL TCR/Thy1a Rag-/- transgenic mice were a gift from Nicholas Restifo (National Institutes of Health, Bethesda, MD, USA) and maintained as homozygotes. C57BL/6 mice were purchased from Jackson Laboratories (Bar Harbor, ME, USA). All mice used were 6-8 weeks of age and were maintained according to Johns Hopkins University's Institutional Review Board.

5.2.2 Reagents and Cell Lines

Kb-Ig and Db-Ig soluble MHC-Ig dimer were prepared and loaded with peptides as described.[208] Briefly, Kb-Ig and Db-Ig producing hybridoma cell lines were expanded in hybridoma serum free media (Thermo Fisher Scientific; Waltham, MA) supplemented with L-glutamine. After one to two weeks, the supernatant was harvested and run over an NP sepharose column. Dimer was then eluted from the column with NIP-e-Aminocaproic acid and concentrated by membrane ultrafiltration with a Vivaspin 20 50 kDa MWCO (GE Healthcare, Little Chalfont, Buckinghamshire, UK). Concentration and molecular weight were measured by a Nanodrop ND-1000 Spectrophotometer and SCL-10A Shimadzu HPLC. Dimers were biotinylated with EZ-Link Sulfo-NHS-Biotinylation (Thermo Fisher Scientific) according to the manufacturer’s protocol, adding 20x molar

excess biotin. Loading of Db-Ig with gp100 peptide was performed by first denaturing the dimer with an acidic (pH=6.5) buffer, adding 50x molar excess gp100 peptide (GenScript, Piscataway, NJ) and incubating at 37º C for 1 hour. Two-fold molar excess of human beta 2 microglobulin (Bio-Rad Laboratories, Hercules, CA) was added and solution was brought back to neutral pH (pH=7.4) and allowed to refold at 4º C for 24 hours. Excess peptide was removed by washing 3X with PBS using membrane ultrafiltration with a Vivaspin 20 50 kDa MWCO (GE Healthcare). Loading of Kb-Ig with trp2 peptide was performed by first denaturing the dimer with a basic (pH=11.5) buffer, equilibrating at room temperature for 15 min, and adding 50x molar excess trp2 peptide (GenScript) and bringing back to neutral pH (pH=7.4). Loaded dimer was allowed to refold at 4º C for 48 hours, and excess peptide was removed as above.

Anti-CD28 clone 37.51 and anti-4-1BB clone 3H3 were purchased from BioXCell (West Lebanon, NH). Biotinylated anti-CD28 antibody clone 37.51 and anti-CD27 antibody clone LG.3A10 were purchased from BD Biosciences (San Jose, CA). Fluorescently labeled monoclonal antibodies were purchased from BioLegend (San Diego, CA, USA). B16-F10 was a gift from Charles Drake (Johns Hopkins University, MD, USA). RMA-S cells were a gift from Michael Edidin (Johns Hopkins University, MD, USA).

5.2.3 Particle synthesis and characterization

For transgenic CD8+ T cell stimulation studies, anti-biotin coated 100 nm iron-dextran nanoparticles were purchased from Miltenyi Biotec (Cologne, Germany). A two-fold excess of biotinylated MHC-Ig dimers and co-stimulatory molecules were allowed to conjugate to particles in PBS overnight at 4º C, and excess unbound antibody was

removed by washing with PBS over an MS column (Miltenyi Biotec, Cologne, Germany). 100 nm streptavidin-coated polystyrene particles were purchased from Micromod (Rostock, Germany) and conjugated as above. Excess unbound antibody was removed by washing with PBS 3x for 20 min at 22,000xg at 4º C.

For different sized particles and endogenous expansion experiments, antibodies were directly conjugated to amine-functionalized iron-oxide particles according to the manufacturer's protocol (Micromod, Rostock, Germany). Briefly, antibodies of interest were thiolated with Traut's reagent (Sigma-Aldrich, St. Louis, MO) in a PBS-EDTA buffer at pH 7.6. Excess Traut's reagent was removed by running the antibody sample over a PD10 column (GE Healthcare) and concentration was measured by a Nanodrop ND-1000 Spectrophotometer. Particles were functionalized with maleimide by incubating particles in 10x PBS with a Sulfo-SMCC crosslinker (ProteoChem, Hurricane, UT) for one hour at room temperature with continuous mixing. Excess Sulfo-SMCC was removed by washing the particles over an LS column (Miltenyi Biotech) according to the manufacturer's protocol. Maleimide functionalized particles were mixed with thiolated proteins in a PBS-EDTA buffer at room temperature overnight. Excess unbound antibody was removed by washing with PBS over an LS column (Miltenyi Biotec) or by using an EasySep Magnet (STEMCELL Technologies, Vancouver, Canada).

Particle size was determined by nanoparticle tracking analysis using a Nanosight LM10. To characterize protein conjugation, a standard curve relating absorbance to particle concentration was first made using a Beckman Coulter AD340 plate reader and Nanosight LM10. Briefly, a serial dilution of each particle size at a known concentration from the manufacturer was made, and absorbance was read for each sample (**Figure 5-1**).

A standard curve relating absorbance to particle concentration was made for each size. Particles were then subsequently measured for absorbance to determine concentration based on the standard curve. The amount of specific antibody per particle was determined by staining the particles with fluorescently-labeled secondary monoclonal antibodies against the antibody of interest. Excess antibody was removed by running the particles over an MS column (Miltenyi Biotec), and antibody concentration was measured by comparing particle fluorescence to a standard curve and correlating with the total bead concentration.

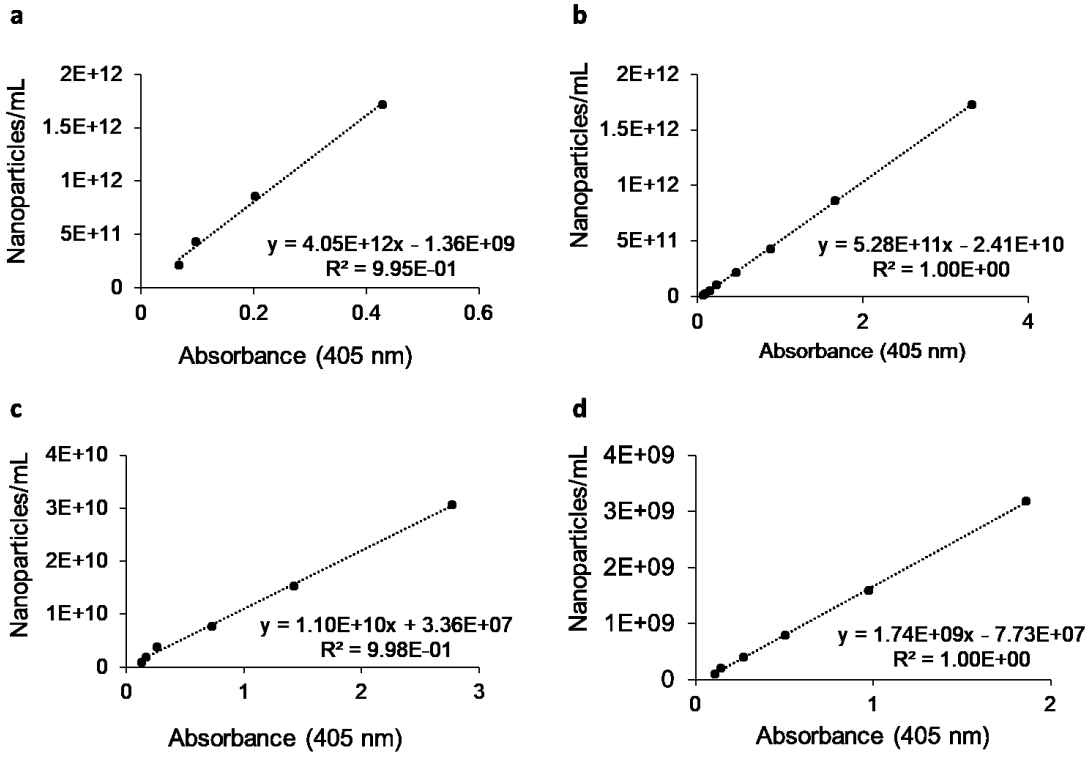

Figure 5-1. *Standard curves relate absorbance to particle concentration of nanoparticles. Serial dilutions were made for each particle size at known concentrations as specified by the manufacturer, and absorbance was measured. Standard curves relating absorbance to particle concentration were made for 30 nm (a), 100 nm (b), 300 nm (c), and 500 nm (d) particles.*

5.2.4 CD8+ T cell aAPC stimulation

PMEL or C57BL/6 CD8+ T cells were isolated from naïve spleens by negative selection with the Miltenyi CD8a+ isolation kit IIa following the manufacturer's protocol (Miltenyi Biotec). For transgenic studies and polyclonal C57BL/6 studies, $CD44^{lo}$ CD8+ T cells were isolated by including anti-CD44-biotin during CD8+ negative selection. For endogenous stimulation, CD8+ T cells were enriched prior to expansion with signal 1 only or traditional aAPC, as specified, using a previously established protocol.[194] Briefly, CD8+ T cells were incubated with the particles of interest at 4º C for 1 hour. Cells bound to particles were then isolated by positive selection using an MS column (Miltenyi Biotec) and only the positive fraction was then plated for expansion. This "enrichment" step was nor performed for the studies described in Fig. 3c where non-paramagnetic nanoparticles were used—the complete un-enriched endogenous CD8+ T cell repertoire was expanded.

For expansion, CD8+ T cells isolated from either of the above methods were mixed with the particles of interest and cultured in 24-well or 96-well culture plates in RPMI supplemented with L-glutamine, non-essential amino acids, vitamin solution, sodium pyruvate, β-mercaptoethanol, 10% FBS, ciproflaxin, and a cocktail of T cell growth factors. To produce a magnetic field, culture plates were fixed between two 1/2 in. neodymium N52 disk magnets and placed at 4º C for 1 hour, followed by 37º C for the first three days of culture. CFSE fluorescence was measured on day three using a BD FacsCalibur flow cytometer and analyzed using FlowJo (TreeStar). Fold expansion was measured by using a trypan blue exclusion test to exclude dead cells and counting cells seven days after stimulation. In endogenous cell stimulation studies, cells were stained

with a biotinylated MHC-Ig dimer and other fluoresecently labeled antibodies of interest seven days after activation followed by a fluorescently labeled streptavidin and read on a BD FacsCalibur.

5.2.5 Specific lysis assay

PMEL CD8+ T cells were stimulated with the particles indicated. After seven days, cells were harvested and incubated with cognate B16-F10 cells at the indicated T cell-target cell ratio in a 96-well plate for four hours at 37º C. Lysis was measured using a CytoTox-Glo Cytotoxicity Assay kit (Promega, Madison, WI) according to the manufacturer's protocol. Luminescence was read on a Tropix TR717 Microplate Luminometer (Applied Biosystems, Bedford, MA).

5.2.6 Particle clustering analysis

Anti-PE and anti-APC nanoparticles (Miltenyi Biotec) were conjugated with PE-labeled and APC-labeled MHC-Ig Db-gp100 dimer and anti-CD28 mAb, respectively. MHC-Ig Db-gp100 dimer and anti-CD28 mAb were fluorescently labeled with a PE/R-Phycoerythrin and APC Conjugation kit (Abcam), respectively, according to the manufacturer's protocol. Particles were incubated with naïve $CD44^{lo}$ PMEL CD8+ T cells for one hour at 4º C followed by one hour at 37º C in a magnetic field. Cells were fixed with 2% PFA at room temperature for 20 minutes then imaged on a Zeiss LSM510-Meta laser scanning confocal microscope at 100X magnification. To measure clustering of signal 1 and signal 2 particles, confocal images were analyzed in Matlab.

For cluster number and size analysis, nanoparticles ranging from 30-500 nm were conjugated with Kb-SIY as described in *Particle synthesis and characterization*. Particles were incubated with cognate 2C CD8+ T cells for one hour at 4º C followed by one hour

in a magnetic field. For confocal imaging, cells were stained with fluorescently labeled antibodies against CD8 and the MHC-Ig dimer on the nanoparticles, fixed, and read by confocal microscopy. Cluster analysis was performed in ImageJ (National Institutes of Health) using the build-in particle analyzer. 15-25 cells were analyzed per condition. Cells were also imaged by SEM.

5.2.7 Matlab clustering analysis

LSM images were imported into Matlab. For each image, the cell borders were first detected. To do so, the gradient was calculated for the white color image, normalized, and thresholded. The image was then morphologically closed. Cell borders were identified using the function *imfindcircles* in the image processing toolbox using the Hough transform method.

For each identified cell, its border was expanded internally and externally by 35%, and then divided equally into 150 voxels. A cell was only included in the analysis if it was fully visual within the field of view of the image and expressed red and green levels above background. For each voxel, the average red and green value was calculated and normalized to the maximum. Co-localization score for each cell was calculated by multiplying the normalized red and green values in each voxel, summing over the entire cell border, and dividing by the Euclidian distance of the normalized red and green values. For no magnetic field, 47 total cells were analyzed. For magnetic field, 58 total cells were analyzed.

5.2.8 Fold-enrichment studies

CD8+ T cells were isolated from Thy1.1+ PMEL and Thy1.2+ C57BL/6 spleens by negative isolation. PMEL CD8+ T cells were doped into Thy1.2+ wild type C57BL/6 CD8+ T cells at a 1:1000 ratio. Cell mixture was enriched with signal 1 only Db-gp100 particles, signal 1/2 Db-gp100/anti-CD28 aAPC, or noncognate aAPC, as above. Enriched fraction was stained with a fluorescently labeled Thy1.1 monoclonal antibody and read on a BD FacsCalibur.

5.2.9 Endogenous CD8+ T cell cytokine functionality

To assess functionality of expanded cells, CD8+ T cells were isolated on day 7 post expansion. CD8+ T cells were co-cultured with cognate and non-cognate peptide-pulsed RMA-S cells with anti-CD107a-FITC, GolgiStop, and GolgiPlug for five hours. Cells were then stained for surface markers, then fixed and permeabilized with BD Cytofix/Cytoperm and stained with fluorescently labeled antibodies against intracellular cytokines according to the manufacturer's protocol. Labeled cells were read on an LSR II and analyzed with FlowJo.

5.2.10 *In vivo* adoptive transfer studies

CD8+ T cells were isolated from Thy1.2+ C57BL/6 mice on day -7. CD8+ T cells were split into three groups and stimulated with either 1) traditional Kb-trp2/anti-CD28 aAPC, 2) Kb-trp2 particles and anti-CD28 particles using the separate particle platform, or 3) Kb-trp2 particles, anti-CD28 particles, and anti-4-1BB particles at a 75/25% anti-CD28/anti-4-1BB ratio. All stimulations were done as in *5.2.4 CD8+ T cell aAPC stimulation* and were normalized by the total amount of co-stimulation. 10^7 CD8+ T cells

from host mice were stimulated via the enrichment and expansion protocol per 1 donor mouse.

On day -1, all Thy1.1+ C57BL/6 host mice were irradiated with 500 cGy sublethal dose of irradiation. On day 0, expanded cells were harvested and injected via retro-orbital injection into host mice. 30,000 U IL-2/mouse were injected into all host mice via intraperitoneal injection on days 0 and 1. Mice were sacrificed and organs harvested on day 21. Cells were stained with a fluorescently labeled antibody against Thy1.2 to detect transferred cells and read on an LSR II.

5.3 Results

5.3.1 Separate particle platform activates CD8 cells

To study the impact of altering composition and ratio of costimulatory signals, we developed a separate paramagnetic nanoparticle platform. The separate particle platform enables T cell activation by using an external magnetic field to cluster paramagnetic nanoparticles separately conjugated with signal 1 or signal 2. The separate particles are then added to culture at defined combinations and ratios to optimize T cell stimulation (**Figure 5-2A, schematic**).

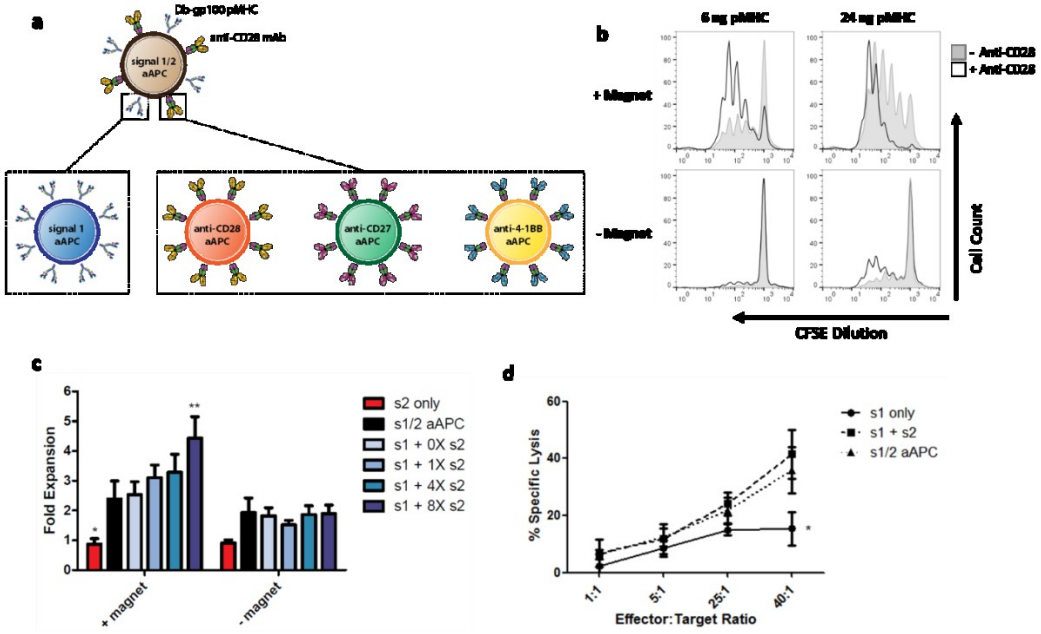

Figure 5-2. *CD8+ T cells are activated by nanoparticles separately expressing signal 1 and signal 2 when particles are clustered within a magnetic field. (a) Schematic comparing standard aAPC co-expressing stimulatory signals on the same nanoparticle, and separate signal 1 + 2 particle platform with each stimulatory signal conjugated to distinct nanoparticles. (b) TCR transgenic PMEL CD8+ T cells were stimulated with signal 1 only Db-gp100 dimer particles in the presence (black) or absence (grey) of signal 2 only anti-CD28 particles. CFSE dilution was measured after three days. Decreased fluorescence indicates increased proliferation. Cells proliferate when signal 1 and signal 2 are presented on separate particles, only when clustered within a magnetic field. (c) PMEL CD8+ T cells were stimulated with anti-CD28 signal 2 (s2) only particles, standard signal 1/2 aAPC (aAPC) expressing Db-gp100, or signal 1 (s1) only Db-gp100 particles with 0-8X molar ratio of signal 2 only anti-CD28 particles. Significance measured by two-way ANOVA with Bonferroni post-test. Signal 2 only particles and s1+8X s2 particles induce significantly different expansion compared to traditional aAPC within a magnetic field. (d) PMEL CD8+ T cells were incubated with signal 1 only particles, signal 1 and 2 expressed on separate particles (s1 + s2), or traditional signal 1/2 aAPC with 12 ng total signal 1. On day seven post stimulation, cells were isolated and co-incubated with cognate B16-F10 tumor cells for 4 hours. Cytotoxicity was measured. Significance measured by two-way ANOVA with Bonferroni post-test. (*p<0.05, **p<0.01)*

One hundred nanometer paramagnetic iron-dextran particles were chosen as the base of the separate particle platform which we previously showed can be clustered on the T cell surface by an external magnetic field.[60] Thus, nanoparticles separately conjugated with T cell stimulatory signals can be brought into the close proximity required for T cell activation. Though signal 1 and signal 2 separated onto distinct stimulatory complexes cannot activate T cells,[209,210] clustering of paramagnetic particles mimics stimulation by a single, larger signal 1 and signal 2 complex.

We first demonstrated proof-of-principle of the system using separately conjugated signal 1 and signal 2 nanoparticles in the PMEL TCR transgenic murine model. While transgenic T cells may be less sensitive to changes in co-stimulation, the large numbers of identical T cell receptors provide an ideal system for validation. Anti-CD28 was chosen as the co-stimulatory molecule and Db-gp100 pMHC as the initial signal 1 to stimulate TCR transgenic PMEL CD8+ T cells, all of which are specific for the gp100 peptide presented by Db MHC I.

Separately conjugated Db-gp100 dimer only and anti-CD28 mAb only particles were incubated with naïve PMEL CD8+ T cells at a 1:1 molar ratio in the presence or absence of a magnetic field. There was significant expansion of the cells by the separate particle platform in the presence of a magnetic field ($p<0.001$) which increased in a dose dependent fashion with increasing signal 2:signal 1 ratio (slope=0.2±0.09, $p=0.02$). In contrast, in the absence of a magnetic field, there was little to no CD8+ T cell proliferation in the presence of low or high doses of signal 1 and regardless of whether signal 2 was present. This was seen by both CFSE dilution (**Figure 5-2B**) and day 7 cell counts (**Figure 5-2C**). As expected, signal 2 alone did not cause T cell expansion, indicating that the magnetic field clustering alone does not non-specifically activate the cells.

CD8+ T cells stimulated with the separate particle platform had equivalent cytotoxicity to those stimulated with traditional aAPC, maximally ~40% specific lysis (**Figure 5-2D**). Signal 1 only activated cells had significantly less cytotoxic activity as expected, as signal 1 alone has been demonstrated previously to produce anergic cells[211]. Thus, the separate particle platform stimulates CD8+ T cells equivalently to traditional

aAPC and maintains the requirement for signal 2, recapitulating the natural biology of T cell stimulation.

5.3.2 Dependence of particle size

Based on data that T cell signaling starts on a nanoscale level,[53] we hypothesized that increasing the particle size would limit the activity of the separate particle platform because this would intrinsically limit the co-clustering of the individual molecules. Thus, we next sought to evaluate the working parameters of particle diameter using the separate particle platform.

We synthesized signal 1 and signal 2 only particles ranging in diameter from 30 nm to 4500 nm. Naïve PMEL CD8+ T cells were stimulated with each pair of matching diameter signal 1 and signal 2 only particles within a magnetic field, normalized to total signal 1 amount, and fold expansion was measured after seven days. Standard aAPC based activation (i.e. signal 1 and 2 on the same particle, in the absence of a magnetic field) results in increasing CD8+ T cell activation with increasing particle diameter (**Figure 5-3**). This is a well-documented phenomena due to the higher radius of curvature of larger particles and thus higher surface area of contact between the T cell and aAPC.[59,65] In contrast, the opposite effect is seen with the separate particle platform—particles with a diameter of 30 nm resulted in the greatest expansion over the course of one week, almost three times more than expansion by 4500 nm particles (**Figure 5-4A**). Magnetic clustering had no effect on activation by particles with diameters of 500 nm and above (**Figure 5-4B**), whereas smaller diameter particles only stimulated a CD8+ T cell response when clustered within a magnetic field. This effect was not correlated with cluster size or the number of clusters on the cell surface (**Figure 5-5A,C**). 100 nm and

300 nm particles resulted in significantly fewer numbers of clusters per cell than 30 nm or 500 nm particles despite producing intermediate levels of T cell activation. Similarly, cluster size did not vary significantly based on particle size, although 300 nm trended toward the largest diameter clusters (**Figure 5-5B,C**). SEM imaging further confirmed the consistency of cluster size (**Figure 5-5D,E**). This data indicates that the signaling molecules must be presented on particles less than 500 nm in diameter to enable signal 1 and 2 co-clustering at sufficiently small length scales. Particles with diameters smaller than 500 nm enable the signaling molecules to cluster within the nanoscale proximity required for activation.

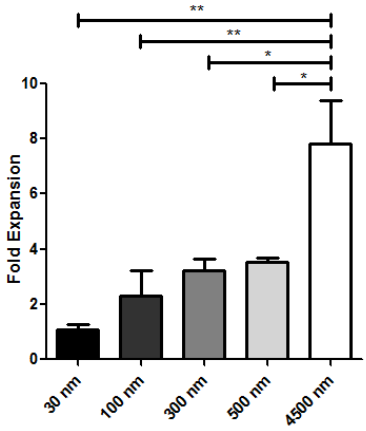

Figure 5-3. *Traditional aAPC activate a more robust T cell response at larger particle sizes. TCR transgenic PMEL CD8+ T cells were stimulated with traditional Db-gp100/anti-CD28 aAPC varying in diameter from 30 nm to 4500 nm with 18 ng total signal 1. Cell counts were taken on day seven and fold expansion calculated. Maximal expansion occurred when cells were stimulated with 4500 nm aAPC. Significance measured by one-way ANOVA with Tukey's post-test. Data combined from three independent experiments. (*p<0.05, **p<0.01)*

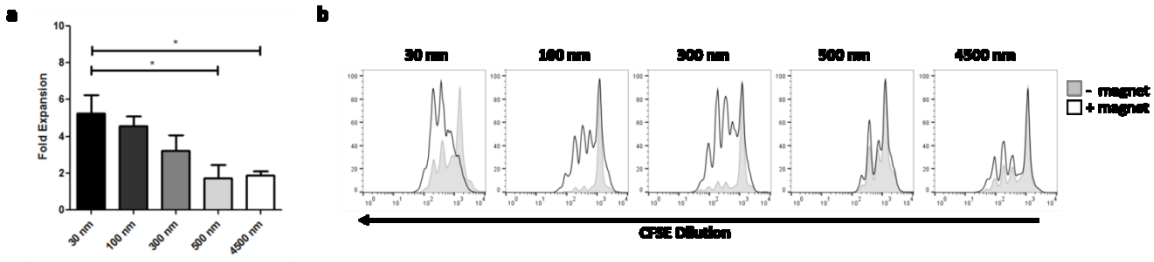

Figure 5-4. *Separate particle platform requires particles on the nanometer size scale for efficient CD8+ T cell stimulation. (a) TCR transgenic PMEL CD8+ T cells were stimulated with different size Db-gp100 and anti-CD28 particles presented on separate particles within a magnetic field. Cell counts were taken on day seven and fold expansion calculated. Maximal expansion occurred when cells were stimulated with 30 nm separately conjugated particles. Significance measured by one-way ANOVA with Tukey's post-test. (b) CFSE labeled PMEL CD8+ T cells were stimulated with different size Db-gp100 and anti-CD28 particles presented on separate particles in the presence (black) or absence (grey) of a magnetic field. CFSE dilution was read by flow cytometry on day three post stimulation. (*p<0.05)*

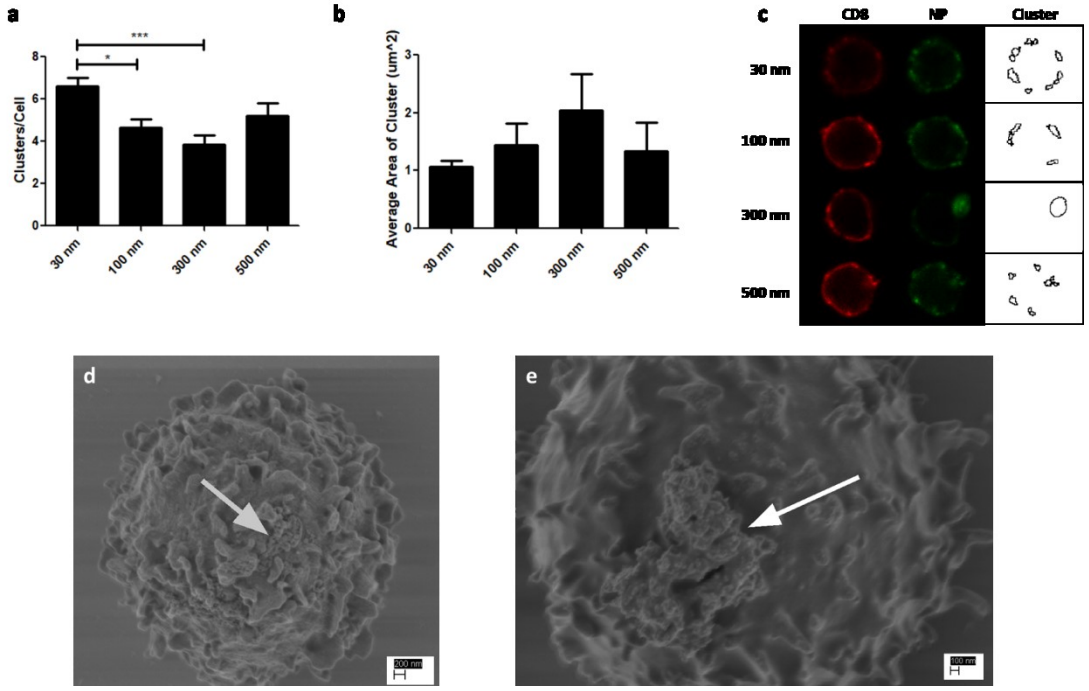

Figure 5-5. *Number of nanoparticle clusters per cell is affected by particle size. (a) 100 nm and 300 nm particles produce significantly fewer numbers of clusters per cell than 30 nm particles. (b) 300 nm particles trend toward a larger average cluster size per cell. Significance for (a,b) measured by one-way ANOVA with Tukey's post-test. (c) Representative confocal images show CD8 (red), nanoparticles (NP; green), and cluster identification for each size nanoparticle. 15-25 cells per condition were analyzed. SEM Imaging shows clusters of 30 nm particles (d) and 300 nm particles (e) on the surface of CD8+ T cells. (*p<0.05, ***p<0.001)*

5.3.3 Dependence of signal co-clustering

To study the importance of clustering both signal 1 and signal 2, we synthesized nanoparticles from paramagnetic or non-paramagnetic materials to control which particles, and thus which signals, co-cluster when a magnetic field is applied. While it is known that during endogenous T cell activation the signal 1 and CD28 molecules co-localize within the immune synapse,[212,213] since our platform utilizes external forces to co-cluster the molecules it may intrinsically change the properties of activation and alter the requirement for co-clustering of signal 1 and signal 2 molecules.

Db-gp100 dimer and anti-CD28 mAb were separately conjugated to the surface of 100 nm paramagnetic iron-dextran particles, or 100 nm non-paramagnetic polystyrene particles (**Figure 5-6**). Each type of signal 1 only and signal 2 only particle were combined with PMEL CD8+ T cells within a magnetic field to produce co-clustering of the signaling molecules, signal 1 or 2 only clustering, or no clustering of either signaling molecule (**Figure 5-7A, schematic**).

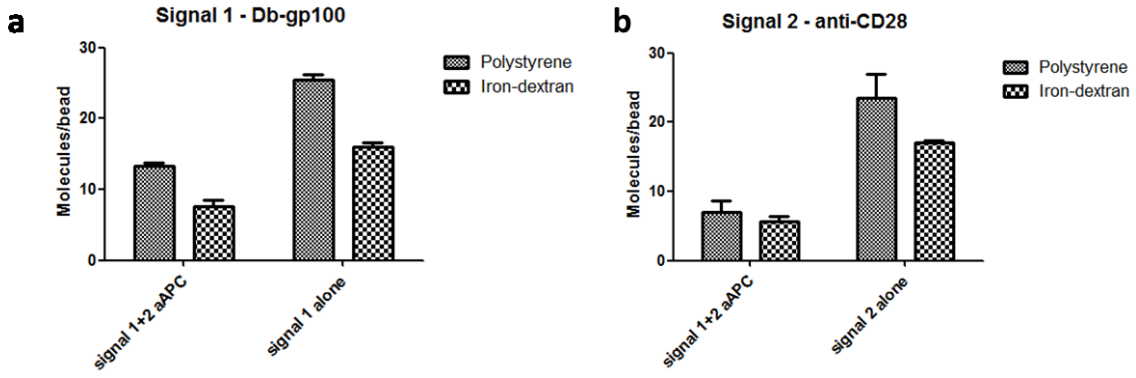

Figure 5-6. *Polystyrene and iron-dextran nanoparticles have similar protein densities. 100 nm diameter polystyrene particles had the same or greater amounts of signal 1 pMHC dimer (a) and signal 2 anti-CD28 mAb (b) conjugated to their surface as 100 nm diameter iron-dextran particles. Analysis performed on three independent samples.*

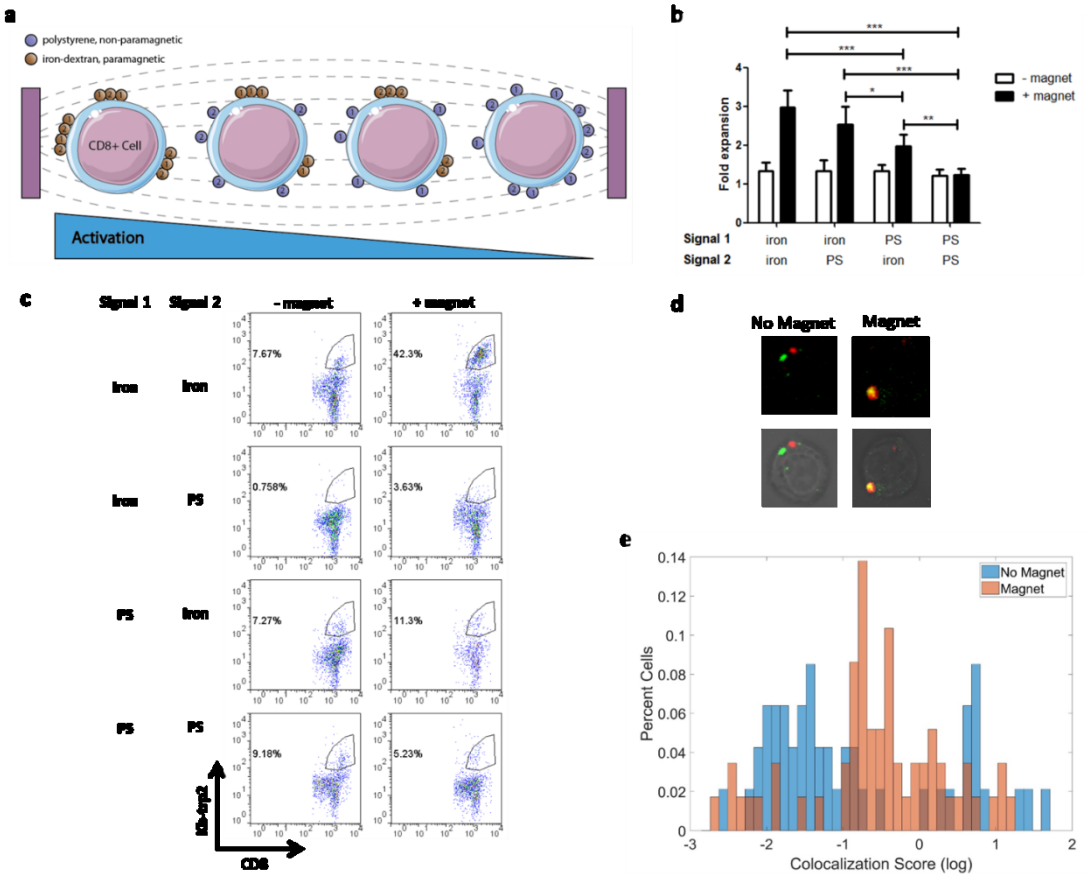

Figure 5-7. *Signal 1 and signal 2 only nanoparticles must be co-clustered on the cell surface for efficient CD8+ T cell activation. (a) Schematic of stimulatory conditions and subsequent CD8+ T cell activation measured in (b). (b) PMEL CD8+ T cells were stimulated with signal 1 only Db-gp100 and signal 2 only anti-CD28 nanoparticles with either an iron or polystyrene (PS) core. Cells were counted after seven days. The greatest proliferation was measured when both signal 1 and signal 2 were presented on paramagnetic iron-dextran particles. Significance measured by two-way ANOVA with Bonferroni post-test. (c) C57BL/6 CD8+ T cells were stimulated with separately conjugated Kb-trp2 signal 1 only and anti-CD28 signal 2 only particles with an iron or polystyrene core. Cells were stained for CD8 and Kb-trp2 cognate dimer after seven days. When both signals were presented on iron-dextran particles, there was a maximum of 42.3% Kb-trp2+ CD8+ T cells. (d) Naïve PMEL CD8+ T cells were incubated with fluorescently labeled Db-gp100 signal 1 only (red) and anti-CD28 signal 2 only (green) nanoparticles for 60 min +/- a magnetic field. Representative confocal images are shown. (e) Cells incubated +/- magnetic field were analyzed and each given a colocalization score quantifying the colocalization between signal 1 and signal 2 particles (see Materials and Methods). Cells incubated within a magnetic field had significantly higher colocalization between signal 1 and signal 2 measured by a Mann-Whitney test ($p=0.0401$). (*$p<0.05$, **$p<0.01$, ***$p<0.001$)*

Optimal expansion occurred when both signals were co-clustered on the surface of iron-dextran particles and decreased when either signal was presented on non-

paramagnetic polystyrene particles (**Figure 5-7B**). Clustering of signal 1 alone decreased cell expansion by approximately 17% and clustering of signal 2 alone decreased cell expansion by approximately 33%. All conditions resulted in little to no expansion in the absence of magnet-induced clustering.

While transgenic T cells provide an important tool for proof-of-principle validation studies, they do not fully recapitulate endogenous naïve T cell activation. Thus, we sought to assess the clustering of signal 1 and signal 2 on the separate nanoparticle platform to expand endogenous T cell populations from naïve wild-type mice. To study this, we conjugated the Kb-trp2 pMHC dimer or anti-CD28 mAb to the surface of iron-dextran or polystyrene 100 nm particles, as above. CD8+ T cells were expanded over the course of one week with each combination of paramagnetic and non-paramagnetic signal 1 and signal 2 only particles in a magnetic field.

After seven days of stimulation, CD8+ T cells were harvested and analyzed (**Figure 5-7C**). When both signal 1 and 2 were clustered on iron-dextran particles, over 40% of cells were specific for Kb-trp2. This is an increase in specificity of up to 400,000-fold, as the estimated pre-curser frequency for Kb-trp2 is approximately 10-100 cells per 10 million, or 0.001-0.0001%.[214] This decreased to less than 12%, a greater than one third reduction, when signal 1 and/or 2 was not clustered on polystyrene particles, indicating the necessity for co-clustering of the signals in endogenous CD8+ T cell expansion.

Next, we sought to visualize and quantify the co-clustering of signal 1 and signal 2 particles in the presence and absence of a magnetic field. Fluorescently labeled Db-gp100 (red) and anti-CD28 (green) particles were co-incubated with naïve PMEL CD8+ T cells for one hour in the presence or absence of a magnetic field. Cells were then fixed

and analyzed by confocal microscopy. Visually, it was evident that the two types of particles were co-clustered when incubated within a magnetic field (**Figure 5-7D**). Co-clustering was quantified in Matlab by assigning each cell from each condition a co-localization score that indicates the level of clustering between the two particle types at the cell level, with a higher co-localization score indicating increased clustering (*see 5.2.7 Matlab clustering analysis*). The median co-localization score for cells within a magnetic field was more than double that for cells in the absence of a magnetic field—0.560 and 0.271, respectively—and the two groups differed significantly by a Mann-Whitney test (**Figure 5-7E**).

5.3.4 Increased expansion of antigen-specific endogenous CD8 cells

We have shown previously that paramagnetic nano-aAPC can be used to enrich for clonal populations of CD8+ T cells from an endogenous repertoire on a magnetic column prior to *in vitro* expansion.[194] Enrichment prior to expansion reduces the competition for cytokines and MHC binding and has been shown to increase the expansion of cognate CD8+ T cells greater than 10-fold over non-enriched cells.[194] However, traditional aAPC are conjugated with anti-CD28 mAb in addition to the cognate signal 1 molecule and thus may lead to non-specific binding and decreased enrichment potential. We hypothesized that since we can separate signal 1 and signal 2 on the nanoparticle platform, the separate particle platform could be utilized to obtain more highly enriched cells with the use of signal 1 only particles, followed by the addition of signal 2 particles to stimulate expansion.

We first modeled the difference in enrichment potential of traditional aAPC versus signal 1 only particles in PMEL CD8+ T cells. To study this, fluorescently labeled

naïve PMEL CD8+ T cells were doped into CD8+ T cells from a naïve C57BL/6 mouse at a 1:1000 ratio. aAPC expressing both Db-gp100 and anti-CD28 or Db-gp100 alone were then used to enrich for the cognate PMEL CD8+ T cells, normalized by the total amount of Db-gp100. Signal 1-only particles resulted in a final purity of 1% PMEL CD8+ T cells, a 10-fold enrichment over the original cell mixture (**Figure 5-8A**). Traditional aAPC enriched PMEL CD8+ T cells to a final purity of only 0.5%, 50% less than signal 1 alone. Non-cognate particles did not enrich for PMEL CD8+ T cells. Both signal 1 alone and traditional aAPC resulted in approximately 80% or more recovered PMEL CD8+ T cells (**Figure 5-9**).

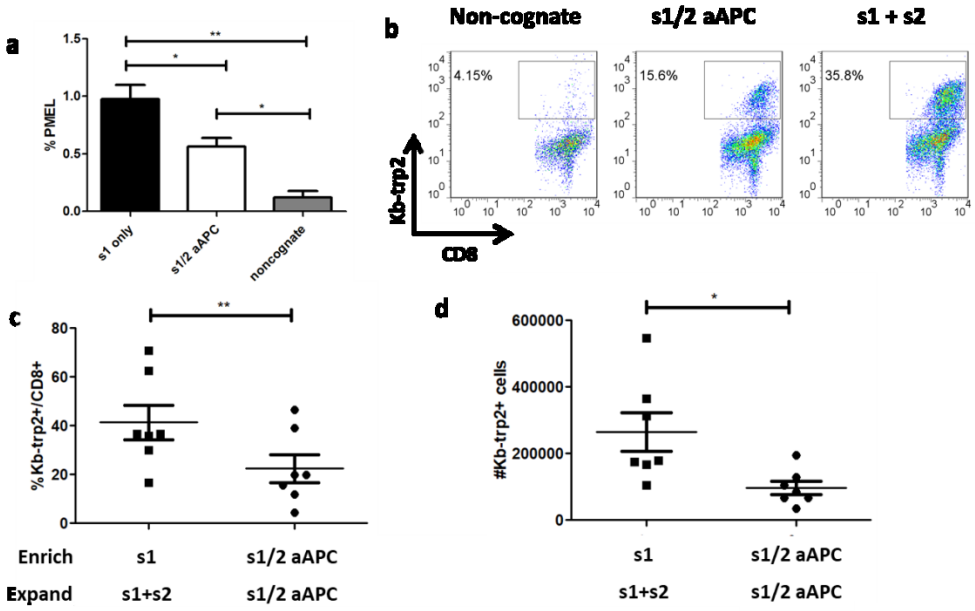

Figure 5-8. *Separate particle platform results in greater expansion of functional cognate CD8+ T cells. (a) Thy1.1+ TCR transgenic PMEL CD8+ T cells were doped into Thy1.2+ wild type C57BL/6 CD8+ T cells at a 1:1000 ratio. Cell mixture was enriched with signal 1 only Db-gp100 particles, signal 1/2 Db-gp100/anti-CD28 aAPC, or noncognate aAPC. Signal 1 only enrichment resulted in a final purity of approximately 1% cognate PMEL cells, while signal 1/2 aAPC had a final purity of approximately 0.5%. Noncognate cells did not enrich for PMEL cells. Significance measured by one-way ANOVA with Tukey's post-test. (b) C57BL/6 cells were enriched and expanded with Kb-trp2 signal 1 dimer presented on traditional aAPC or the separate particle platform within a magnetic field. Representative staining shows that separate particle platform increases the percentage of expanded cognate cells from an endogenous response after seven days. (c) Percent of cognate dimer positive cells seven days post enrichment and expansion. (d) Number of Kb-trp2+ CD8+ T cells seven days post enrichment per one million expanded CD8+ T cells. Significance measured by two-tailed paired t-test of seven independent experiments. (*p<0.05, **p<0.01)*

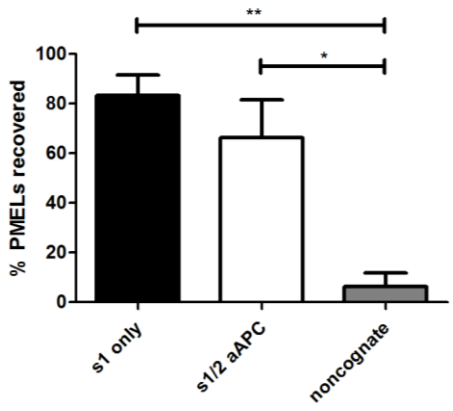

Figure 5-9. *Percent recovery of cognate T cells is equivalent with aAPC and separate particle platform. Enrichment with signal 1 only or traditional signal 1/2 aAPC recovered a similar amount of total PMEL CD8+ T cells, approximately 70-80%. Significance measured by one-way ANOVA with Tukey's post-test. Data combined from three independent experiments. (*p<0.05, **p<0.01)*

Next, we sought to determine if the increased enrichment by signal 1 only particles corresponds with a greater expansion of endogenous CD8+ T cell populations from naïve C57BL/6 mice by the separate particle platform compared to traditional aAPC. CD8+ T cells isolated from naïve C57BL/6 mice were enriched with either traditional aAPC or signal 1 only Kb-trp2 particles. Anti-CD28 mAb signal 2 only particles were added to cells enriched with signal 1 only Kb-trp2 particles, and both traditional aAPC and separate signal 1 and 2 particle cultures were expanded in a magnetic field for one week. All cultures were normalized by the total amount of signal 1 and 2 which were present at an approximate 1:1 molar ratio.

After one week, cells were harvested, counted, and stained with Kb-trp2. Cells enriched with signal 1 only particles then expanded with signal 1 and signal 2 only particles contained 35.8% Kb-trp2+ cells, more than double that of traditional aAPC, 15.6% (**Figure 5-8B**). This effect was consistent in multiple independently repeated experiments (**Figure 5-8C**) as well as with different signal 1 peptides (**Figure 5-10**). The

total number of Kb-trp2+ cells also increased nearly 2-fold when enriched and expanded with the separate particle platform (**Figure 5-8D**).

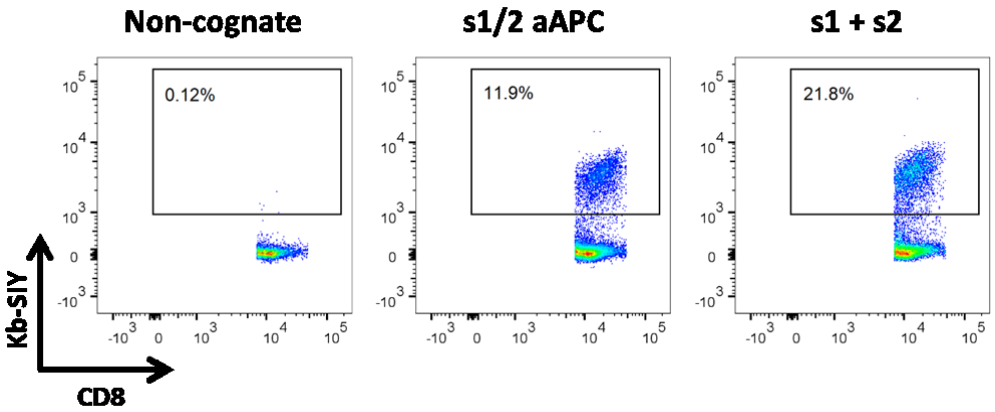

Figure 5-10. *Separate particle platform improves T cell expansion against various antigens. Endogenous C57BL/6 CD8+ T cells were enriched and expanded with Kb-SIY signal 1 dimer presented on traditional s1/2 aAPC or the separate particle platform within a magnetic field. Representative staining shows that the separate particle platform approximately doubles the percentage of expanded Kb-SIY+ cognate cells from an endogenous response after seven days.*

The functionality of the cells expanded by the separate particle platform was assessed by measuring cytokine secretion and degranulation markers. Seven days after stimulation, the cells were harvested and re-stimulated with trp2-pulsed RMA-S cells and cytokine secretion and CD107 expression, a degranulation marker, was measured. Cells expanded with the separate particle platform secreted the same or higher level of all cytokines measured—IFN-γ, IL-2, and TNF-α—and had equivalent expression of CD107 (**Figure 5-11**). Thus, the separate particle platform results in greater expansion of highly functional antigen-specific CD8+ T cells compared to traditional aAPC.

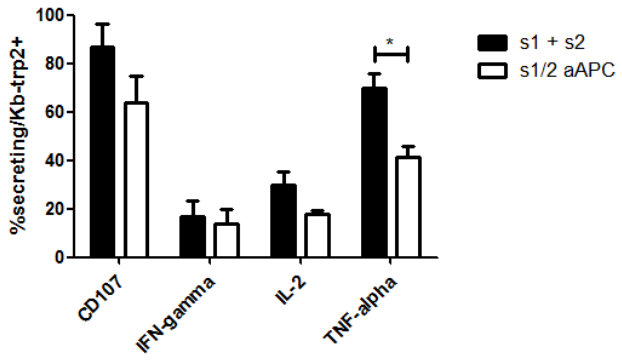

Figure 5-11. *Separate particle platform results in greater or equal T cell cytokine secretion. Shown is the percent of cognate dimer positive cells secreting cytokines after seven day enrichment and expansion with traditional s1/2 aAPC or separate particle platform (s1 + s2). Separate particle platform results in significantly greater TNF-α secretion and equivalent secretion of all other cytokines as compared with traditional aAPC. Data combined from three independent experiments. (*p<0.05)*

5.3.5 High throughput co-stimulatory molecule customization

A valuable goal of the development of this platform is the ability to easily customize the type, combination, and specific ratios of co-stimulatory signal 2 molecules during CD8+ T cell expansion. We thus sought to use the separate particle platform to investigate how altering co-stimulatory molecule type and ratio affects endogenous CD8+ T cell expansion and phenotype. Four stock particle types were synthesized expressing anti-CD3, anti-CD28, anti-4-1BB, or anti-CD27 mAb. Anti-CD3 bypasses the pMHC-TCR recognition and was used as the signal 1 to stimulate endogenous polyclonal CD8+ T cells.

CD8+ T cells were isolated from C57BL/6 mice on day 0 and incubated with signal 1 particles and a constant total amount, but varied ratio, of anti-CD28 and anti-4-1BB mAb signal 2 particles within a magnetic field. After seven days, total cell counts were recorded. Despite the total amount of signal 2 in all stimulatory conditions being equivalent, changing the ratio of signal 2 molecules significantly impacted CD8+ T cell proliferation (**Figure 5-12A**). All combinations of anti-CD28 and anti-4-1BB resulted in

equivalent or greater CD8+ T cell expansion than either signal 2 molecule alone. At a 75/25% ratio of anti-CD28/anti-4-1BB, CD8+ T cells reached nearly 13-fold expansion, approximately 50% more proliferation than anti-CD28 alone and 95% more than anti-4-1BB alone. Also of note, signal 1 alone induced little to no cell proliferation of endogenous antigen-specific CD8+ T cells. Similarly, we showed how the separate particle platform allows for streamlined signal 2 customization by also testing various combinations of anti-CD28 and anti-CD27 mAb during a seven day activation. Interestingly, at a 50/50% ratio of anti-CD28/anti-CD27 mAb, there was a significant increase in the number of CD8+ T cells with a memory phenotype despite no significant difference in total CD8+ T cell expansion (**Figure 5-13**). This data indicates that altering signal 2 composition can impact skewing toward specific T cell subsets in addition to overall expansion.

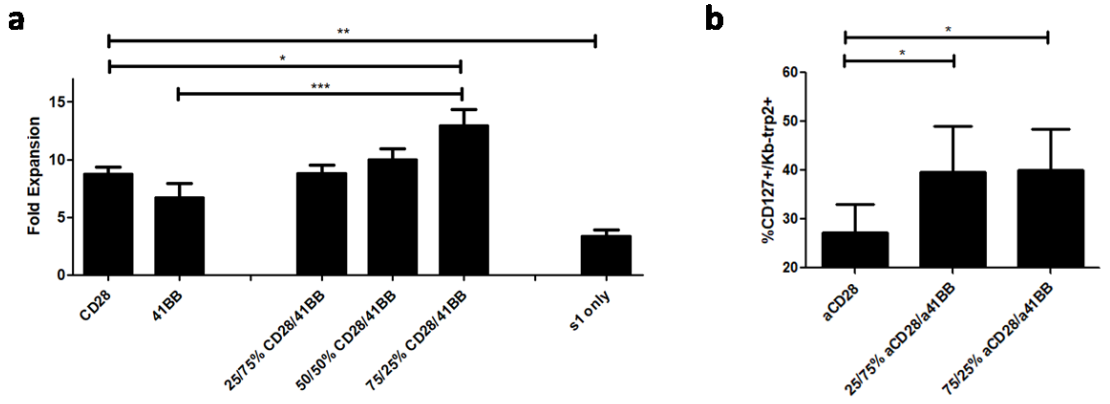

Figure 5-12. *Separate particle platform allows for manipulation of co-stimulatory signal 2 composition. (a) Naïve CD44^{lo} CD8+ T cells from C57BL/6 mice were stimulated for seven days with separate particle platform. Anti-CD3 mAb was used as signal 1, and anti-CD28 and/or anti-4-1BB mAb were used as signal 2. Total signal 2 amount remained constant, only ratio varied. A 75/25% anti-CD28/anti-4-1BB ratio significantly increased expansion over either signal 2 alone. (b) C57BL/6 cells were enriched and expanded with Kb-trp2 signal 1 dimer presented on the separate particle platform within a magnetic field. Signal 2 ratio varied as in (a). On day seven, cells were harvested and stained for Kb-trp2 and CD127. The addition of anti-4-1BB significantly increased the percent of Kb-trp2+ cells expressing CD127. Significance measured by one-way ANOVA with Dunnett's post-test. (*p<0.05, **p<0.01, ***p<0.001)*

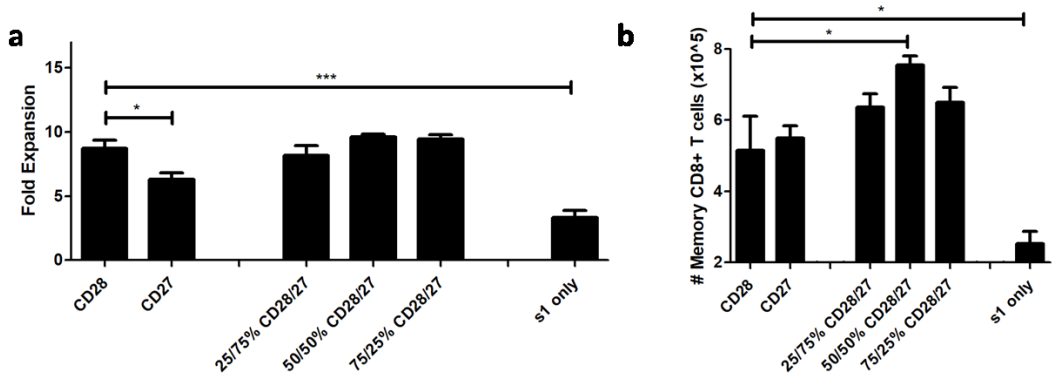

Figure 5-13. *Separate particle platform enables customization of co-stimulation. (a) CD8+ T cells from C57BL/6 mice were stimulated for seven days with separate particle platform. Anti-CD3 mAb was used as signal 1, and anti-CD28 and/or anti-CD27 mAb were used as signal 2. Total signal 2 amount remained constant, only ratio varied. Significance measured by one-way ANOVA with Dunnett's post-test. (b) Resultant CD8+ T cells were stained for CD62L and CD44 on day seven post activation. The percentage of memory ($CD44^{hi}CD62L^{hi}$) CD8+ T cell responders were assessed. At a 50/50% ratio of anti-CD28/anti-CD27 mAb, there is a significant increase in the number of memory CD8+ T cells. Significance to anti-CD28 alone is measured by one-way ANOVA with Dunnett's post-test. Data from three independent experiments combined. (*p<0.05, ***p<0.001)*

Finally, we assessed the ability to use the separate particle platform to study how different signal 2 ratios change T cell phenotype when expanding endogenous antigen-specific CD8+ T cells. C57BL/6 mice were enriched with signal 1 only Kb-trp2 particles, and different ratios of anti-CD28 and anti-4-1BB mAb signal 2 only particles were added during expansion, as above.

Both a 25/75% and 75/25% ratio of anti-CD28 and anti-4-1BB mAb increased the expression of CD127, the IL-7Rα chain, on Kb-trp2+ CD8+ T cells compared to anti-CD28 alone (**Figure 5-12B**). Signaling CD8+ T cells through 4-1BB has previously been shown to increase CD127 expression in CD8+ T cells and may be indicative of cells with a memory rather than exhausted phenotype.[215] Thus, the separate particle platform presents a streamlined method to customize stimulatory conditions to optimize the phenotype of T cells for immunotherapeutic applications.

5.3.6 Co-stimulatory molecule selection impacts memory formation *in vivo*

Our *in vitro* data indicated that a 75/25% ratio of CD28/4-1BB co-stimulation improves the expansion and skews toward a memory phenotype of CD8+ T cells. Thus, we sought to assess the ability of the separate particle platform to extend the persistence of adoptively transferred antigen-specific CD8+ T cells *in vivo* and demonstrate a therapeutic use case.

CD8+ T cells were isolated from Thy1.2+ C57BL/6 mice and stimulated *in vitro* with Kb-trp2/anti-CD28 traditional aAPC, identical signals on the separate particle platform, or the separate particle platform with a 75/25% ratio of anti-CD28/anti-4-1BB. After one week, expanded cells were injected retro-orbitally into Thy1.1+ C57BL/6 mice and mice were treated with IL-2 on the day of and day after transfer. Short-term and long-term persistence of the cells were analyzed by sacrificing mice 7 and 21 days post-adoptive transfer and staining for Th1.2+ cells.

At twenty-one days after adoptive transfer, cells stimulated with the optimal anti-CD28/anti-4-1BB signals were detected at significantly higher levels than either other stimulus (**Figure 5-14**). The frequency of the transferred cells was approximately 5-fold higher in the spleen and 10-fold higher in the lymph node than traditional aAPC or the separate particle platform with anti-CD28 alone. There were no significant differences in the blood on day 21, or in any organs on days 3 or 7 (data not shown). Thus, the separate particle platform enables the stimulation of more optimal CD8+ T cells for adoptive transfer.

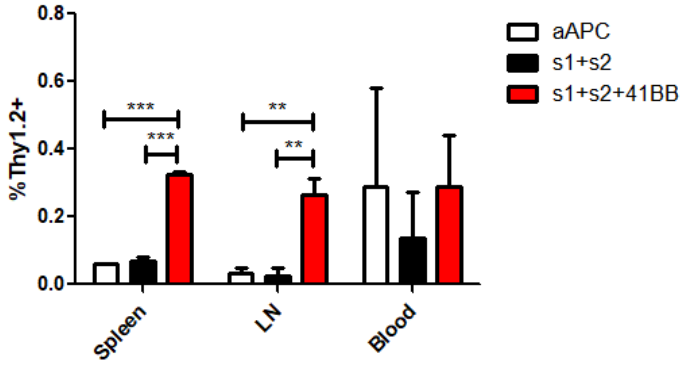

Figure 5-14. *Separate particle platform activates optimal CD8+ T cells for adoptive cell transfer. CD8+ T cells from Thy1.2+ C57BL/6 mice were activated in vitro with Kb-trp2/anti-CD28 traditional aAPC (aAPC), separate particle platform (s1+s2), or separate particle platform with a 75/25% ratio of anti-CD28/anti-4-1BB. After seven days, expanded cells were injected retro-orbitally into Thy1.1+ C57BL/6 mice. Adoptively transferred cells activated with anti-4-1BB on the separate particle platform were present at significantly higher frequencies than either other stimulus on day 21 post transfer. Significance in each organ was analyzed by a one-way ANOVA with Tukey's post-test (**p<0.01, ***p<0.001).*

5.4 Discussion and conclusions

Here, we have developed and validated a system that can combine high throughput synthesis of single-molecule paramagnetic "aAPC" with magnetic fields to demonstrate a reductionist platform capable of studying and optimizing T cell activation. While upcoming cancer immunotherapies such as adoptive cell transfer are promising for generating patient-specific cytotoxic T cell responses, approaches that use homogenous microscale aAPC cannot take full advantage of the nanoscale organization and co-stimulus diversity that has demonstrated importance in generating long-lived functional T cell populations. Additionally, few platforms exist that enable the more fundamental study of T cell co-stimulus clustering in a three-dimensional system. We show proof of concept for this platform to easily customize co-stimulatory signals, study the clustering of signaling molecule clustering during activation, and isolate and activate higher purity endogenous T cell populations.

Various recent studies have shown the impact of the composition of co-stimulatory molecules on the expansion and phenotype of activated T cells. Simply changing the ratio of co-stimulatory molecules without altering the total amount of signal on aAPC can impact the expansion of T cells.[10] The previous approach to study co-stimulus composition on three dimensional platforms involves synthesizing new aAPC for each condition.[6,10] This limits throughput and can present difficulty in accurately studying such effects as it has been documented that unexpected experimental artifacts in the preparation of aAPC with defined ratios of molecules are common.[206] The separate particle platform simplifies nanoparticle synthesis and quality control assessment while maintaining a similar, if not higher, level of T cell activation. The importance of co-stimulatory signal medication was further emphasized *in vivo* where the separate particle platform with a specific anti-CD28/anti-4-1BB ratio significantly extended the persistence of adoptively transferred CD8+ T cells.

This platform allowed us to easily investigate ten different co-stimulatory conditions, whereas previous reports have investigated five or fewer.[6,10] We demonstrated proof of concept for ability to alter the frequency and phenotype of CD8+ T cells by incorporating anti-4-1BB and anti-CD27 mAbs at defined ratios, although it could easily be extended to study additional conditions. This platform also provides a technique to customize co-stimulation on a case-by-case basis. For example, it can be hypothesized that in the future of adoptive cell therapy, one may wish to co-stimulate with molecules that synergize with checkpoint blockade[5] in some patients, but molecules that improve expansion and function in the presence of signal 1 alone in others.[6,7] Information gained about co-stimulatory requirements using this approach may also help to guide

optimization of approved therapies such as CAR T cells in terms of which co-stimuli to incorporate.

In addition to providing a mechanism for high-throughput co-stimulus customization, by design, this platform also enables the three-dimensional study of signal co-clustering. Prior studies that manipulate signal clustering at the nanoscale often utilize two dimensional platforms that poorly simulate endogenous activation.[18,48] By incorporating the separate signaling molecules on different sized paramagnetic and non-paramagnetic particles, we showed that pMHC and anti-CD28 require co-clustering at length scales smaller than 500 nm. This size-dependent effect did not seem to be associated with a change in cluster size, as 30 nm particles did not result in any significant change in cluster size or number as compared to 500 nm particles. However, all particles resulted in cluster sizes that average 1 μm^2 or greater, correlating with a cluster radius greater than 500 nm. It is likely that the magnetic field-induced clustering decreases the degree of particle internalization by the T cells and thus prolongs extracellular activation time, especially of the 30-100 nm particles, as it has been shown that particles with diameters of 40-60 nm have the shortest internalization time.[216] Likewise, this approach can be used to investigate clustering requirements for less studied co-stimulatory or co-inhibitory molecules. While some previous reports analyzed 4-1BB co-localization at the immune synapse during T cell activation,[217] little to no information is known about the clustering of other co-stimulatory molecules such as CD27, CD40L, and OX40.

Finally, the separate particle platform results in greater expansion of specific T cell clones from an endogenous repertoire. Previous work from our lab established an

Enrichment and Expansion protocol to enrich for specific CD8+ T cell clones using paramagnetic aAPC prior to expansion.[194] The success of enrichment prior to expansion was demonstrated to be due to reduced competition for growth factors and pMHC binding and results in approximately a 10-40-fold increase in frequency after one week compared to expansion alone. Likewise, we showed that by further increasing enrichment using particles that only have cognate signal 1 molecule followed by the addition of co-stimulatory particles for expansion, we further doubled the frequency and total number of activated cognate CD8+ T cells. This is especially relevant as next generation expansion protocols could incorporate other co-stimulatory molecules that are not specific to the T cells of interest and would decrease enrichment. This platform enables a mechanism to eliminate that obstacle.

Because magnetic clustering is required to stimulate T cells with this platform, it is likely that this approach would be limited to *in vitro* stimulation protocols. This may include serving as a tool for assessing T cell activation conditions or customizing conditions for adoptive cell transfer where *ex vivo* stimulation is required. We have demonstrated the ability of this platform to activate all T cells or specific T cell subsets depending on the type of signal 1 stimulation. For adoptive cell therapy, this separate particle approach could be used to activate specific T cell populations using an MHC-Ig dimer loaded with a specific tumor peptide, or could be used in combination with anti-CD3-coated particles to non-specifically activate T cells in a more high-throughput manner. Additionally, we have only studied how changes in co-stimulation composition and clustering impact murine T cell activation. It is likely that co-stimulatory composition differentially affects expansion of murine and human T cells, and the

efficacy of this approach for stimulating human T cells needs to be investigated. Finally, it is important to note that in contrast to other methods, this separate particle approach creates homogenous single signal “islands” which may not directly translate to a homogenous distribution of the molecules. Further studies need to be performed to investigate how these too approaches compare in the context of T cell activation.

We have developed a reductionist T cell activation platform that simplifies and streamlines customized co-stimulatory conditions. This platform is a robust tool for the study of the composition and clustering of signaling molecules for T cell activation by altering particle size, material, and molecules conjugated to their surface. This will allow for further study of T cell signal clustering and composition to better understand the signaling pathways as well as optimize activation for cell-based immunotherapies such as adoptive cell transfer.

Chapter 6. Improving the Efficacy of Biodegradable Artificial Antigen Presenting Cell Platforms[3]

6.1 Introduction

Biomimetic materials that target the immune system hold promise for cancer immunotherapy.[218] Synthetic immunotherapies can be designed with defined characteristics and therefore often outperform their cell-based counterparts. These platforms can be engineered in terms of biodegradability,[87] controlled release of immuno-modulators,[219] and physical parameters including shape and size.[65] Biomimetic materials can be customized to incorporate combination therapies in an all-in-one therapeutic and are therefore an exciting platform for the future of cancer immunotherapy. Despite their potential, current development of combinatorial immunotherapies utilizing biomaterials has been limited as their interaction with other existing therapeutics must first be understood.

Synthetic artificial antigen presenting cells (aAPC), a biomaterial-based immunotherapy, have shown success in generating an anti-tumor immune response *in vitro* and *in vivo*.[70,75,205,220] aAPC are three-dimensional platforms that minimally express the two signals required for T cell activation – a signal 1, peptide-MHC (pMHC) to provide T cell receptor (TCR) specificity, and a signal 2, such as anti-CD28 monoclonal antibody (mAb) to provide the co-stimulatory "go" signal. aAPC can be functionalized

[3] Sections of this chapter reprinted (adapted) from "Kosmides, A.K.*, Meyer, R.A.*, Hickey, J.W., Aje, K., Cheung, K.N., Green, J.J., and Schneck, J.P. Biomimetic Biodegradable Artificial Antigen Presenting Cells Synergize with PD-1 Blockade to Treat Melanoma. *Biomaterials* **2017**, *118*, 16-26."
*authors contributed equally

with tumor-specific pMHC to activate a patient's immune system against cancer antigens and mediate tumor rejection.[71,72,221] They can be utilized in adoptive cell transfer (ACT) of *ex vivo* activated autologous T cells[68,71,222] or directly administered intravenously (IV) for *in vivo* anti-tumor T cell activation.[200,223] Synthetic aAPC platforms have distinct advantages over cellular systems in terms of long-term storage and the ability to optimize T cell activation and biocompatibility.[224] Unlike biological antigen presenting cells used as cellular therapy, biomaterial-based aAPC have the advantage of being able to maintain an "always on" state that cannot be down-regulated by the microenvironment as well as flexibility for manufacturing as an acellular product. Compared to poly(lactic-*co*-glycolic acid) (PLGA)-based drug delivery particles for cancer therapy, the anti-cancer drugs must reach and destroy every cancer cell to ultimately be effective. In contrast, PLGA-based aAPC particles for immunotherapy need only reach tumor specific T cells that can recognize the tumor antigen for the aAPC to then be able to direct a robust systemic immunotherapy response against the cancer cells. Biomimetic modifications of PLGA-based aAPC materials that greatly enhance their effector capacity, including controlling the shape of the aAPC[65,66] or slowly releasing pro-inflammatory cytokines from their core,[54,97] have demonstrated the benefit of bringing novel materials engineering concepts to the development of immunotherapeutics.

In addition to amplifying positive regulators of the immune system, inhibiting negative regulators has also shown success in generating anti-tumor immune responses. Checkpoint molecules, including programmed death 1 (PD-1) and CTLA-4, are negative regulators of T cell function. These molecules are upregulated on tumor infiltrating lymphocytes and on activated T cells expanded during ACT, being described as a

rheostat of the immune system.[39] PD-1 signaling inhibits CD8+ T cell effector function upon ligation with its ligand, programmed death ligand 1 (PD-L1), and is one of the methods by which tumors escape immune surveillance. Checkpoint blockade with monoclonal antibodies against PD-1 and PD-L1 delay tumor growth in murine tumor models,[168,187] and FDA approved monoclonal anti-PD-1 and anti-CTLA-4 antibodies have shown significant overall response rates and long-term survival benefits. However, clinical responses only reach approximately 30%[41,189–191] indicating that there is a necessity for improvement.

Single-targeted approaches have limited efficacy because cancerous cells utilize multiple mechanisms to avoid immune surveillance and the immune system internally suppresses prolonged strong activation.[28] The combination of checkpoint inhibitors with other immunotherapies that boost T cell effector functions or promote cancer cell recognition by the immune system have potential to increase anti-tumor effectiveness. Checkpoint blockade in conjunction with T cell costimulatory antibodies resulted in tumor regression in multiple murine tumor models[43,44,170] and increased effector functions of exhausted CD8+ T cells by forcing them out of quiescence.[5] These studies suggest that checkpoint blockade can boost the effects of other immune-stimulatory approaches, although their interaction with biomaterial-based antigen-specific T cell stimulation has not been studied.

Here, we investigate the synergy between a biomimetic material, biodegradable PLGA-based aAPC, and anti-PD-1 monoclonal antibody treatment for the activation of tumor-specific CD8+ T cells. Combinatorial treatment enhances CD8+ T cell effector functions *in vitro* and significantly delays tumor growth *in vivo*. These results

demonstrate the effectiveness of PLGA-based aAPC in combination immunotherapy, and identify a molecule that could potentially be incorporated and released from polymeric aAPC for increased effectiveness.

6.2 Methods

6.2.1 Artificial antigen presenting cell synthesis and characterization

PLGA artificial antigen presenting cells were synthesized in a two-step core particle formation and functionalization. Particles cores were synthesized from poly (lactic-co-glycolic acid) (PLGA 50:50 lactic acid to glycolic acid ratio, MW 34,000-58,000 Da) that was purchased commercially (Sigma Aldrich; St. Louis, MO). For a typical microparticle synthesis, 100 mg of PLGA was dissolved in 5 mL dichloromethane and homogenized into a 50 mL, 1% poly vinyl alcohol (PVA) solution by an T-25 digital ULTRA-TURRAX IKA tissue homogenizer at a speed of 5,000 rpm (IKA Works; Wilmington, NC). The resulting microparticle emulsification was then added to 100 mL of 0.5% PVA solution. The dichloromethane was then allowed to evaporate over the course of 4 hrs. After particle hardening, the particles were washed three times in water through centrifugation at 3000 g for 5 min. The washed microparticle solution was flash frozen in liquid nitrogen and lyophilized for 1 day prior to characterization and use.

PBAE/PLGA aAPC were synthesized by mixing PLGA and PBAE at defined ratios during the emulsion process. Briefly, PBAEs were synthesized by polymerizing a base chain diacrylate group and a hydroxyl amine in solvent free conditions at 90 °C. The terminal acrylate groups on the resulting PBAE were end capped with an amine coupled functional group to enhance the PBAE efficacy. PLGA was purchased at a 50:50 wt/wt ratio of monomers. PLGA/PBAE particles were synthesized by single emulsion at

a 3:1 PLGA:PBAE ratio with or without a fluorescent dye. After particle hardening, the particles were washed three times in water through centrifugation at 3000 g for 5 min. The washed microparticle solution was flash frozen in liquid nitrogen and lyophilized for 1 day prior to characterization and use.

Functionalization of both PLGA aAPC and PLGA/PBAE aAPC was achieved through EDC/NHS chemistry to conjugate carboxylic acid terminated PLGA to amines on the proteins of interest. Lyophilized particles were dissolved in 0.1 M MES buffer at pH 6.0 at a concentration of 2 mg/mL. 100 µL of EDC/NHS (Sigma Aldrich; St. Louis, MO) stock solution at 40 mg/mL and 48 mg/mL respectively were added to each sample and the particles were activated for 30 min. The resulting surface activated particles were washed in PBS through centrifugation at 5,000 g for 5 min. The particles were resuspended in PBS at 2 mg/mL. 8 µg MHC IgG dimer loaded with the antigen of choice and 10 µg anti-CD28 monoclonal antibody (mAb) (BD Biosciences; San Jose, CA) was added to each sample and the particles were allowed to react with the proteins overnight at 4 ºC. The resulting aAPC were washed 3x in PBS through centrifugation at 5,000 g and then dissolved in 400 µL of 100 mg/mL endotoxin free sucrose. The resulting suspension was then lyophilized overnight.

Particle imaging was conducted with a Leo FESEM scanning electron microscope. To prepare samples for analysis, lyophilized particles were mounted onto carbon tape (Nisshin EM Co.; Tokyo, Japan) and placed upon aluminum tacks (Electron Microscopy Services; Hatfield, PA). The excess particles were removed by blowing air across the surface of the tack and the sample was then sputter coated with a 20 nm thick

layer of gold-palladium. The samples were then loaded into the microscope and imaged. The images were processed in ImageJ to obtain size information.

To determine the amount of protein on the surface, conjugated aAPC microparticles were stained with Alexa Fluor 647 goat anti-mouse IgG for the dimer and Alexa Fluor 546 goat anti-hamster IgG for the anti-CD28 (Life Technologies; Grand Island, NY) for 1 hour at 4 °C. The particles were subsequently washed with PBS three times and fluorescence readings of particles were evaluated for fluorescence with a BioTek Synergy 2 plate reader (Biotek; Winooski, VT). The mass of protein on the particle was calculated to evaluate conjugation efficiency. Conjugation efficiency was calculated as (Protein Calculated on Particles)/(Protein Added to Conjugation Media) *100%.

6.2.2 Anti-PD1 monoclonal antibody synthesis

Anti-PD-1 mAb clone G4 was grown from the G4 hybridoma cell line. Hybridoma cells were grown in hybridoma serum free media supplemented with L-glutamine. After one week, the supernatant was harvested and run over a HiTrap protein G column (GE Healthcare, Little Chalfont, Buckinghamshire, UK), then eluted according to the manufacturer's protocol. G4 mAb was concentrated by membrane ultrafiltration with a Vivaspin 20 50 kDa MWCO (GE Healthcare) and concentration was measured by Nanodrop ND-1000 Spectrophotometer.

6.2.3 *In vitro* artificial antigen presenting cell T cell stimulation

To determine the effectiveness of the aAPC at stimulating antigen specific T cells, we used primary CD8+ T cells isolated from PMEL or 2C mouse splenocytes. All mice were maintained according to Johns Hopkins University's Institutional Review Board.

The mice were sacrificed and then the spleen was dissected out and homogenized through a cell strainer. The CD8+ T cells were then isolated using the Miltenyi CD8a+ Isolation Kit (Miltenyi; Auburn, CA). The cells were then stained with Vybrant Cell Tracker carboxyfluorescein succinyl ester (CFSE) (Life Technologies; Grand Island, NY) dye following the manufacturer's protocol. CFSE stained cells were incubated with the particle bearing the antigen of choice at a concentration of 1 mg, 0.1 mg, or 0.01 mg aAPC (polymer weight)/100,000 CD8+ T cells in RPMI supplemented with L-glutamine, non-essential amino acids, vitamin solution, sodium pyruvate, β-mercaptoethanol, 10% FBS, ciproflaxin, and a cocktail of T cell growth factors. CFSE dilution was then assessed after three days of incubation through flow cytometry analysis on a BD FACSCalibur. Each generation is defined as a distinct peak of the flow cytometry CFSE histogram, as the CFSE dye is diluted in half with each cell division. Generational analysis was assessed using the built in function in FlowJo (TreeStar). Total proliferation after seven days was assessed by cell counting on a hemocytometer and using a trypan blue exclusion test to exclude dead cells.

6.2.4 *In vitro* anti-PD-1 mAb functionality assay

To evaluate the functional effectiveness of the synthesized anti-PD-1 mAb, we utilized an *in vitro* assay of repeated CD8+ T cell stimulation to upregulate PD-1 expression, as PD-1 expression is low on naïve CD8+ T cells. On day 0, primary splenocytes were isolated from naïve 2C transgenic mouse (Jackson Labs; Bar Harbor, ME) spleens through cell straining. Cells were treated with 4 mL of ACK lysis buffer for 1 minute to lyse red blood cells. CD8+ T cells were isolated by negative selection with the Miltenyi CD8a+ Isolation Kit following the manufacturer's protocol (Miltenyi;

Auburn, CA). Micro anti-CD3 (145.2C11)/anti-CD28 (37.51) aAPC were synthesized on 4.5μm M-450 Epoxy Dynabeads (Life Technologies; Grand Island, NY) at a 1:1 protein ratio, following manufacturer's protocol. Anti-CD3 and anti-CD28 antibodies were purchased from BioXCell (West Lebanon, NH). 2C CD8+ T cells were mixed with micro aAPC at a 1:1 ratio and cultured in RPMI supplemented with L-glutamine, non-essential amino acids, vitamin solution, sodium pyruvate, β-mercaptoethanol, 10% FBS, ciproflaxin, and a cocktail of T cell growth factors. On day 4, additional T cell growth factors and anti-CD3/anti-CD28 beads were added at a 2:1 bead:cell ratio. On day 6, B16-SIY and B16-F10 cells were cultured in RPMI supplemented with L-glutamine, non-essential amino acids, vitamin solution, sodium pyruvate, β-mercaptoethanol, 10% FBS, ciproflaxin, and 20 ng/ml recombinant murine IFN-γ (R&D Systems, Minneapolis, MN) to upregulate PD-L1 expression.

On day 8, B16-F10 and B16-SIY were harvested and washed three times to remove all IFN-γ, as confirmed by ELISA. CD8+ T cells were also harvested, washed three times, and aAPC were removed with a magnet. PD-1 and PD-L1 expression was confirmed on CD8 and B16 cells by flow cytometry using fluorescently labeled anti-PD-1 and anti-PD-L1 antibodies (Biolegend). CD8+ T cells and B16-SIY or B16-F10 cells were mixed at a 1:1 effector target ratio in the presence of 10 μg/ml anti-PD-1 mAb or Armenian hamster IgG isotype control antibody. The cells were co-incubated for 18 hours at 37 ˚C, then supernatants were collected. IFN-γ was measured by ELISA using the ebioscience murine IFN-γ Ready-SET-Go! Kit (San Diego, CA).

6.2.5 *In vitro* anti-PD-1 mAb and aAPC assay

To evaluate the synergistic effect of aAPC and anti-PD-1 mAb treatment, we utilized an *in vitro* T cell and tumor cell co-incubation assay. CD8+ T cells were stimulated at a single earlier time-point prior to the start of the assay to allow for resting time before the secondary stimulation. On day -5, primary splenocytes were isolated from naïve 2C transgenic mouse (Jackson Labs; Bar Harbor, ME) spleens through cell straining, and incubated with a 1:1 ratio of anti-CD3/anti-CD28 microbeads as above. Additional T cell growth factors and media were added on day -2. On day -2, B16-SIY and B16-F10 cells were cultured in the presence of 20 ng/ml IFN-γ, as above. On day 0, B16-F10 and B16-SIY were harvested and washed three times to remove all IFN-γ, as confirmed by ELISA. 2C cells were also harvested, washed three times, and aAPC were removed with a magnet. Cells were stained with PE anti-PD-1, PE anti-PD-L1, PE anti-PD-L2, and isotype control antibody (Biolegend) and read on a BD FacsCalibur to confirm expression. CD8+ T cells and B16-SIY or B16-F10 cells were mixed at a 1:1 effector target ratio, and anti-PD-1 mAb and PLGA aAPC were added into culture at titrating amounts. The cells were incubated for 18 hours at 37˚, then supernatants were collected. IFN-γ was measured by ELISA using the ebioscience murine IFN-γ Ready-SET-Go! Kit (San Diego, CA).

6.2.6 *In vivo* particle and cell biodistribution study

To evaluate the influence of the combination of adoptively transferred cells on the biodistribution of our aAPC, we used near infrared (IR) fluorescence to track the aAPC upon intravenous administration. The particles and aAPC were synthesized as previously described except that 1 mg of a custom synthesized hydrophobic dye from LI-COR

biotechnologies fluorophore (LICOR Biosciences; Lincoln, NE) was added to the dichloromethane mixture to be encapsulated into the particles. Labeled aAPC were split up into two different treatment groups. For group 1, Thy 1.2+ C57BL/6 mice (Jackson Laboratories; Bar Harbor, ME) received intravenously 2 mg of the IR labeled aAPC alone. For group 2, Thy 1.2+ C57BL/6 mice received intravenously 2 mg of IR labeled aAPC with $1x10^6$ Thy1.1+ PMEL CD8+ T cells that had been pre-incubated for 1 hour at 4 °C. Blood was collected retroorbitally at 10, 20, 30, and 40 min post injection to monitor elimination from the bloodstream and was imaged in the LI-COR Pearl Impulse. At 24 hours, mice were sacrificed and the liver, kidney, spleen, heart, and lung were dissected out and imaged in the LI-COR Pearl Impulse (LICOR Biosciences; Lincoln, NE) to determine biodistribution of the particles over 24 hrs. All fluorescence was quantified by ImageJ for normalized measurements of particle concentration. For retroorbital bleeds, the data for each mouse was normalized to the fluorescence value of the initial time point collected. This data was then fit to a single exponential decay curve using the GraphPad non-linear regression analysis module (GraphPad Software; La Jolla, CA). For organ distribution, the fluorescence readings were normalized to the sum of the fluorescence values across all organs to get a percent distribution across the organs analyzed.

6.2.7 *In vivo* tumor treatment study

To evaluate the efficacy of dual treatment *in vivo* we utilized an adoptive immunotherapy murine melanoma treatment model. Thy 1.2+ C57BL/6 mice (Jackson Laboratories; Bar Harbor, ME) were inoculated subcutaneously on the right flank with $3x10^5$ B16-F10 melanoma cells four days prior to treatment. One day prior to treatment,

the mice were irradiated with a central dose of 500 cGy, a sublethal dose to induce transient lymphopenia as per standard approaches to adoptive immunotherapy.[225] On the day of treatment, mice were subdivided into four groups randomly by cage: 1) no treatment, 2) CD8 adoptive transfer + anti-PD-1 mAb, 3) CD8 adoptive transfer + aAPC, or 4) CD8+ T cell adoptive transfer + anti-PD-1 mAb + aAPC. All injection volumes were 100 μL. All injections were completed intravenously, and group 1 received mock injections of PBS, labeled as no treatment control. Group 2 received an injection of $1x10^6$ Thy 1.1+ PMEL CD8+ T cells and 200 μg of anti-PD-1 antibody intraperitoneally. Group 3 received an injection of $1x10^6$ Thy 1.1+ PMEL CD8+ T cells that had been pre-incubated with 2 mg of PLGA aAPC particles for one hour at 4˚C. Group 4 received an injection of $1x10^6$ Thy 1.1+ PMEL CD8+ T cells that had been pre-incubated with 2 mg of PLGA aAPC particles as well as 200 μg of anti-PD-1 antibody intraperatoneally. One day post treatment, Groups 2 and 4 received an additional 100 μg of anti-PD-1 antibody intraperitoneally. At six, ten, and thirteen days post treatment, the mice were bled retroorbitally to analyze peripheral blood. Red blood cells were lysed with 4 min of treatment in ACK lysis buffer and then the remaining white blood cells were stained with anti-CD8a-APC (BD Biosciences; San Jose, CA) and anti-Thy1.1-Alexa Fluor 488 (BioLegend). The cells were then analyzed by flow cytometry on a BD FACSCalibur to evaluate the percentage of antigen specific Thy1.1+ CD8+ T cells in the periphery at the indicated time points. Beginning seven days after treatment, all tumor areas were measured by multiplying the length of the longest dimension by the length of the perpendicular dimension. The mice were sacrificed once tumor size progressed past 200 mm^2.

To evaluate the efficacy of PLGA/PBAE hybrid particles *in vivo*, wild type C57BL/6 mice (n=6/group) were injected with $3x10^5$ B16-F10 cells subcutaneously on day 0. On days 4, 11, and 18, half of the mice were treated with 2 mg aAPC intravenously. All mice, including the non-treated group, received 200 ug and 100 ug of anti-PD-1 monoclonal antibody on days 4 and 5, respectively. Beginning on day 7, all tumor areas were measured by multiplying the length of the longest dimension by the length of the perpendicular dimension. The mice were sacrificed once tumor size progressed past 200 mm^2.

6.2.8 *In vivo* CD8+ T cell harvest and analysis

To further probe the effect of treatment on CD8+ T cells, we used the same *in vivo* set up as used in Section 2.7. However, at day 11 post treatment tumor size was measured. Also on day 15 mice were sacrificed and spleen and tumors were harvested and homogenized through a cell strainer. Tumor infiltrating lymphocytes (TILs) were isolated by a density separation technique, using Lympholyte-M (Cedarlane; Burlington, Ontario, Canada) according to the manufacturer's protocol. Splenocytes were treated with 4 mL of ACK lysis buffer for 1 minute to lyse red blood cells. Total immune cells were measured from the spleen and TILs with manual counting on a hemocytometer and a Trypan blue exclusion test to exclude dead cells. Immune cells were stained with surface staining antibodies anti-PD-1-PE/Cy7, anti-Thy1.1-APC, anti-CD8-APC/Cy7(Biolegend); Live/Dead-FITC (Life Technologies; Carlsbad, CA) for 30 minutes at 4 °C. No more than 200,000 cells were used for any given condition. One sample per treatment group per organ was stained with anti-PD-1 mAb isotype antibody

anti-RIgG2a-PE/Cy7. All samples were then washed and analyzed by flow cytometry on a BD FACSCalibur.

To look at the stimulatory potential of CD8+ T cells isolated from tumor-bearing animals of this *in vivo* experiment, we stimulated splenocytes isolated with micro-aAPC. Techniques previously described in *2.3. In Vitro Artificial Antigen Presenting Cell T-Cell Stimulation* were followed with minor modifications. Briefly, micro Db-GP100/anti-CD28 mAb (37.51) aAPC on 4.5μm M-450 Epoxy Dynabeads (Life Technologies) were made at a 1:1 protein ratio, following manufacturer's protocol. Anti-CD28 monoclonal antibody was purchased from BioXCell (West Lebanon, NH). Splenocytes were stained with CFSE and Db-GP100/anti-CD28 mAb micro aAPC were added to isolated splenocytes at a 1:1 ratio. Total dilution was assessed after three days of incubation by flow cytometry. Percent of diluted CD8+ T cells was measured by comparing flow cytometry histograms to non-stimulated controls for each condition studied.

6.3 Results

6.3.1 PLGA-based aAPC synthesis and characterization

PLGA-based aAPC were made as recently described.[65] Briefly, the core PLGA particle was synthesized by a single emulsion technique. The particles were subsequently functionalized by EDC/NHS chemistry with two proteins to mimic the surface of the natural APC which relays two critical signals to CD8+ T cells.[65] We used a soluble major histocompatibility complex (MHC) Class I-Ig fusion protein to mimic signal 1 in the aAPC/CD8+ T cell interaction, and an agonistic monoclonal anti-CD28 antibody to serve as a costimulatory molecule to mimic signal 2.[66] In this way, the aAPC were able to

activate only a particular cognate CD8+ T cell that recognizes the specific MHC with loaded melanoma antigen peptide as signal 1.

Initially we evaluated the physical and chemical properties of the PLGA-based aAPC by imaging lyophilized particles by scanning electron microscopy (SEM) to determine particle morphology and size (**Figure 6-1A**). SEM images revealed that the conjugated particles were spherical in nature. Image analysis determined an average particle size of 4.42 μm with a standard deviation of 1.45 μm (**Figure 6-1B**). We designed the aAPC to be approximately 4-5 μm in size as this is large enough to mimic the length scale of biological antigen presenting cells and also small enough to avoid pulmonary embolism following systemic injection. To evaluate the surface protein content, we stained the particles with fluorescent monoclonal antibodies for the conjugated proteins, and measured the effect of incubation time of activated particle and protein on conjugation efficiency over a 48 hour period (**Figure 6-1C**). There is a clear increase in both pMHC and anti-CD28 mAb content at longer incubation times, maximally approximately 10% and 3% at 48 hours, respectively. Thus, we synthesized all subsequent particles for this study by incubating for 48 hours with protein.

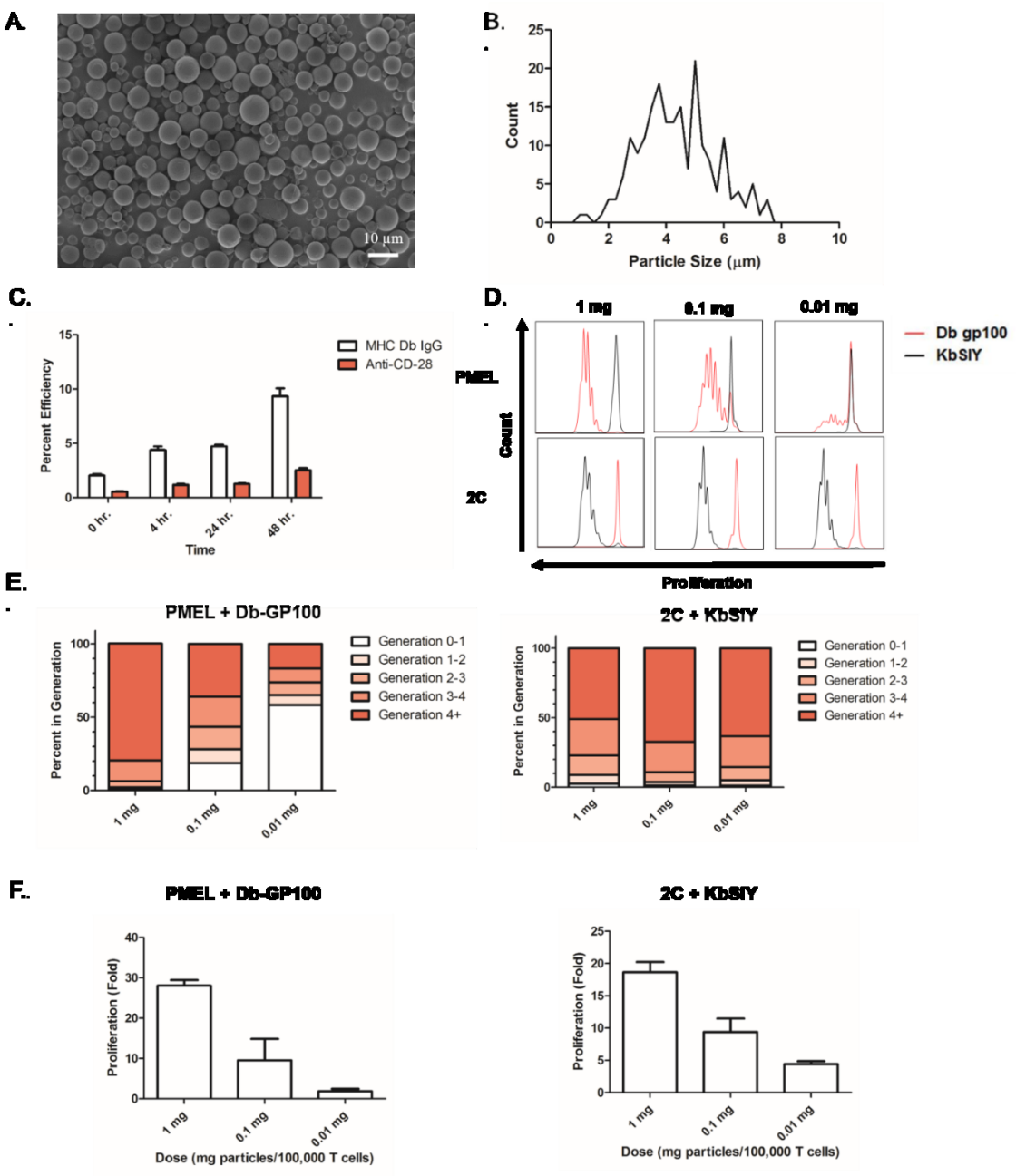

Figure 6-1. *aAPC characterization and functional assessment. (a) SEM micrographs of conjugated aAPC microparticles. (b) Particle size distribution of conjugated aAPC microparticles as evaluated by image analysis of SEM micrographs. (c) Particle protein content on aAPC microparticles as evaluated by fluorescent antibody staining of the particles and measured by a fluorescent plate reader. Conjugation efficiency is defined in Materials and Methods. (d) Antigen specific CD8+ T cell stimulation capabilities of aAPC microparticles. CFSE dilution of CD8+ T cells from either PMEL or 2C TCR transgenic mice incubated for 3 days with indicated dose of particles (1 mg, 0.1 mg, 0.01 mg) functionalized with the indicated antigen, GP100 or SIY peptide. (e) Generation analysis of CFSE dilution data in (d) indicates antigen specific proliferation of PMEL and 2C CD8+ T cells in response to stimulation by Db-GP100 (left) or Kb-SIY (right) aAPC microparticles. (f) Fold proliferation calculated by day 7 cell counts after stimulation with the Db-GP100 (left) or Kb-SIY (right) aAPC microparticles indicates antigen specific proliferation of CD8+ T cells. Error bars are SEM of n=3 replicates.*

6.3.2 aAPC stimulate peptide-specific CD8+ T cells

Biologically, one of the most important properties of an aAPC is the capability to specifically stimulate T cells of interest. To that end we evaluated the ability of our aAPC to specifically stimulate CD8+ T cells from two primary transgenic mice (PMEL or 2C) whose CD8+ T cells are all specific for the same peptide-MHC. The particles were functionalized with either Db-GP100 (cognate to PMEL CD8+ T cells) or Kb-SIY (cognate to 2C CD8+ T cells) peptide-MHC and an anti-CD28 co-stimulatory monoclonal antibody. CD8+ T cell activation was quantified by two measurements of cell proliferation – CFSE dilution and day 7 cell counts.

Each particle type was separately incubated with CFSE-labeled 2C or PMEL CD8+ T cells, and CFSE dilution was analyzed by flow cytometry after three days. In this assay, if the CD8+ T cells are stimulated by the aAPC, they rapidly divide, diluting the CFSE dye between daughter cells following each division. Effective stimulation of CD8+ T cells occurred only in the case of a cognate antigen/CD8+ T cell match as seen by CFSE dilution (**Figure 6-1D**). Nearly all CD8+ T cells divided one or more times at the highest 1 mg dose of aAPC. CD8+ T cell expansion was dose dependent as evidenced by CD8+ T cell generation analysis of CFSE data (**Figure 6-1D,E**). Nearly 80% of PMEL CD8+ T cells divided 4 or more times at a 1 mg particle dose as compared to only 15% at a 0.01 mg dose. For 2C CD8+ T cells, which have a lower activation threshold, robust proliferation was seen across all doses studied (**Figure 6-1D,E**).

Cell counts after 7 days of stimulation confirmed the dose-dependence of aAPC-based activation in both transgenic systems (**Figure 6-1F**). At the highest aAPC particle dose of 1 mg, PMEL CD8+ T cells reached approximately 30-fold expansion and 2C

CD8+ T cells reached approximately 20-fold expansion which is similar to our previously reported proliferation levels for spherical PLGA aAPCs.[65]

6.3.3 Anti-PD-1 mAb and aAPC activate cognate CD8 cells *in vitro*

We hypothesized that simultaneous PD-1 blockade would further enhance activation of cognate cells for adoptive cell transfer. To investigate this, we first developed an *in vitro* system to mimic some of the major immunosuppressive characteristics of the tumor microenvironment. We utilized PD-L1^{hi} target tumor cells and pre-activated CD8+ T cells that express PD-1 (**Figure 6-2A, schematic**).

To establish the *in vitro* system, 2C CD8+ T cells were stimulated with cognate aAPC on days 0 and 4 to upregulate PD-1 expression. This resulted in elevated PD-1 expression by day 8 compared to naïve cells (**Figure 6-2B**). B16-SIY murine melanoma cells which express the cognate Kb-SIY pMHC, and noncognate B16-F10 murine melanoma cells, were treated with IFN-γ for 48 hours to upregulate PD-L1 expression (**Figure 6-2C**). All IFN-γ was removed from B16-SIY cells from prior treatment, as confirmed by undetectable levels of the cytokine from B16-SIY cells alone (**Figure 6-2D**).

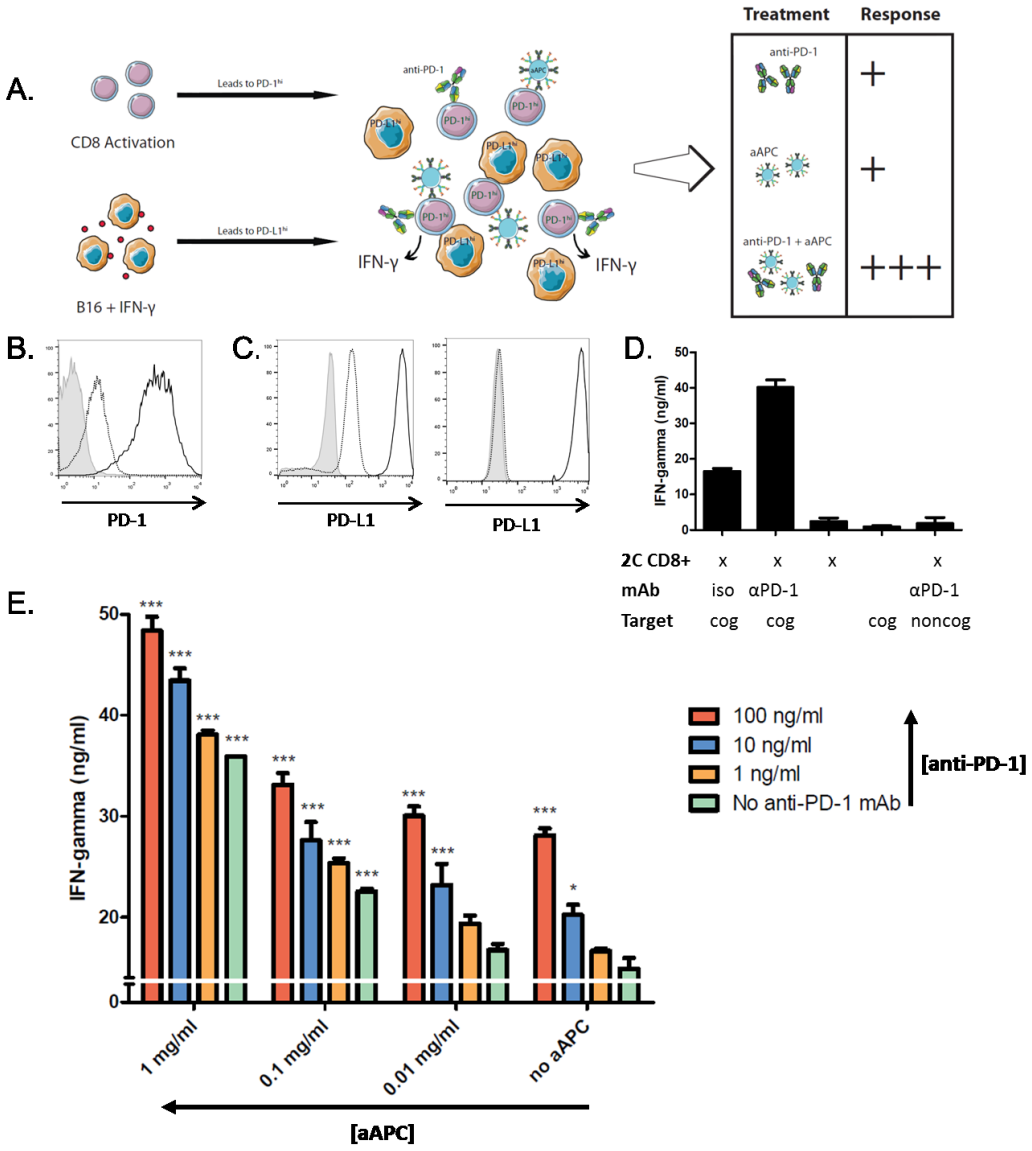

Figure 6-2. *aAPC and anti-PD-1 mAb show greater CD8+ T cell activation in combination. (a) Schematic of in vitro tumor microenvironment model system. 2C CD8+ T cells were isolated and stimulated with a 1:1 cell:aAPC ratio and B16-SIY and B16-F10 cells were incubated with 20 ng/ml IFN-γ. Activated 2C CD8+ T cells and B16 cells were purified from aAPC and IFN-γ, respectively, and combined at a 1:1 effector to target ratio with additional aAPC in the presence or absence of anti-PD-1 mAb. IFN-γ release was measured by ELISA after 18 hours. (b) CD8+ T cells are PD-1^{hi} after dual aAPC activation (black), compared to expression on naive cells (dotted) and isotype (grey). (c) B16-SIY (left) and B16-F10 (right) are PD-L1^{hi} after IFN-γ treatment (black) as compared to untreated cells (dotted) and isotype (grey). (d) PD-1^{hi} 2C CD8+ T cells and target PD-L1^{hi} B16-SIY (cognate; cog) or B16-F10 (noncognate; noncog) were co-incubated at a 1:1 ratio in the presence of 10 ug/ml anti-PD1 mAb or isotype control (iso). Anti-PD-1 mAb increased CD8+ T cell IFN-γ release as compared to isotype. No IFN-γ release was measured in response to CD8+ T cells and noncognate B16-F10 cells incubated with anti-PD-1 mAb. Significance was measured by one-way ANOVA with Dunnett's post-test. (e) CD8+ T cells secrete more IFN-γ in response to increasing doses of both aAPC and anti-PD-1 mAb. Error bars represent SEM, and significance compared to no treatment (i.e. no aAPC, anti-PD-1) is shown (* = $p<0.05$, ** = $p<0.01$, *** = $p<0.001$). Both aAPC and anti-PD-1 significantly affect IFN- γ ($p<0.001$; $F_{3,40}=226.4$ and $F_{3,40}=88.32$, respectively) by two-way ANOVA.*

To validate that the resultant cell phenotypes can model the effect of PD-1 blockade *in vitro*, we first assessed IFN-γ release from CD8+ T cells in response to anti-PD-1 mAb alone. 8-day activated PD-1^{hi} 2C CD8+ T cells and 48 hour treated PD-$L1^{hi}$ B16-SIY cells were co-incubated at a 1:1 ratio in the presence or absence of 10 μg/ml anti-PD-1 mAb or isotype control antibody. IFN-γ secretion, a marker of T cell activation, was 2.5-fold higher in the presence of anti-PD-1 mAb (**Figure 6-2D**). Importantly, anti-PD-1 mAb did not stimulate CD8+ T cells in the absence of a cognate signal 1, indicated by co-incubation with noncognate B16-F10 cells. These results demonstrate that this model can assess synergy between anti-PD-1 mAb and aAPC-based CD8+ T cell activation *in vitro*.

Next, we sought to investigate the combinatorial power of aAPC and anti-PD-1 mAb treatment *in vitro*. We hypothesized that this two-hit approach would disrupt the inhibitory PD-1/PD-L1 pathway which is upregulated during stimulation and therefore lead to greater CD8+ T cell activation by aAPC. 2C CD8+ T cells were stimulated for five days with cognate aAPC and B16-SIY cells were primed with IFN-γ as previously described. CD8+ T cells and B16 cells were co-incubated at a 1:1 ratio in the presence of titrating amounts of cognate PLGA aAPC and anti-PD-1 mAb alone or in combination, and response was quantified by IFN-γ release (**Figure 6-2A, schematic**). While CD8+ T cells secreted minimal levels of IFN-γ with no aAPC or anti-PD-1 mAb treatment, and either treatment alone increased activation in a dose-responsive manner (**Figure 6-2E**), the combination of aAPC and anti-PD-1 mAb resulted in the greatest activation – over 3.5-fold more IFN-γ secretion over no treatment. No further increase in IFN-γ release was seen with higher anti-PD-1 mAb doses.

6.3.4 PLGA aAPC biodistribution

We next sought to demonstrate the biodistribution of aAPC with and without adoptively transferred CD8+ T cells. PLGA aAPC particles encapsulating a near infrared dye were injected intravenously into C57BL/6 mice. Particles were injected either alone or after a co-incubation with cognate CD8+ T cells to assess their impact on particle distribution. We serially collected blood and imaged the samples to track fluorescence of the particles (**Figure 6-3A**). There was a noticeably faster elimination of the particles in the presence of cells compared to particles alone. A single exponential decay curve was fit to each data set, and it was determined that the effective half-life of the aAPC alone was 11.6 min and aAPC in the presence of cells was 2.8 min. At 30 and 40 minutes post injection, there were significantly more aAPC particles still in circulation when particles were injected alone as compared to particles co-injected with cells.

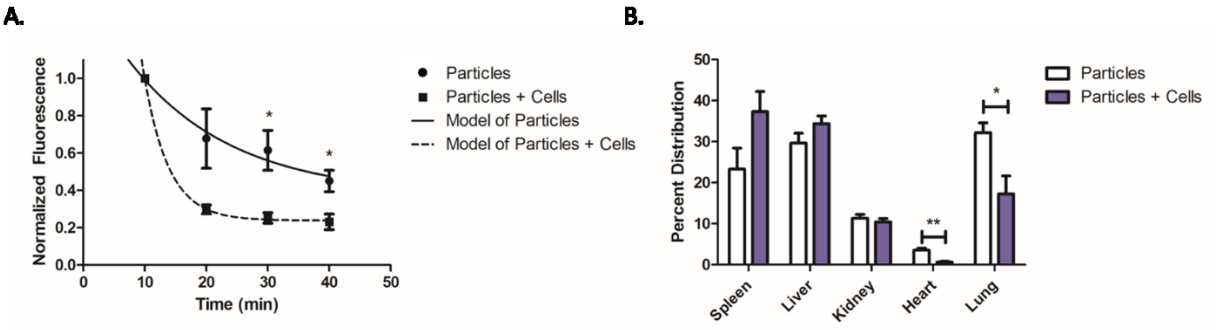

Figure 6-3. *Co-administration of aAPC with CD8+ T cells impacts aAPC biodistribution. (a) Blood was collected retroorbitally following intravenous administration of IR fluorescence labeled particles alone or incubated with cells. Blood was imaged and fluorescence was quantified and normalized to the first time point collected. Asterisk indicates time points at which normalized data was significantly different between the two groups. Lines through the points denote first order exponential decay curves fit to the data. In the presence of cells, the aAPC particles are eliminated faster than without cells. (b) At 24 hrs post-aAPC administration, the organs were dissected out, imaged, and quantified for fluorescence. In the presence of cells, the aAPC particles resist getting trapped in the lungs ($p<0.05$) or the heart ($p<0.01$), and trend towards accumulating more in the spleen ($p=0.1$). Error bars are SEM of $n=3$ replicates. (*=$p<0.05$, **=$p<0.01$)*

24 hours post administration, the animals were sacrificed and the spleen, liver, kidney, heart, and lung were harvested for fluorescence quantification (**Figure 6-3B**). In both the aAPC alone and the aAPC with cells groups the major organs for accumulation were the spleen and the liver. The aAPC in the presence of cells potentially had 60.1% greater accumulation in the spleen than the aAPC alone. With regard to the lung ($p<0.05$) and heart ($p<0.01$) it was concluded that there were fewer aAPC particles trapped in these tissues when the aAPC were in the presence of cells compared to aAPC alone.

This biodistribution study also demonstrated that systemic injection of the aAPC particles with or without cells did not cause an acute safety risk such as embolism. Systemic injection of these micron-scale biomimetic aAPC is a new administration route as we have previously used similar aAPC particles only sub-cutaneously.[65] We found the intravenous injections to be well tolerated in all animals. This approach used for the biodistribution studies also highlights another potential advantage of these particular PLGA aAPC biomaterials as it validates that they are capable of co-encapsulating imaging or other agents internally, while orthogonally allowing presentation of biomolecules from their surfaces.

6.3.5 Combination therapy delays tumor growth and extend survival

To evaluate the therapeutic potential of combination biodegradable aAPC and anti-PD-1 mAb therapies, we assessed their efficacy alone or in combination in an adoptive immunotherapy melanoma tumor treatment model. Thy1.2+ C5BL/6 mice were inoculated subcutaneously in the right flank with B16-F10 murine melanoma cells (**Figure 6-4A, schematic**). Three days later, all mice were irradiated with a sub-lethal

dose of radiation to induce transient lymphopenia. On the following day, naïve cognate Thy1.1+ PMEL CD8+ T cells alone or co-incubated with PLGA aAPC were injected intravenously into treated mice. Anti-PD-1 mAb was given intraperitoneally on the same day and the day after aAPC and CD8+ T cell treatment, as per standard anti-PD-1 mAb treatment. Peripheral blood samples were taken from the mice to evaluate antigen specific CD8+ T cell proliferation of the adoptively transferred cells, and tumor size was measured every other day.

Analysis of the circulating CD8+ T cell population revealed a proliferative advantage of the adoptively transferred cells in the dual treatment group (**Figure 6-4B**). Significantly higher percentages of Thy1.1+ antigen specific CD8+ T cells were seen in the periphery of mice treated with the combined aAPC and anti-PD-1 mAb treatment as opposed to aAPC or anti-PD-1 mAb alone. There was on average a 3-4 fold increase in proliferation of CD8+ T cells in the combination treatment group over the anti-PD-1 mAb alone group and a 2-3 fold proliferative advantage of the combination treatment group over the aAPC alone group.

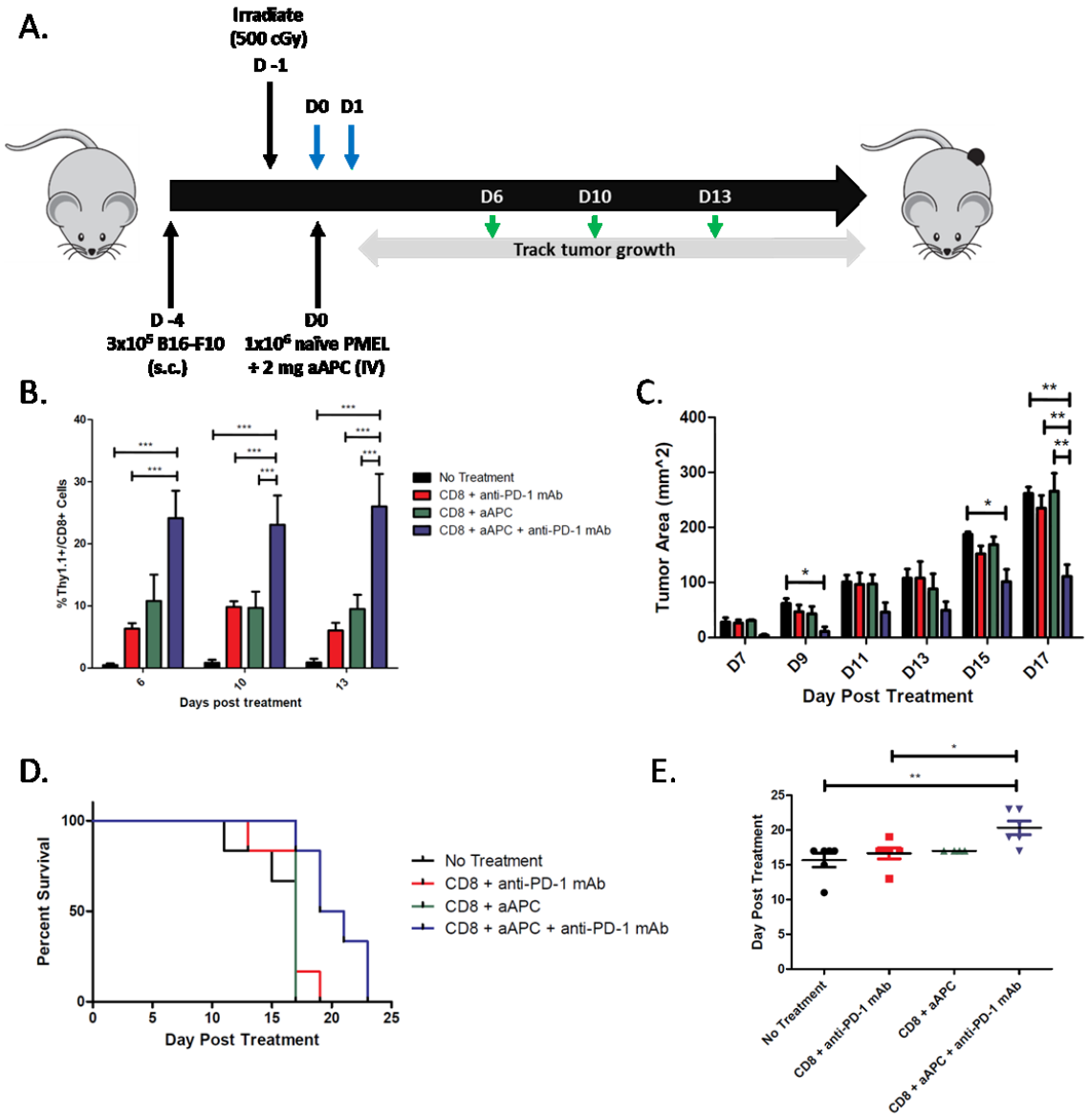

Figure 6-4. *Anti-PD1 mAb and aAPC synergize to mediate anti-tumor activity in vivo. (a) Schematic of the adoptive transfer experiment. Blue arrows indicate anti-PD-1 mAb treatment, green arrows indicate blood sampling days. (b) Percent of CD8+ T cells in peripheral blood that are Thy1.1+. Anti-PD1 mAb and aAPC dual therapy mediated the best proliferation of antigen-specific CD8+ T cells in vivo. Significance evaluated with two-way ANOVA with Bonferroni post-test. (c) Tumor measurements indicate an anti-tumor response was mediated by the dual therapy group. Significance measured by two-way ANOVA with Bonferroni post-test. (d) Kaplan-Meier survival plots indicate that dual therapy mediates the best survival. Only combination treatment resulted in significantly extended survival compared to no treatment by Log-rank test ($p<0.01$). (e) Survival distributions illustrate a statistically significant survival advantage of the dual therapy regimen compared to no treatment and anti PD-1 mAb alone. Significance measured by one-way ANOVA with Dunnett's post-test. Error bars represent the standard error of n=4-6 mice/group. Results from one representative experiment are shown. Experiment was repeated with the same overall result. (*$p<0.05$, **$p<0.01$, ***$p<0.001$)*

A therapeutic benefit of the combination treatment was also seen as determined by inhibition of tumor growth and prolonged survival (**Figure 6-4C-E**). There was a statistically significant reduction in tumor burden for the combination treatment group compared to no treatment, whereas either treatment alone had no effect (**Figure 6-4C**). By day 17, the combination treatment group had an average tumor size of 111 mm^2 – over a 50% reduction in tumor size from the no treatment and single treatment groups with all p values being less than 0.01. Additionally, the survival of the animals was extended only in the combination treatment group (**Figure 6-4D**), with the median survival increasing 24% from 17 days for no treatment and all single treatment groups to 21 days for the combination therapy (**Figure 6-4E**). This survival advantage was statistically significant compared to the no treatment and anti-PD-1 mAb treatment groups.

6.3.6 Combination therapy increases T cell functionality

To understand mechanistically how the combination of aAPC and anti-PD-1 mAb treatment affects tumor-specific CD8+ T cells *in vivo*, we analyzed phenotypic and functional changes in adoptively transferred CD8+ T cells in the various treatment groups. Thy1.2+ C5BL/6 mice were inoculated subcutaneously in the right flank with B16-F10 murine melanoma cells and sublethally irradiated after three days. Mice received either Thy1.1+ PMEL CD8+ T cells alone or co-incubated with aAPC, and were treated with anti-PD-1 mAb as described above. Eleven days after treatment, tumor infiltrating lymphocytes (TILs) and splenocytes were harvested and adoptively transferred cells were identified by the presence of Thy1.1+ on the cell surface.

Thy1.1+ CD8+ adoptively transferred PMEL T cells in the TILs expressed significantly higher levels of the immunosuppressive PD-1 molecule in the absence of anti-PD-1 treatment (**Figure 6-5A**). A similar trend was evident in the spleen, where adoptively transferred cells expressed higher PD-1 levels in the absence of any additional treatment (**Figure 6-5B**). Additionally, there was about half the percentage of Thy1.1+ CD8+ T cells in the spleen of mice lacking aAPC treatment as compared to dual treated mice (**Figure 6-5C**).

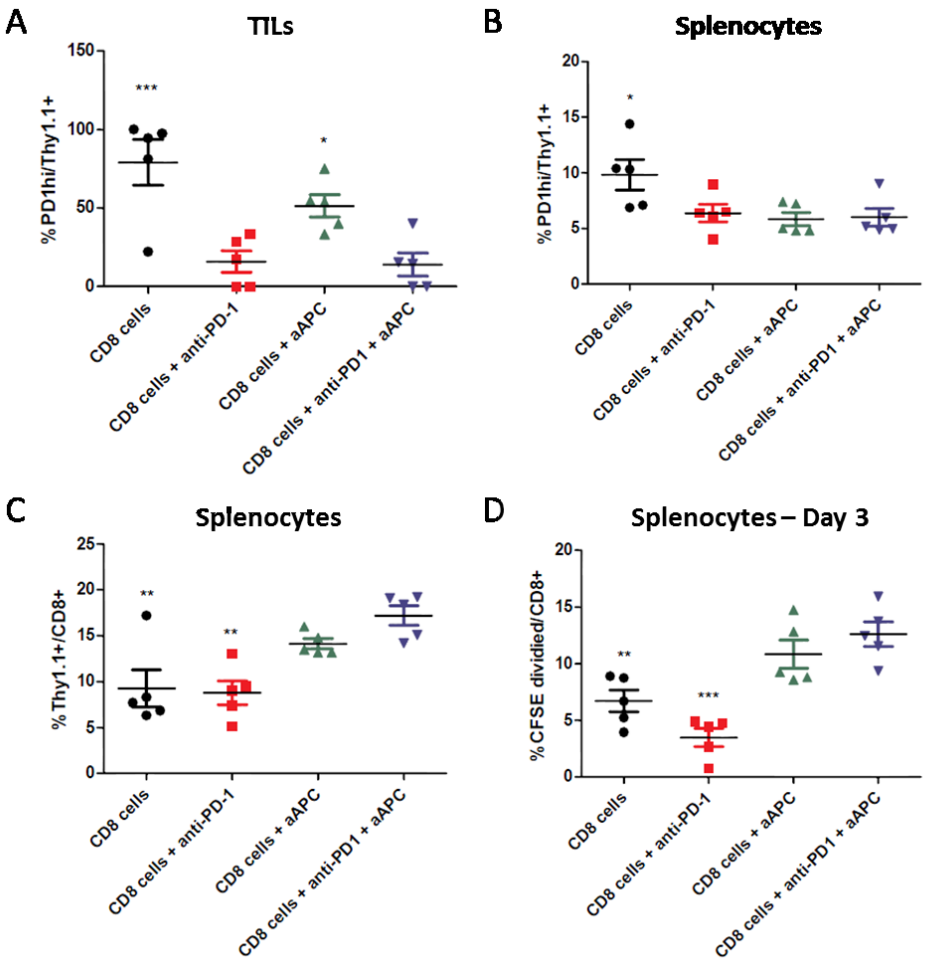

Figure 6-5. *Anti-PD1 mAb and aAPC combination therapy decreases PD-1 expression and increases expansion of tumor-specific CD8+ T cells. C57BL/6 mice were inoculated with B16-F10 tumors on day -4 and sublethally irradiated on day -1. On day 0, mice received an IV injection of PMEL Thy1.1+ CD8+ T cells either alone or co-incubated with cognate aAPC. Two of the groups also received an IP injection of anti-PD-1 mAb on days 0 and 1. Splenocytes and TILs were harvested on day 11. (a) Thy1.1+ TILs of mice not treated with anti-PD-1 mAb had significantly elevated PD-1 expression as compared to dual treated mice. (b) Thy1.1+ cells in the spleen of non-treated mice also had significantly elevated PD-1 expression as compared to dual treatment. (c) CD8+ T cells within the spleen of mice not treated with aAPC had a significantly lower percentage of Thy1.1+ tumor-specific cells as compared to dual treatment. (d) Splenocytes were CFSE stained and re-stimulated with Db-GP100/anti-CD28 mAb aAPC, and CFSE dilution was assessed after 3 days. There was significantly less expansion of tumor-specific CD8+ T cells in mice not treated with aAPC. Significance measured by one-way ANOVA with Dunnett's post-test comparing all groups to dual treatment (*p<0.05, **p<0.01, ***p<0.001).*

To investigate the functional capacity of the tumor-specific cells, we studied their ability to expand in response to re-stimulation. Isolated splenocytes from each mouse were stained with a CFSE dye and re-stimulated *in vitro* with aAPC expressing cognate

Db-GP100 pMHC and anti-CD28 mAb to expand only tumor-specific cells. After three days, CFSE dilution was assessed by flow cytometry and expanded cells identified. CD8+ T cells from dual treated mice expanded about 2-3 fold more in response to antigen-specific re-stimulation than compared to non-treated and anti-PD-1 mAb only treated mice (**Figure 6-5D**). Together, this data shows that dual aAPC and anti-PD-1 mAb treatment leads to a change in expression of checkpoint molecules and increases the proliferative capacity of CD8+ T cells both within the tumor microenvironment and secondary lymphoid tissue. PD-1 blockade reduces CD8+ T cell PD-1 expression and aAPC treatment increases tumor-specific CD8+ T cell expansion and re-activation potential. Thus, combination therapy leads to a superior CD8+ T cell population by facilitating both lower expression of the immunosuppressive PD-1 molecule and increased proliferative and functional capacity.

6.3.7 PLGA/PBAE hybrid aAPC outperforms traditional PLGA

Next, we sought to develop an aAPC with greater efficacy that could further increase the anti-tumor effect, activate an endogenous anti-tumor T cell response, and potentially eliminate established tumors upon combination with checkpoint blockade. Particle material has been shown to affect the ability to activate a T cell response because of changes in protein density, shape, surface charge, size, and stiffness among other factors. Particle material can also enable further modifications such as the ability to encapsulate drugs or deliver gene-modifying agents. Thus, we assessed the changes in T cell activation by aAPC synthesized with polymeric materials demonstrated in other drug delivery fields to enable surface protein conjugation, drug encapsulation, and gene delivery. The success of this new type of aAPC would allow for exciting combination

therapies in future iterations, such as siRNA-mediated knock-down of checkpoint molecules that is restricted to antigen-specific T cell populations or paracrine delivery of inflammatory cytokines.

A blend of PLGA and a poly(beta-amino ester) (PBAE) was chosen as the base material for particle synthesis. PLGA enables conjugation of proteins to the surface, whereas PBAEs have demonstrated the ability to delivery siRNA intracellular in other cell types.[226,227] PLGA/PBAE or PLGA only aAPC, each approximately 1 μm in diameter, were synthesized by single emulsion and subsequently characterized. SEM analysis showed that morphologically the particles we identical in surface features and spherical shape (**Figure 6-6A-B**). We assessed size via ImageJ analysis of the collected SEM micrographs and found the size to be statistically similar after counting 100 particles each (**Figure 6-6C**). In addition, the size distributions were essentially identical between the two particle populations (**Figure 6-6D**).

PLGA/PBAE hybrid or PLGA aAPC were conjugated with Kb-SIY dimer signal 1 and anti-CD28 mAb signal 2 via EDC/NHC chemistry. To characterize the amount of protein immobilized on the surface of the particles, we used signal 1 and signal 2 proteins pre-conjugated to fluorophores and assessed fluorescent content of the particles after protein conjugation (**Figure 6-6E**). Interestingly, we found that the PLGA/PBAE particle immobilized a significantly higher amount of protein after the conjugation compared to the PLGA particles and that a large fraction of the protein was bound non-specifically in the absence of conjugation reagents. PLGA/PBAE aAPC thus increase the maximum achievable signal density on the particle surface, a characteristic shown to be important for T cell activation.[47,48]

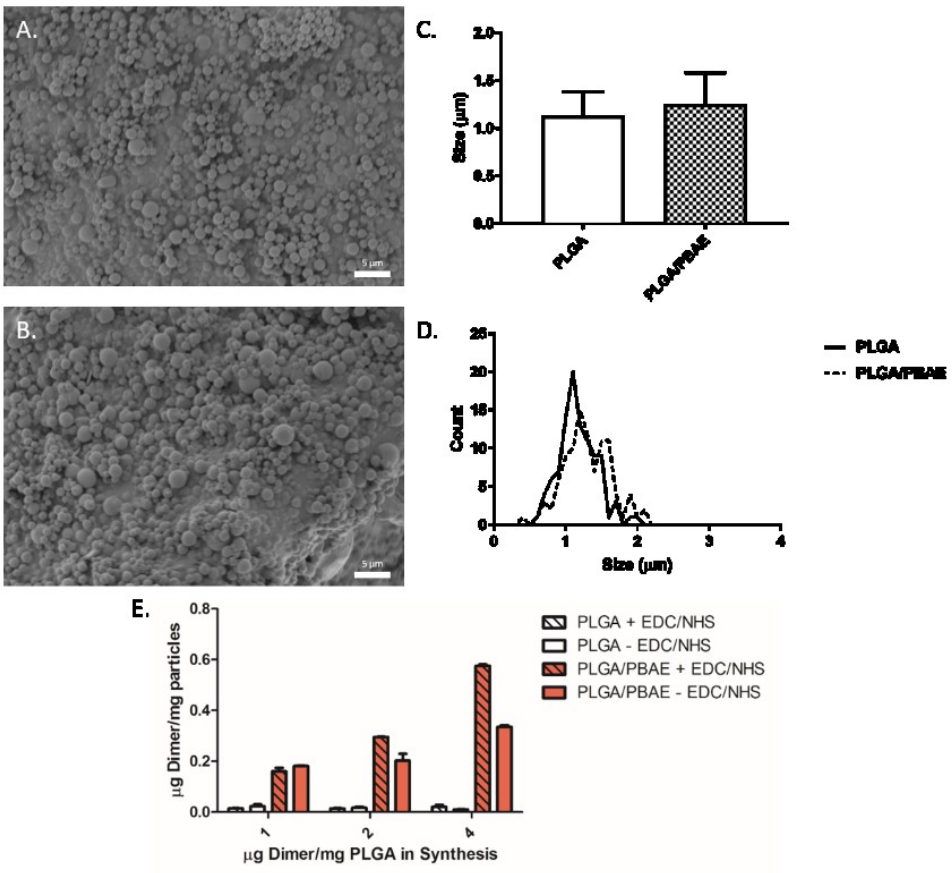

Figure 6-6. *PLGA/PBAE and PLGA particle characterization. SEM images of (a) PLGA and (b) PLGA/PBAE microparticles synthesized by single emulsion. (c) Average size and standard error of 100 representative particles for both materials. (d) Size distributions for particles for both materials. (e) Protein conjugation efficacy for PLGA and PLGA/PBAE particles with and without EDC/NHS conjugation reagents.*

To assess the stimulatory potential of the PLGA/PBAE hybrid particles, PLGA or PLGA/PBAE particles were incubated with cognate 2C transgenic CD8+ T cells at titrating doses. All CD8+ T cells from a 2C transgenic mouse recognize the Kb-SIY peptide MHC complex making it a useful system for studying CD8+ T cell activation potential *in vitro*. PLGA/PBAE aAPC resulted in equivalent expansion of 2C CD8+ T cells as their PLGA counterparts at 100X lower doses (**Figure 6-7A-B**). We then studied how changing the length of the carbon chain in the PBAE backbone affects the stimulatory potential of the hybrid particles. Our standard PBAE has a 4 carbon length

chain, and we studied the effect of 3 and 5 carbon length chains. Interestingly, this had no effect on CD8+ T cell activation across three doses–all PLGA/PBAE hybrid aAPC stimulated cells to a greater extent than PLGA aAPC (data not shown). The effect of PBAE ratio in the hybrid particles was also investigated as it affects T cell activation. This is important to study, as the PBAE ratio alters the biodegradation rate as well as siRNA encapsulation ability. It may therefore be necessary to slightly alter the PBAE ratio to optimize future plans for siRNA encapsulation and *in vivo* kinetics. The standard hybrid particles contain 25% PBAE and were compared to particles containing 15% PBAE. Again, this resulted in no difference in CD8+ T cell stimulatory potential (data not shown). Thus, PLGA/PBAE hybrid particles are robust stimulators of a cognate CD8+ T cell response and are relatively insensitive to PBAE construct and concentration.

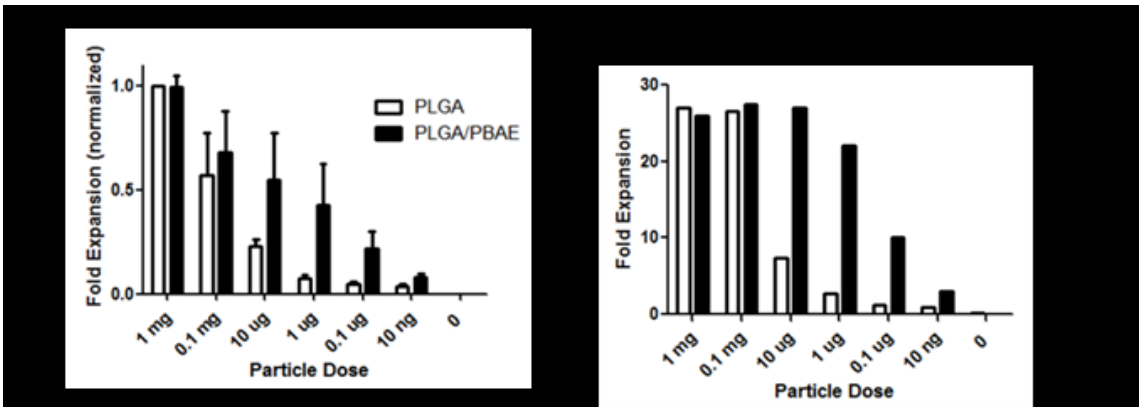

Figure 6-7. *PLGA/PBAE hybrid particles activate cognate CD8+ T cells. (a) Fold expansion of 2C CD8+ T cells incubated with Kb-SIY/anti-CD28 PLGA or PLGA/PBAE aAPC, normalized to 1 mg PLGA. Significant by two-way ANOVA ($p<0.05$). (b) Representative total expansion of 2C CD8+ T cells incubated with PLGA or PLGA/PBAE aAPC.*

For optimal activity of the hybrid particles, it is important for the aAPC to have high specificity for cognate cells expressing the correct signal 1. Thus, to further study how the PLGA/PBAE particles interact with the cells of interest, we performed confocal

microscopy and flow cytometry with aAPC encapsulating a fluorescent dye. Confocal microscopy showed that the PLGA/PBAE aAPC bound cognate but not non-cognate CD8+ T cells, as expected (**Figure 6-8A**). Additionally, PLGA/PBAE aAPC bound cognate cells at a higher frequency than PLGA only aAPC, as shown by 2D and 3D reconstructed images (**Figure 6-8B**). The higher binding capacity was further confirmed by flow cytometry. Neither aAPC showed significant binding to non-cognate cells. However, the hybrid aAPC bound more cells and at a higher level than the traditional PLGA aAPC (**Figure 6-8C**).

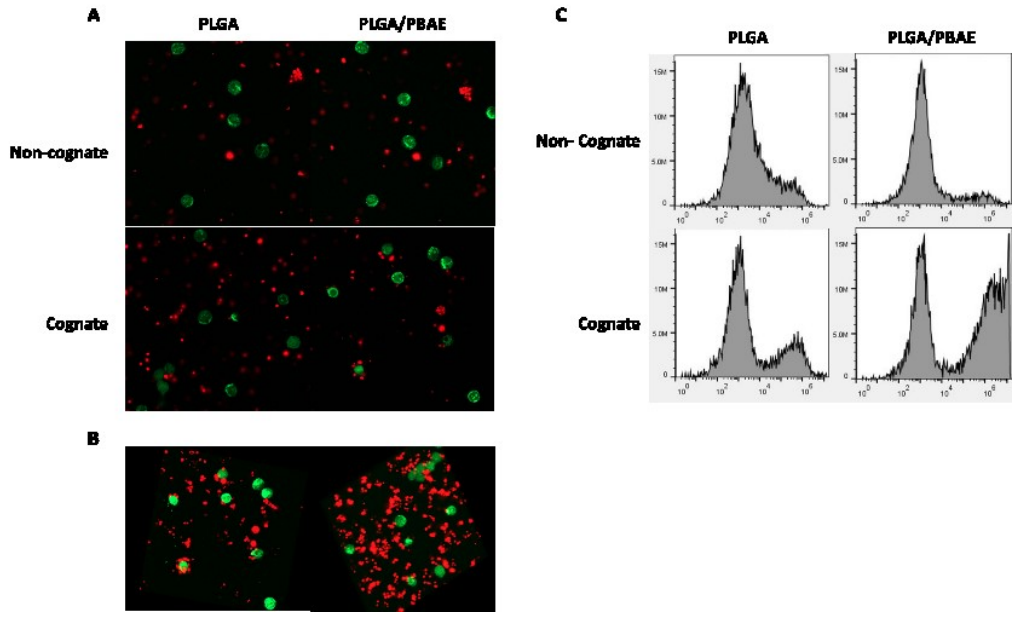

Figure 6-8. *PLGA/PBAE bind cognate cells at a higher level than PLGA aAPC. (a) Confocal images show PLGA/PBAE aAPC (red) bind cognate cells (green) at a higher frequency than PLGA aAPC (red). (b) 3D reconstruction of confocal image. (c) Flow cytometry showing higher binding of PLBA/PBAE aAPC to cognate cells than PLGA aAPC.*

Finally, we assessed the ability of our PLGA/PBAE aAPC to inhibit tumor growth *in vivo*. We investigated this in a tumor treatment study without any adoptive transfer of tumor-specific cells. PLGA/PBAE aAPC were synthesized as above, and

conjugated with Kb-trp2 and Db-gp100 signal 1, and anti-CD28 mAb signal 2. Wild type C57BL/6 mice (n=6/group) were injected with $3x10^5$ B16-F10 cells, which express Kb-trp2 and Db-gp100, subcutaneously on day 0. On days 4, 11, and 18, half of the mice were treated with 2 mg aAPC intravenously. All mice, including the non-treated group, received 200 ug and 100 ug of anti-PD-1 monoclonal antibody on days 4 and 5, respectively, a dose we have shown to have no effect on tumor growth when given as a monotherapy (data not shown). Mice that received aAPC injection had significantly delayed tumor growth (**Figure 6-9A**). Additionally, treated mice lived significantly longer – non-treated mice died on day 13 on average, while aAPC treatment extended this until day 16 (**Figure 6-9B**).

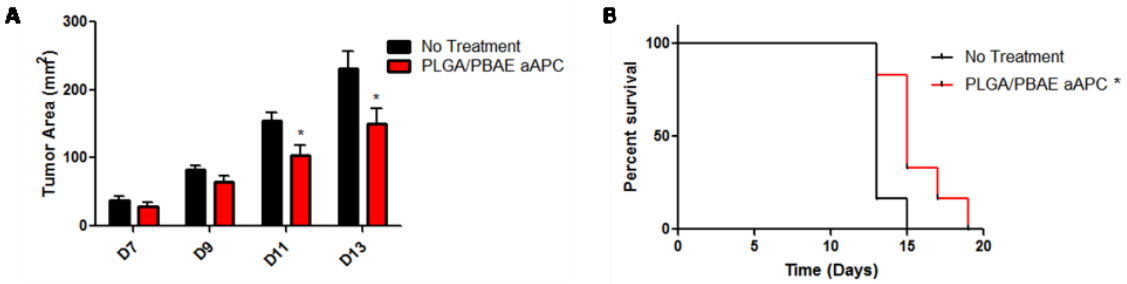

Figure 6-9. *PLGA/PBAE aAPC inhibit tumor growth. C57BL/6 mice were inoculated with B16-F10 tumors on day 0. Mice were treated with anti-PD-1 mAb +/- PLGA/PBAE aAPC expressing Db-gp100 and Kb-trp2. (a) PLGA/PBAE aAPC treatment inhibits growth of established B16-F10 tumors. (b) Treatment also extends survival.*

6.4 Discussion and conclusions

Stimulating a tumor-specific cytotoxic CD8+ T cell response is a promising approach in cancer immunotherapy, although several hurdles still exist in generating a population of cells that is both optimally effective and persistent. Often, very large numbers of activated T cells, up to 10^{11},[68] are necessary for an objective response.

Advancements in biomimetic and biodegradable aAPC have made robust activation for clinical therapy possible, although strong activation upregulates immunosuppressive surface molecules on the CD8+ T cells such as PD-1. As progress is made in the field of biomaterials for robust T cell activation, it is likewise necessary to understand their interaction with other conventional immunotherapeutics, including new clinical standards of care, to counterbalance the resultant inhibitory phenotype.

Here, we have characterized the synergistic interaction between biodegradable PLGA aAPC and PD-1 checkpoint blockade for murine tumor control in an adoptive transfer model. PLGA-based aAPC were chosen as they are effective T cell stimulators, and, due to well-known experience with PLGA particles in the body, offer translational potential for tumor-specific CD8+ T cell expansion *in vivo*. We showed antigen-specific stimulation of CD8+ T cells in response to PLGA aAPC conjugated with two different peptide-MHC complexes. The aAPC are able to induce robust expansion in each of the tested cell types.

However, the immune system has developed ways to self-regulate itself by upregulating immunosuppressive molecules in response to activation. In this nature, activated CD8+ T cells express high levels of PD-1 which is important biologically to control autoimmunity, but detrimental in cancer immunotherapy where a strong anti-tumor response is desired. Tumors take advantage of this biological process and express the ligand for PD-1, PD-L1, to inhibit an anti-tumor CD8+ T cell response. Our *in vitro* model of PD-1^{hi} CD8+ T cells and PD-$L1^{hi}$ tumor cells, mimicking those that would be found within the tumor microenvironment of a patient, showed increased CD8+ T cell activation in response to the combination of aAPC stimulation and PD-1 blockade. While

both therapeutics alone increased activation, the combination was able to stimulate CD8+ T cells while turning off their "rheostat" and led to a further enhanced antigen-specific response.

We also sought to study the effectiveness of combination treatment *in vivo* since the dynamics of the tumor microenvironment can play a significant role in the response. The aAPC were first demonstrated to circulate systemically, both with and without a co-injection of cognate CD8+ T cells. When aAPC were co-injected with CD8+ T cells, they spent less time in circulation and accumulated less in off-target sites such as the lung and heart. This comparison is both interesting and important, as the intrinsic honing capabilities of CD8+ T cells may cause accumulation of aAPC in immune-dense sites. Indeed, we did see a trend towards higher aAPC accumulation in secondary lymphoid tissue - the spleen. While this >50% change in distribution was not significant under the conditions studied, it may help to explain the statistically shorter circulation half-life of particles co-injected with cells along with the greater accumulation of tumor-specific CD8+ T cells in the spleens of mice treated with particles and cells *in vivo*.

Combination of aAPC expressing tumor antigens and anti-PD-1 mAb treatment resulted in delayed tumor growth and extended survival *in vivo* in an adoptive transfer model. Importantly, this is the first time this PLGA aAPC-based therapeutic was effective in a therapeutic rather than prophylactic tumor model as well as the first time that it has been evaluated following systemic administration.[65] The therapeutic effect was shown to be due to increased proliferation of the adoptively transferred tumor-specific cells both in the peripheral blood and spleen in response to aAPC transfer, as well as decreased PD-1 expression by these cells in the spleen and tumor in response to anti-PD-1 mAb

treatment. Importantly, this strong stimulation of the tumor-specific CD8+ T cells did not lead to unresponsiveness—CD8+ T cells from the spleen of the dual treatment group also expanded the greatest amount upon re-stimulation *ex vivo*.

Finally, we synthesized and characterized a new hybrid material that increases the activation potential of aAPC. These PLGA/PBAE aAPC demonstrated maximal T cell proliferation at doses 100x less than PLGA alone. The data suggests that this is due to significantly enhanced protein conjugation, leading to a higher signal density and increased binding to cognate T cells. This new aAPC material is exciting not only because of the improved activation that could potentially further increase anti-tumor activity when combined with anti-PD-1 mAb, but also because of the doors it opens for next generation aAPC. PBAE-based particles have been shown to efficiently deliver intracellular genetic material to cells and can be used to create a dual-functioning aAPC in future work. For example, siRNA that knocks down expression of inhibitory molecules like PD-1 could be encapsulated within the aAPC and activate clonal T cell populations on an extracellular (i.e. aAPC) and intracellular (i.e. siRNA delivery) level. This may lead to a new therapeutic capable of eradicating established tumors and decreasing side effects experienced with systemic immune activation.

In summary, anti-PD-1 immunotherapy unleashes more of the aAPC-activated CD8+ T cells to perform effector function whereas without anti-PD-1 mAb therapy more aAPC-activated CD8+ T cells were ineffective due to the immunosuppressive tumor cells expressing PD-L1. Furthermore, aAPC activate and increase the number of CD8+ T cells that anti-PD1 therapy can target and affect. CD8+ T cells not activated by aAPC do not proliferate as much or upregulate PD1, thus decreasing the total effect of the checkpoint

blockade immunotherapy. Therefore, both therapies complement and synergize to provide a more potent tumor immunotherapy.

Here we have developed a biomaterial-based combinatorial cancer immunotherapy. This therapeutic simultaneously activates cytotoxic CD8+ T cells while reducing the immune dampening effects of the tumor microenvironment. We have developed a biomimetic PLGA-based aAPC that can, in an antigen specific fashion, stimulate cancer-targeting CD8+ T cells and synergize with PD-1 checkpoint blockade. The aAPC particles generate a cytotoxic response against melanoma cells *in vitro* and, for the first time, these aAPC have been shown effective in an *in vivo* tumor treatment model following a single intravenous injection. The combined therapy was able to mediate a reduction in tumor burden and increase median survival time. As the aAPC are composed of PLGA, a biodegradable material that has a track-record of safe use in the clinic with related technologies, these advanced immunostimulatory materials may be promising for combination treatment in the clinical application of cancer immunotherapy.

Chapter 7. Conclusions

7.1 Summary of work

Cancer immunotherapies aim to increase the ability of a patient's immune system to recognize and eliminate cancerous cells. The immune system is complex and involves both antigen-specific recognition, such as the case of the T cell receptor on T cells, as well as non-antigen-specific modulators, including co-stimulatory molecules, co-inhibitory checkpoint molecules, and cytokines. Current immunotherapies target one or more of these various pathways with the goal of stimulating the most robust anti-tumor response with minimal systemic effects.

Artificial antigen presenting cells, aAPC, are one of the most common approaches for antigen-specific T cell stimulation. These synthetic particles present a tumor antigen in the context of an MHC molecule along with the necessary co-stimulatory signals. Synthetic aAPC have many advantages over cell-based APC because of their ability to be engineered to explicit specifications and reduced cost and extended shelf-life. However, aAPC have been limited by their ability to induce a sufficiently persistent and robust anti-tumor T cell response capable of eliminating established tumors.

Due to the complexities of the nano- and micro-scale interactions necessary for T cell activation, aAPC that are several microns in diameter are the most effective at stimulating T cells. However, their reduced biocompatibility makes micron-scale particles infeasible for *in vivo* because of their rapid clearance and poor bioavailibility. In this dissertation, I described how aAPC efficacy can be improved through combination therapies and by altering particle material and surface protein composition. Chapter 6

showed how simply modifying the material of the aAPC platform can increase activation up to 100x. Previous work from our lab demonstrated how magnetic field-induced clustering could increase T cell activation induced by nano-aAPC. In Chapter 5, I described how this type of approach could be further improved to more than double the stimulatory potential of nano-aAPC. No previous aAPC platforms were optimized to take advantage of the diversity of co-stimulatory molecules that affect T cell phenotype and function. However, the importance of this was demonstrated by the fact that the incorporation of additional co-stimulation significantly extended T cell persistence *in vivo* following adoptive transfer. Additionally, due to the nature of the approach, it also provides a mechanism for analyzing the necessity of nano-and micro-scale clustering of T cell signaling molecules or signal clustering on other types of immune or non-immune cells. This information could be further used to improve more biocompatible aAPC.

In addition to directly increasing T cell stimulation through the modification of the aAPC platform, Chapter 6 demonstrated how direct aAPC-induced T cell stimulation can be improved through combination immunotherapy. Biodegradable aAPC were shown to synergize with anti-PD-1 mAb checkpoint blockade and delay tumor growth at doses where neither treatment alone had any effect. These studies begin to bring nano-aAPC into the playing field for adoptive cell transfer. The data also indicates that improvements in aAPC-based activation can take the form of engineering enhancements or combinations with therapies that target activation through non-overlapping pathways.

aAPC have the advantage of targeting antigen-specific T cells. However, this requires *a priori* selection of a tumor antigen which can be difficult, expensive, and allow for antigen-escape. The opposing approach is to target pathways that are utilized by all T

cells, the downside being that non-specific immune activation may lead to off-target toxicities. Thus, I described in Chapter 4 how nanoparticles can both increase the synergy between combination non-specific immunotherapies, as well as target the drug delivery to the tumor site to decrease off-target effects. I demonstrated how these immunoswitch particles can reverse or eliminate tumor growth as a standalone therapy to stimulate a polyclonal anti-tumor immune response that forms a memory response.

Together, these approaches demonstrate the various ways by which nanotechnology can be used to improve immunotherapies and study T cell activation. Many of the studies also utilize combination immunotherapy, combining T cell activation with checkpoint blockade, which has been shown by others as well to significantly improve the anti-tumor immune response.

7.2 Future directions

Much of the work presented here is primarily proof-of-concept studies with various interesting future directions. In terms of the immunoswitch particles described in Chapter 4, next steps include further optimization of the platform and analysis of the mechanism of action. For example, the particles were constructed with a 1:1 anti-PD-1 to anti-4-1BB mAb ratio on 100 nm particles, but other ratios or other particle sizes may prove to be more efficacious. Altering the relative antibody densities may affect their cell targeting abilities or biodistribution *in vivo*. Likewise, we predict that the size of the particle will have an impact on efficacy. Smaller particles may be preferential in terms of the resultant intercellular distance, but may have conflicting effects compared to the size-induced change in biodistribution or avidity. Immunoswitch particles may also have

further increased efficacy if pre-coated on tumor-specific CD8+ T cells prior to adoptive cell transfer.

It will also be important to perform immunohistochemistry experiments and *in vivo* imaging to assess immunoswitch particle interactions within the tumor microenvironment. The data presented here indicates that primarily a CD8+ T cell response is induced, although it does not prove that the response is caused by a direct interaction with immunoswitch particles and tumor cells *in vivo*. Other immune cell types express both PD-L1 and 4-1BB including dendritic cells and CD4+ T cells and the interaction of immunoswitch particles with these other cell types may also play a role. Finally, TCR sequencing analysis demonstrated that immunoswitch particles select for the expansion of a single T cell clone in the B16-SIY murine melanoma model. Experiments to determine if this type of response is preserved against other tumors lacking a dominant antigen and the impact of this monoclonal-skewed response would be interesting and important.

The T cell stimulation platform described in Chapter 5 showed how this approach can be used to manipulate various aspects of activation. I demonstrated how altering the size or material of particles can alter the clustering of different signaling molecules. It would be interesting to use this approach to study the impact of clustering of other less-studied co-stimulatory molecules such as OX40 or CD40L, or on other immune or non-immune cell types. I also demonstrated how this platform can be used to customize the ratio and combination of co-stimulation and how this affects T cell phenotype. Future studies that utilize this platform to further investigate the importance of additional co-

stimulatory combinations would be interesting and important to the future of adoptive immunotherapy.

Chapter 6 demonstrated how checkpoint blockade synergizes with micro-scale aAPC. Further studies to investigate if this synergy is maintained with more biocompatible nano-aAPC would be important to the field. Additionally, the polymeric particles could potentially have anti-PD-1 mAb secreted from their core to localize the delivery of checkpoint blockade to cognate T cells. Further optimization should also be conducted for the PLGA/PBAE hybrid aAPC. This particle formulation was originally chosen due to its potential ability to encapsulate and deliver genetic material in other cell types. Interesting future work would explore the potential to encapsulate siRNA to selectively give cognate T cells a proliferative advantage, such as an siRNA to turn off PD-1 expression. The polymeric aAPC could then be used to both activate cognate T cells at a cell membrane level, as well as genetically modify the T cells to reduce the toxicities associated with checkpoint blockade.

Bibliography

1. Kosmides, A. K.; Sidhom, J. W.; Fraser, A.; Bessell, C. A.; Schneck, J. P. Dual Targeting Nanoparticle Stimulates the Immune System to Inhibit Tumor Growth. *ACS Nano* **2017**, *11*, 5417–5429.
2. Kosmides, A. K.; Meyer, R. A.; Hickey, J. W.; Aje, K.; Cheung, K. N.; Green, J. J.; Schneck, J. P. Biomimetic Biodegradable Artificial Antigen Presenting Cells Synergize with PD-1 Blockade to Treat Melanoma. *Biomaterials* **2017**, *118*, 16–26.
3. Smith-Garvin, J. E.; Koretzky, G. A.; Jordan, M. S. T Cell Activation. *Annu. Rev. Immunol.* **2009**, *27*, 591–619.
4. Cannons, J. L.; Lau, P.; Ghumman, B.; DeBenedette, M. A.; Yagita, H.; Okumura, K.; Watts, T. H. 4-1BB Ligand Induces Cell Division, Sustains Survival, and Enhances Effector Function of CD4 and CD8 T Cells with Similar Efficacy. *J. Immunol.* **2001**, *167*, 1313–1324.
5. Buchan, S. L.; Manzo, T.; Flutter, B.; Rogel, A.; Edwards, N.; Zhang, L.; Sivakumaran, S.; Ghorashian, S.; Carpenter, B.; Bennett, C. L.; Freeman, G. J.; Sykes, M.; Croft, M.; Al-Shamkhani, A.; Chakraverty, R. OX40- and CD27-Mediated Costimulation Synergizes with Anti-PD-L1 Blockade by Forcing Exhausted CD8+ T Cells to Exit Quiescence. *J. Immunol.* **2015**, *194*, 125–133.
6. Zeng, W.; Su, M.; Anderson, K. S.; Sasada, T. Artificial Antigen-Presenting Cells Expressing CD80, CD70, and 4-1BB Ligand Efficiently Expand Functional T Cells Specific to Tumor-Associated Antigens. *Immunobiology* **2014**, *219*, 583–592.
7. Chacon, J. A.; Wu, R. C.; Sukhumalchandra, P.; Molldrem, J. J.; Sarnaik, A.; Pilon-Thomas, S.; Weber, J.; Hwu, P.; Radvanyi, L. Co-Stimulation through 4-1BB/CD137 Improves the Expansion and Function of CD8(+) Melanoma Tumor-Infiltrating Lymphocytes for Adoptive T-Cell Therapy. *PLoS One* **2013**, *8*, e60031.
8. Zhang, H.; Snyder, K. M.; Suhoski, M. M.; Maus, M. V; Kapoor, V.; June, C. H.; Mackall, C. L. 4-1BB Is Superior to CD28 Costimulation for Generating CD8+ Cytotoxic Lymphocytes for Adoptive Immunotherapy. *J. Immunol.* **2007**, *179*, 4910–4918.

9. Oh, H. S.; Choi, B. K.; Kim, Y. H.; Lee, D. G.; Hwang, S.; Lee, M. J.; Park, S. H.; Bae, Y.-S.; Kwon, B. S. 4-1BB Signaling Enhances Primary and Secondary Population Expansion of CD8+ T Cells by Maximizing Autocrine IL-2/IL-2 Receptor Signaling. *PLoS One* **2015**, *10*, e0126765.

10. Rudolf, D.; Silberzahn, T.; Walter, S.; Maurer, D.; Engelhard, J.; Wernet, D.; Bühring, H.-J.; Jung, G.; Kwon, B. S.; Rammensee, H.-G.; Stevanović, S. Potent Costimulation of Human CD8 T Cells by Anti-4-1BB and Anti-CD28 on Synthetic Artificial Antigen Presenting Cells. *Cancer Immunol. Immunother.* **2008**, *57*, 175–183.

11. Zheng, G.; Wang, B.; Chen, A. The 4-1BB Costimulation Augments the Proliferation of CD4+CD25+ Regulatory T Cells. *J. Immunol.* **2004**, *173*, 2428–2434.

12. Resta, R.; Thompson, L. F. T Cell Signalling through CD73. *Cell Signal* **1997**, *9*, 131–139.

13. Debenedette, M. A.; Shahinian, A.; Mak, T. W.; Watts, T. H. Costimulation of CD28- T Lymphocytes by 4-1BB Ligand. *J. Immunol.* **1997**, *158*, 551–559.

14. Lillemeier, B. F.; Mörtelmaier, M. A.; Forstner, M. B.; Huppa, J. B.; Groves, J. T.; Davis, M. M. TCR and Lat Are Expressed on Separate Protein Islands on T Cell Membranes and Concatenate during Activation. *Nat. Immunol.* **2010**, *11*, 90–96.

15. Hashimoto-Tane, A.; Saito, T. Dynamic Regulation of TCR-Microclusters and the Microsynapse for T Cell Activation. *Front. Immunol.* **2016**, *7*, 1–8.

16. Yokosuka, T.; Kobayashi, W.; Sakata-Sogawa, K.; Takamatsu, M.; Hashimoto-Tane, A.; Dustin, M. L.; Tokunaga, M.; Saito, T. Spatiotemporal Regulation of T Cell Costimulation by TCR-CD28 Microclusters and Protein Kinase C Translocation. *Immunity* **2008**, *29*, 589–601.

17. Dustin, M. L.; Depoil, D. New Insights into the T Cell Synapse from Single Molecule Techniques. *Nat. Rev. Immunol.* **2011**, *11*, 672–684.

18. Bashour, K. T.; Tsai, J.; Shen, K.; Lee, J.-H.; Sun, E.; Milone, M. C.; Dustin, M. L.; Kam, L. C. Cross Talk between CD3 and CD28 Is Spatially Modulated by Protein Lateral Mobility. *Mol. Cell. Biol.* **2014**, *34*, 955–964.

19. Zhu, J. T Helper Cell Differentiation, Heterogeneity, and Plasticity. *Cold Spring Harb. Perspect. Biol.* **2017**, a030338.

20. Luckheeram, R. V.; Zhou, R.; Verma, A. D.; Xia, B. CD4+T Cells: Differentiation and Functions.

Clin. Dev. Immunol. **2012**, *2012*.

21. Tesmer, L. A.; Lundy, S. K.; Sarkar, S.; Fox, D. A. Th17 Cells in Human Disease. *Immunol Rev* **2008**, *223*, 87–113.
22. Josefowicz, S. Z.; Lu, L.-F.; Rudensky, A. Y. Regulatory T Cells: Mechanisms of Differentiation and Function. *Annu. Rev. Immunol.* **2012**, *30*, 531–564.
23. Zhang, N.; Bevan, M. J. CD8+ T Cells: Foot Soldiers of the Immune System. *Immunity* **2011**, *35*, 161–168.
24. Schumacher, T. N.; Schreiber, R. D. Neoantigens in Cancer Immunotherapy. *Science* **2015**, *348*, 69–74.
25. Bobisse, S.; Foukas, P. G.; Coukos, G.; Harari, A. Neoantigen-Based Cancer Immunotherapy. *Ann. Transl. Med.* **2016**, *4*, 262–262.
26. Vigneron, N. Review Article Human Tumor Antigens and Cancer Immunotherapy. *Hindawi* **2015**, *2015*, 1–17.
27. Vasievich, E. a; Huang, L. The Suppressive Tumor Microenvironment: A Challenge in Cancer Immunotherapy. *Mol. Pharm.* **2011**, *8*, 635–641.
28. Chen, D. S.; Mellman, I. Oncology Meets Immunology : The Cancer-Immunity Cycle. *Immunity* **2013**, *39*, 1–10.
29. Snyder, A.; Makarov, V.; Merghoub, T.; Yuan, J.; Zaretsky, J. M.; Desrichard, A.; Walsh, L. a.; Postow, M. a.; Wong, P.; Ho, T. S.; Hollmann, T. J.; Bruggeman, C.; Kannan, K.; Li, Y.; Elipenahli, C.; Liu, C.; Harbison, C. T.; Wang, L.; Ribas, A.; *et al.* Genetic Basis for Clinical Response to CTLA-4 Blockade in Melanoma. *N. Engl. J. Med.* **2014**, *371*, 2189–2199.
30. Mcgranahan, N.; Furness, A. J. S.; Rosenthal, R.; Ramskov, S.; Lyngaa, R.; Saini, S. K.; Jamal-hanjani, M.; Wilson, G. A.; Birkbak, N. J.; Hiley, C. T.; Watkins, T. B. K.; Shafi, S.; Murugaesu, N.; Mitter, R.; Akarca, A. U.; Linares, J.; Marafioti, T.; Henry, J. Y.; Allen, E. M. Van. Clonal Neoantigens Elicit T Cell Immunoreactivity and Sensitivity to Immune Checkpoint Blockade. *Science* **2016**, *351*, 1463–1469.
31. Germano, G.; Lamba, S.; Rospo, G.; Barault, L.; Magrì, A.; Maione, F.; Russo, M.; Crisafulli, G.; Bartolini, A.; Lerda, G.; Siravegna, G.; Mussolin, B.; Frapolli, R.; Montone, M.; Morano, F.; de

Braud, F.; Amirouchene-Angelozzi, N.; Marsoni, S.; D'Incalci, M.; *et al.* Inactivation of DNA Repair Triggers Neoantigen Generation and Impairs Tumour Growth. *Nature* **2017**, *552*, 116–120.

32. Rabinovich, G. a; Gabrilovich, D.; Sotomayor, E. M. Immunosuppressive Strategies That Are Mediated by Tumor Cells. *Annu. Rev. Immunol.* **2007**, *25*, 267–296.

33. Garrido, F.; Algarra, I. MHC Antigens and Tumor Escape from Immune Surveillance. *Adv. Cancer Res.* **2001**, *83*, 117–158.

34. Baghdadi, M.; Jinushi, M. The Impact of the TIM Gene Family on Tumor Immunity and Immunosuppression. *Cell. Mol. Immunol.* **2014**, *11*, 41–48.

35. Wang, Q.; Liu, F.; Liu, L. Prognostic Significance of PD-L1 in Solid Tumor: An Updated Meta-Analysis. *Medicine (Baltimore).* **2017**, *96*.

36. Birnbaum, M. E.; Berry, R.; Hsiao, Y.-S.; Chen, Z.; Shingu-Vazquez, M. A.; Yu, X.; Waghray, D.; Fischer, S.; McCluskey, J.; Rossjohn, J.; Walz, T.; Garcia, K. C. Molecular Architecture of the Aβ T Cell receptor–CD3 Complex. *Proc. Natl. Acad. Sci.* **2014**, *111*, 17576–17581.

37. Chen, L.; Flies, D. B. Molecular Mechanisms of T Cell Co-Stimulation and Co-Inhibition. *Nat. Rev. Immunol.* **2013**, *13*, 227–242.

38. Shuford, W. W.; Klussman, K.; Tritchler, D. D.; Loo, D. T.; Chalupny, J.; Siadak, a W.; Brown, T. J.; Emswiler, J.; Raecho, H.; Larsen, C. P.; Pearson, T. C.; Ledbetter, J. a; Aruffo, A.; Mittler, R. S. 4-1BB Costimulatory Signals Preferentially Induce CD8+ T Cell Proliferation and Lead to the Amplification in Vivo of Cytotoxic T Cell Responses. *J. Exp. Med.* **1997**, *186*, 47–55.

39. Okazaki, T.; Chikuma, S.; Iwai, Y.; Fagarasan, S.; Honjo, T. A Rheostat for Immune Responses: The Unique Properties of PD-1 and Their Advantages for Clinical Application. *Nat. Immunol.* **2013**, *14*, 1212–1218.

40. Postow, M. A.; Chesney, J.; Pavlick, A. C.; Robert, C.; Grossmann, K.; McDermott, D.; Linette, G. P.; Meyer, N.; Giguere, J. K.; Agarwala, S. S.; Shaheen, M.; Ernstoff, M. S.; Minor, D.; Salama, A. K.; Taylor, M.; Ott, P. A.; Rollin, L. M.; Horak, C.; Gagnier, P.; *et al.* Nivolumab and Ipilimumab versus Ipilimumab in Untreated Melanoma. *N. Engl. J. Med.* **2015**, *372*, 2006–2017.

41. Callahan, M. K.; Wolchok, J. D. At the Bedside: CTLA-4- and PD-1-Blocking Antibodies in Cancer Immunotherapy. *J. Leukoc. Biol.* **2013**, *94*, 41–53.

42. Spranger, S.; Koblish, H. K.; Horton, B.; Scherle, P. a; Newton, R.; Gajewski, T. F. Mechanism of Tumor Rejection with Doublets of CTLA-4, PD-1/PD-L1, or IDO Blockade Involves Restored IL-2 Production and Proliferation of CD8(+) T Cells Directly within the Tumor Microenvironment. *J. Immunother. cancer* **2014**, *2*, 3.

43. Chen, S.; Lee, L.-F.; Fisher, T. S.; Jessen, B.; Elliott, M.; Evering, W.; Logronio, K.; Tu, G. H.; Tsaparikos, K.; Li, X.; Wang, H.; Ying, C.; Xiong, M.; VanArsdale, T.; Lin, J. C. Combination of 4-1BB Agonist and PD-1 Antagonist Promotes Antitumor Effector/Memory CD8 T Cells in a Poorly Immunogenic Tumor Model. *Cancer Immunol. Res.* **2014**, *3*, 149–160.

44. Shindo, Y.; Yoshimura, K.; Kuramasu, A.; Watanabe, Y.; Ito, H. H.; Kondo, T.; Oga, A.; Ito, H. H.; Yoshino, S.; Hazama, S.; Tamada, K.; Yagita, H.; Oka, M. Combination Immunotherapy with 4-1BB Activation and PD-1 Blockade Enhances Antitumor Efficacy in a Mouse Model of Subcutaneous Tumor. *Anticancer Res* **2015**, *35*, 129–136.

45. Vezys, V.; Penaloza-macmaster, P.; Barber, D. L.; Ha, S.-J.; Konieczny, B.; Freeman, G. J.; Mittler, R. S.; Ahmed, R. 4-1BB Signaling Synergizes with Programmed Death Ligand 1 Blockade to Augment CD8 T Cell Responses during Chronic Viral Infection. *J. Immunol.* **2011**, *187*, 1634–1642.

46. Doh, J.; Irvine, D. J. Immunological Synapse Arrays: Patterned Protein Surfaces That Modulate Immunological Synapse Structure Formation in T Cells. *Proc. Natl. Acad. Sci.* **2006**, *103*, 5700–5705.

47. Delcassian, D.; Depoil, D.; Rudnicka, D.; Liu, M.; Davis, D. M.; Dustin, M. L.; Dunlop, I. E. Nanoscale Ligand Spacing Influences Receptor Triggering in T Cells and NK Cells. *Nano Lett.* **2013**, *13*, 5608–5614.

48. Matic, J.; Deeg, J.; Scheffold, A.; Goldstein, I.; Spatz, J. P. Fine Tuning and Efficient T Cell Activation with Stimulatory aCD3 Nanoarrays. *Nano Lett.* **2013**, *13*, 5090–5097.

49. Deeg, J.; Axmann, M.; Matic, J.; Liapis, A.; Depoil, D.; Afrose, J.; Curado, S.; Dustin, M. L.; Spatz, J. P. T Cell Activation Is Determined by the Number of Presented Antigens. *Nano Lett.* **2013**, *13*, 5619–5626.

50. Yokosuka, T.; Takamatsu, M.; Kobayashi-Imanishi, W.; Hashimoto-Tane, A.; Azuma, M.; Saito,

T. Programmed Cell Death 1 Forms Negative Costimulatory Microclusters That Directly Inhibit T Cell Receptor Signaling by Recruiting Phosphatase SHP2. *J. Exp. Med.* **2012**, *209*, 1201–1217.

51. Hui, E.; Cheung, J.; Zhu, J.; Su, X.; Taylor, M. J.; Wallweber, H. A.; Sasmal, D. K.; Huang, J.; Kim, J. M.; Mellman, I.; Vale, R. D. T Cell Costimulatory Receptor CD28 Is a Primary Target for PD-1–mediated Inhibition. *Science* **2017**, *355*, 1428–1433.
52. Stephan, M. T.; Ponomarev, V.; Brentjens, R. J.; Chang, A. H.; Dobrenkov, K. V; Heller, G.; Sadelain, M. T Cell-Encoded CD80 and 4-1BBL Induce Auto- and Transcostimulation, Resulting in Potent Tumor Rejection. *Nat. Med.* **2007**, *13*, 1440–1449.
53. Perica, K.; Kosmides, A. K.; Schneck, J. P. Linking Form to Function: Biophysical Aspects of Artificial Antigen Presenting Cell Design. *Biochim. Biophys. Acta* **2015**, *1853*, 781–790.
54. Steenblock, E. R.; Fahmy, T. M. A Comprehensive Platform for Ex Vivo T-Cell Expansion Based on Biodegradable Polymeric Artificial Antigen-Presenting Cells. *Mol. Ther.* **2008**, *16*, 765–772.
55. Oelke, M.; Maus, M. V; Didiano, D.; June, C. H.; Mackensen, A.; Schneck, J. P. Ex Vivo Induction and Expansion of Antigen-Specific Cytotoxic T Cells by HLA-Ig-Coated Artificial Antigen-Presenting Cells. *Nat. Med.* **2003**, *9*, 619–624.
56. Sharma, G.; Valenta, D. T.; Altman, Y.; Harvey, S.; Xie, H.; Mitragotri, S.; Smith, J. W. Polymer Particle Shape Independently Influences Binding and Internalization by Macrophages. *J. Control. Release* **2010**, *147*, 408–412.
57. Champion, J. a; Walker, A.; Mitragotri, S. Role of Particle Size in Phagocytosis of Polymeric Microspheres. *Pharm. Res.* **2008**, *25*, 1815–1821.
58. Manolova, V.; Flace, A.; Bauer, M.; Schwarz, K.; Saudan, P.; Bachmann, M. F. Nanoparticles Target Distinct Dendritic Cell Populations according to Their Size. *Eur. J. Immunol.* **2008**, *38*, 1404–1413.
59. Hickey, J. W.; Vicente, F. P.; Howard, G. P.; Mao, H.-Q.; Schneck, J. P. Biologically Inspired Design of Nanoparticle Artificial Antigen-Presenting Cells for Immunomodulation. *Nano Lett.* **2017**, *17*, 7045–7054.
60. Perica, K.; Tu, A.; Richter, A.; Bieler, J. G.; Edidin, M.; Schneck, J. P. Magnetic Field-Induced T Cell Receptor Clustering by Nanoparticles Enhances T Cell Activation and Stimulates Antitumor

Activity. *ACS Nano* **2014**, *8*, 2252–2260.

61. Champion, J. a; Mitragotri, S. Role of Target Geometry in Phagocytosis. *Proc. Natl. Acad. Sci.* **2006**, *103*, 4930–4934.

62. Gratton, S. E. a; Ropp, P. a; Pohlhaus, P. D.; Luft, J. C.; Madden, V. J.; Napier, M. E.; DeSimone, J. M. The Effect of Particle Design on Cellular Internalization Pathways. *Proc. Natl. Acad. Sci.* **2008**, *105*, 11613–11618.

63. Yoo, J.-W.; Mitragotri, S. Polymer Particles That Switch Shape in Response to a Stimulus. *Proc. Natl. Acad. Sci.* **2010**, *107*, 11205–11210.

64. Barua, S.; Yoo, J.-W.; Kolhar, P.; Wakankar, A.; Gokarn, Y. R.; Mitragotri, S. Particle Shape Enhances Specificity of Antibody-Displaying Nanoparticles. *Proc. Natl. Acad. Sci.* **2013**, *110*, 3270–3275.

65. Sunshine, J. C.; Perica, K.; Schneck, J. P.; Green, J. J. Particle Shape Dependence of CD8+ T Cell Activation by Artificial Antigen Presenting Cells. *Biomaterials* **2014**, *35*, 269–277.

66. Meyer, R. a.; Sunshine, J. C.; Perica, K.; Kosmides, A. K.; Aje, K.; Schneck, J. P.; Green, J. J. Biodegradable Nanoellipsoidal Artificial Antigen Presenting Cells for Antigen Specific T-Cell Activation. *Small* **2014**, *11*, 1519–1525.

67. Dudley, M. E.; Rosenberg, S. A. Adoptive-Cell-Transfer Therapy for the Treatment of Patients with Cancer. *Nat. Rev. Cancer* **2003**, *3*, 666–675.

68. Rosenberg, S. A.; Restifo, N. P. Adoptive Cell Transfer as Personalized Immunotherapy for Human Cancer. *Science* **2015**, *348*, 62–68.

69. Busch, D. H.; Fräßle, S. P.; Sommermeyer, D.; Buchholz, V. R.; Riddell, S. R. Role of Memory T Cell Subsets for Adoptive Immunotherapy. *Semin. Immunol.* **2016**, *28*, 28–34.

70. Oelke, M.; Schneck, J. P. Overview of a HLA-Ig based “Lego-like System” for T Cell Monitoring, Modulation and Expansion. *Immunol. Res.* **2010**, *47*, 248–256.

71. Ye, Q.; Loisiou, M.; Levine, B. L.; Suhoski, M. M.; Riley, J. L.; June, C. H.; Coukos, G.; Powell, D. J. Engineered Artificial Antigen Presenting Cells Facilitate Direct and Efficient Expansion of Tumor Infiltrating Lymphocytes. *J. Transl. Med.* **2011**, *9*, 131.

72. Gong, W.; Ji, M.; Cao, Z.; Wang, L.; Qian, Y.; Hu, M.; Qian, L.; Pan, X. Establishment and

Characterization of a Cell Based Artificial Antigen-Presenting Cell for Expansion and Activation of CD8+ T Cells Ex Vivo. *Cell. Mol. Immunol.* **2008**, *5*, 47–53.

73. Suhoski, M. M.; Golovina, T. N.; Aqui, N. A.; Tai, V. C.; Varela-Rohena, A.; Milone, M. C.; Carroll, R. G.; Riley, J. L.; June, C. H. Engineering Artificial Antigen-Presenting Cells to Express a Diverse Array of Co-Stimulatory Molecules. *Mol. Ther.* **2007**, *15*, 981–988.

74. Dupont, J.; Latouche, J.-B.; Ma, C.; Sadelain, M. Artificial Antigen-Presenting Cells Transduced with Telomerase Efficiently Expand Epitope-Specific, Human Leukocyte Antigen-Restricted Cytotoxic T Cells. *Cancer Res.* **2005**, *65*, 5417–5427.

75. Latouche, J. B.; Sadelain, M. Induction of Human Cytotoxic T Lymphocytes by Artificial Antigen-Presenting Cells. *Nat. Biotechnol.* **2000**, *18*, 405–409.

76. Papanicolaou, G. A.; Latouche, J.-B.; Tan, C.; Dupont, J.; Stiles, J.; Pamer, E. G.; Sadelain, M. Rapid Expansion of Cytomegalovirus-Specific Cytotoxic T Lymphocytes by Artificial Antigen-Presenting Cells Expressing a Single HLA Allele. *Blood* **2003**, *102*, 2498–2505.

77. Deeths, M. J.; Mescher, M. F. B7-1-Dependent Co-Stimulation Results in Qualitatively and Quantitatively Different Responses by CD4+ and CD8+ T Cells. *Eur. J. Immunol.* **1997**, *27*, 598–608.

78. Curtsinger, J.; Deeths, M. J.; Pease, P.; Mescher, M. F. Artificial Cell Surface Constructs for Studying Receptor-Ligand Contributions to Lymphocyte Activation. *J. Immunol. Methods* **1997**, *209*, 47–57.

79. Mescher, M. F. Surface Contact Requirements for Activation of Cytotoxic T Lymphocytes. *J. Immunol.* **1992**, *149*, 2402–2405.

80. Tham, E. L.; Jensen, P. L.; Mescher, M. F. Activation of Antigen-Specific T Cells by Artificial Cell Constructs Having Immobilized Multimeric Peptide-Class I Complexes and Recombinant B7-Fc Proteins. *J. Immunol. Methods* **2001**, *249*, 111–119.

81. Motta, I.; Lone, Y. C.; Kourilsky, P. In Vitro Induction of Naive Cytotoxic T Lymphocytes with Complexes of Peptide and Recombinant MHC Class I Molecules Coated onto Beads: Role of TCR/ligand Density. *Eur. J. Immunol.* **1998**, *28*, 3685–3695.

82. Hammink, R.; Mandal, S.; Eggermont, L. J.; Nooteboom, M.; Willems, P. H. G. M.; Tel, J.;

Rowan, A. E.; Figdor, C. G.; Blank, K. G. Controlling T-Cell Activation with Synthetic Dendritic Cells Using the Multivalency Effect. *ACS Omega* **2017**, *2*, 937–945.

83. Fang, J.; Nakamura, H.; Maeda, H. The EPR Effect: Unique Features of Tumor Blood Vessels for Drug Delivery, Factors Involved, and Limitations and Augmentation of the Effect. *Adv. Drug Deliv. Rev.* **2011**, *63*, 136–151.

84. Perica, K.; De León Medero, A.; Durai, M.; Chiu, Y. L.; Bieler, J. G.; Sibener, L.; Niemöller, M.; Assenmacher, M.; Richter, A.; Edidin, M.; Oelke, M.; Schneck, J. Nanoscale Artificial Antigen Presenting Cells for T Cell Immunotherapy. *Nanomedicine* **2014**, *10*, 119–129.

85. Helle, M.; Rampazzo, E.; Monchanin, M.; Marchal, F.; Guillemin, F.; Bonacchi, S.; Salis, F.; Prodi, L.; Bezdetnaya, L. Surface Chemistry Architecture of Silica Nanoparticles Determine the Efficiency of in Vivo Fluorescence Lymph Node Mapping. *ACS Nano* **2013**, *7*, 8645–8657.

86. Astete, C. E.; Sabliov, C. M. Synthesis and Characterization of PLGA Nanoparticles. *J. Biomater. Sci. Polym. Ed.* **2006**, *17*, 247–289.

87. Danhier, F.; Ansorena, E.; Silva, J. M.; Coco, R.; Le Breton, A.; Préat, V. PLGA-Based Nanoparticles: An Overview of Biomedical Applications. *J. Control. Release* **2012**, *161*, 505–522.

88. Ye, Q.; Song, D.-G.; Poussin, M.; Yamamoto, T.; Best, A.; Li, C.; Coukos, G.; Powell, D. J. CD137 Accurately Identifies and Enriches for Naturally Occurring Tumor-Reactive T Cells in Tumor. *Clin. Cancer Res.* **2014**, *20*, 44–55.

89. Hernandez-chacon, J. A.; Li, Y.; Wu, R. C.; Bernatchez, C.; Weber, J.; Hwu, P.; Radvanyi, L. Co-Stimulation through the CD137/4-1BB Pathway Protects Human Melanoma Tumor-Infiltrating Lymphocytes from Activation-Induced Cell Death and Enhances Anti-Tumor Effector Function. **2012**, *34*, 236–250.

90. Zhang, H.; Snyder, K. M.; Suhoski, M. M.; Maus, M. V; Kapoor, V. 4-1BB Is Superior to CD28 Costimulation for Generating CD8+ Cytotoxic Lymphocytes for Adoptive Immunotherapy. **2013**, *179*, 4910–4918.

91. Jahan, N.; Talat, H.; Curry, W. T. Agonist OX40 Immunotherapy Improves Survival in Glioma-Bearing Mice and Is Complementary with Vaccination with Irradiated GM-CSF–expressing Tumor Cells. *Neuro. Oncol.* **2017**, *20*, 44–54.

92. Tay, N. Q.; Lee, D. C. P.; Chua, Y. L.; Prabhu, N.; Gascoigne, N. R. J.; Kemeny, D. M. CD40L Expression Allows CD8+ T Cells to Promote Their Own Expansion and Differentiation through Dendritic Cells. *Front. Immunol.* **2017**, *8*.

93. Singh, M.; Vianden, C.; Cantwell, M. J.; Dai, Z.; Xiao, Z.; Sharma, M.; Khong, H.; Jaiswal, A. R.; Faak, F.; Hailemichael, Y.; Janssen, L. M. E.; Bharadwaj, U.; Curran, M. A.; Diab, A.; Bassett, R. L.; Tweardy, D. J.; Hwu, P.; Overwijk, W. W. Intratumoral CD40 Activation and Checkpoint Blockade Induces T Cell-Mediated Eradication of Melanoma in the Brain. *Nat. Commun.* **2017**, *8*, 1–10.

94. Poon, I. K. H.; Lucas, C. D.; Rossi, A. G.; Ravichandran, K. S. Apoptotic Cell Clearance: Basic Biology and Therapeutic Potential. *Nat. Rev. Immunol.* **2014**, *14*, 166–180.

95. Bruns, H.; Bessell, C.; Varela, J. C.; Haupt, C.; Fang, J.; Pasemann, S.; Mackensen, A.; Oelke, M.; Schneck, J. P.; Schütz, C. CD47 Enhances in Vivo Functionality of Artificial Antigen-Presenting Cells. *Clin. Cancer Res.* **2015**, *21*, 2075–2083.

96. Curtsinger, J. M.; Mescher, M. F. Inflammatory Cytokines as a Third Signal for T Cell Activation Julie. *Curr Opin Immunol* **2011**, *22*, 333–340.

97. Steenblock, E. R.; Fadel, T.; Labowsky, M.; Pober, J. S.; Fahmy, T. M. An Artificial Antigen-Presenting Cell with Paracrine Delivery of IL-2 Impacts the Magnitude and Direction of the T Cell Response. *J. Biol. Chem.* **2011**, *286*, 34883–34892.

98. Dinauer, N.; Balthasar, S.; Weber, C.; Kreuter, J.; Langer, K.; von Briesen, H. Selective Targeting of Antibody-Conjugated Nanoparticles to Leukemic Cells and Primary T-Lymphocytes. *Biomaterials* **2005**, *26*, 5898–5906.

99. Smith, T. T.; Stephan, S. B.; Moffett, H. F.; McKnight, L. E.; Ji, W.; Reiman, D.; Bonagofski, E.; Wohlfahrt, M. E.; Pillai, S. P. S.; Stephan, M. T. In Situ Programming of Leukaemia-Specific T Cells Using Synthetic DNA Nanocarriers. *Nat. Nanotechnol.* **2017**, *12*, 813.

100. Ramishetti, S.; Kedmi, R.; Goldsmith, M.; Leonard, F.; Sprague, A. G.; Godin, B.; Gozin, M.; Cullis, P. R.; Dykxhoorn, D. M.; Peer, D. Systemic Gene Silencing in Primary T Lymphocytes Using Targeted Lipid Nanoparticles. **2015**, 6706–6716.

101. Stephan, M. T.; Stephan, S. B.; Bak, P.; Chen, J.; Irvine, D. J. Synapse-Directed Delivery of

Immunomodulators Using T-Cell-Conjugated Nanoparticles. *Biomaterials* **2012**, *33*, 5776–5787.

102. Jones, R. B.; Mueller, S.; Kumari, S.; Vrbanac, V.; Genel, S.; Tager, A. M.; Allen, T. M.; Walker, B. D.; Irvine, D. J. Antigen Recognition-Triggered Drug Delivery Mediated by Nanocapsule-Functionalized Cytotoxic T-Cells. *Biomaterials* **2017**, *117*, 44–53.

103. Zheng, Y.; Tang, L.; Mabardi, L.; Kumari, S.; Irvine, D. J. Enhancing Adoptive Cell Therapy of Cancer through Targeted Delivery of Small-Molecule Immunomodulators to Internalizing or Non-Internalizing Receptors. *ACS Nano* **2017**, acsnano.7b00078.

104. Ascierto, P. A.; Simeone, E.; Sznol, M.; Fu, Y. X.; Melero, I. Clinical Experiences with Anti-CD137 and Anti-PD1 Therapeutic Antibodies. *Semin. Oncol.* **2010**, *37*, 508–516.

105. Panelli, M. C.; White, R.; Foster, M.; Martin, B.; Wang, E.; Smith, K.; Marincola, F. M. Forecasting the Cytokine Storm Following Systematic Interleukin (IL)-2 Administration. *J. Transl. Med.* **2004**, *2*, 1–14.

106. Kwong, B.; Gai, S. A.; Elkhader, J.; Wittrup, K. D.; Irvine, D. J. Localized Immunotherapy via Liposome-Anchored Anti-CD137 + IL-2 Prevents Lethal Toxicity and Elicits Local and Systemic Antitumor Immunity. *Cancer Res.* **2013**, *73*, 1547–1558.

107. Zhang, Y.; Li, N.; Suh, H.; Irvine, D. J. Nanoparticle Anchoring Targets Immune Agonists to Tumors Enabling Anti-Cancer Immunity without Systemic Toxicity. *Nat. Commun.* **2018**, *9*, 6.

108. Steinman, R. M. Decisions About Dendritic Cells: Past, Present, and Future. *Annu. Rev. Immunol.* **2012**, *30*, 1–22.

109. Kantoff, P. W.; Higano, C. S.; Shore, N. D.; Berger, R.; Small, E. J.; Penson, D. F.; Redfern, C. H.; Ferrari, A. C.; Dreicer, R.; Sims, R. B.; Xu, Y.; Frohlich, M. W.; Schellhammer, P. F. Sipuleucel-T Immunotherapy for Castration-Resistant Prostate Cancer. *N. Engl. J. Med.* **2010**, *363*, 2373–2383.

110. Paller, C. J.; Antonarakis, E. S. Sipuleucel-T for the Treatment of Metastatic Prostate Cancer. *Hum. Vaccin. Immunother.* **2012**, *8*, 509–519.

111. Gu, L.; Mooney, D. J. Biomaterials and Emerging Anticancer Therapeutics: Engineering the Microenvironment. *Nat. Rev. Cancer* **2015**, *16*, 56–66.

112. Leleux, J.; Alexandra, A.; Roy, K. Engineering Immunity: Modulating Dendritic Cell Subsets and Lymph Node Response to Direct Immune-Polarization and Vaccine Efficacy. *J Control Release*

2015, *219*, 610–621.

113. Reddy, S. T.; Van Der Vlies, A. J. A. J.; Simeoni, E.; Angeli, V.; Randolph, G. J.; O'Neil, C. P.; Lee, L. K.; Swartz, M. A.; Hubbell, J. A. Exploiting Lymphatic Transport and Complement Activation in Nanoparticle Vaccines. *Nat. Biotechnol.* **2007**, *25*, 1159–1164.

114. Fifis, T.; Gamvrellis, A.; Crimeen-Irwin, B.; Pietersz, G. A.; Li, J.; Mottram, P. L.; McKenzie, I. F. C.; Plebanski, M. Size-Dependent Immunogenicity: Therapeutic and Protective Properties of Nano-Vaccines against Tumors. *J. Immunol.* **2004**, *173*, 3148–3154.

115. Kuai, R.; Ochyl, L. J.; Bahjat, K. S.; Schwendeman, A.; Moon, J. J. Designer Vaccine Nanodiscs for Personalized Cancer Immunotherapy. *Nat. Mater.* **2016**, *1*, 1–10.

116. Lee, I. H.; Kwon, H. K.; An, S.; Kim, D.; Kim, S.; Yu, M. K.; Lee, J. H.; Lee, T. S.; Im, S. H.; Jon, S. Imageable Antigen-Presenting Gold Nanoparticle Vaccines for Effective Cancer Immunotherapy in Vivo. *Angew. Chemie - Int. Ed.* **2012**, *51*, 8800–8805.

117. Li, A. V; Moon, J. J.; Abraham, W.; Suh, H.; Seidman, M. A.; Yen, M.; Im, E.; Foley, M. H.; Dan, H. Generation of Effector Memory T Cell–Based Mucosal and Systemic Immunity with Pulmonary Nanoparticle Vaccination. *Sci Transl Med* **2014**, *5*, 204ra130.

118. Liu, H.; Moynihan, K. D.; Zheng, Y.; Szeto, G. L.; Li, A. V.; Huang, B.; Van Egeren, D. S.; Park, C.; Irvine, D. J. Structure-Based Programming of Lymph-Node Targeting in Molecular Vaccines. *Nature* **2014**, *507*, 519–522.

119. Raghuwanshi, D.; Mishra, V.; Suresh, M. R.; Kaur, K. A Simple Approach for Enhanced Immune Response Using Engineered Dendritic Cell Targeted Nanoparticles. *Vaccine* **2012**, *30*, 7292–7299.

120. Cruz, L. J.; Rosalia, R. A.; Kleinovink, J. W.; Rueda, F.; Löwik, C. W. G. M.; Ossendorp, F. Targeting Nanoparticles to CD40, DEC-205 or CD11c Molecules on Dendritic Cells for Efficient CD8+T Cell Response: A Comparative Study. *J. Control. Release* **2014**, *192*, 209–218.

121. Scott, E. A.; Stano, A.; Gillard, M.; Maio-Liu, A. C.; Swartz, M. A.; Hubbell, J. A. Dendritic Cell Activation and T Cell Priming with Adjuvant- and Antigen-Loaded Oxidation-Sensitive Polymersomes. *Biomaterials* **2012**, *33*, 6211–6219.

122. Shutz, C.; Varela, J. C.; Perica, K.; Haupt, C.; Oelke, M.; Schneck, J. P. Antigen-Specific T Cell Redirectors: A Nanoparticle Based Approach for Redirecting T Cells. *Oncotarget* **2016**, *7*, 68503–

68512.

123. Lurie, N.; Slater, J.; McGovern, P.; Ekstrum, J.; Quam, L.; Margolis, K. A Progress Report on the Treatment of 157 Patients with Advanced Cancer Using Lymphokine-Activated Killer Cells and Interleukin-2 of High-Dose Interleukin-2 Alone. *N. Engl. J. Med.* **1993**, *329*, 478–482.

124. Rosenberg, S. A. IL-2: The First Effective Immunotherapy for Human Cancer. *J. Immunol.* **2014**, *192*, 5451–5458.

125. Malek, T. R.; Castro, I. Interleukin-2 Receptor Signaling: At the Interface between Tolerance and Immunity. *Immunity* **2010**, *33*, 153–165.

126. Krieg, C.; Letourneau, S.; Pantaleo, G.; Boyman, O. Improved IL-2 Immunotherapy by Selective Stimulation of IL-2 Receptors on Lymphocytes and Endothelial Cells. *Proc. Natl. Acad. Sci.* **2010**, *107*, 11906–11911.

127. Levin, A. M.; Bates, D. L.; Ring, A. M.; Krieg, C.; Lin, J. T.; Su, L.; Moraga, I. L.; Raeber, M. E.; Bowman, G. R.; Novick, P.; Pande, V. S.; Fathman, C. G.; Boyman, O.; Garcia, K. C.; Vijay, S.; Fathman, C. G.; Boyman, O.; Garcia, K. C. Exploiting a Natural Conformational Switch to Engineer an Interleukin-2 “Superkine.” *Nature* **2012**, *484*, 529–533.

128. Mishra, A.; Sullivan, L.; Caligiuri, M. A. Molecular Pathways: Interleukin-15 Signaling in Health and in Cancer. *Clin Cancer Res* **2014**, *20*, 2044–2050.

129. Rubinstein, M. P.; Kovar, M.; Purton, J. F.; Cho, J.-H.; Boyman, O.; Surh, C. D.; Sprent, J. Converting IL-15 to a Superagonist by Binding to Soluble IL-15Ra. *Proc. Natl. Acad. Sci.* **2006**, *103*, 9166–9171.

130. Zhu, X.; Marcus, W. D.; Xu, W.; Lee, H.-I.; Han, K.; Egan, J. O.; Yovandich, J. L.; Rhode, P. R.; Wong, H. c. Novel Human Interleukin-15 Agonists. *J Immunol* **2009**, *183*, 1–27.

131. Bailey, C. P.; Budak-Alpdogan, T.; Sauter, C. T.; Panis, M. M.; Buyukgoz, C.; Jeng, E. K.; Wong, H. C.; Flomenberg, N.; Alpdogan, O. New Interleukin-15 Superagonist (IL-15SA) Significantly Enhances Graft-versus-Tumor Activity. *Oncotarget* **2017**, *8*, 44366–44378.

132. Neri, D.; Sondel, P. M. Immunocytokines for Cancer Treatment: Past, Present and Future. *Curr Opin Immunol* **2016**, *40*, 96–102.

133. Müller, D. Antibody-Cytokine Fusion Proteins for Cancer Immunotherapy: An Update on Recent

Developments. *BioDrugs* **2014**, *28*, 123–131.

134. Carnemolla, B.; Borsi, L.; Balza, E.; Castellani, P.; Meazza, R.; Berndt, A.; Ferrini, S.; Kosmehl, H.; Neri, D.; Zardi, L. Enhancement of the Antitumor Properties of Interleukin-2 by Its Targeted Delivery to the Tumor Blood Vessel Extracellular Matrix Enhancement of the Antitumor Properties of Interleukin-2 by Its Targeted Delivery to the Tumor Blood Vessel Extracellular Matr. **2013**, *99*, 1659–1665.

135. Liu, B.; Kong, L.; Han, K.; Hong, H.; Marcus, W. D.; Chen, X.; Jeng, E. K.; Alter, S.; Zhu, X.; Rubinstein, M. P.; Shi, S.; Rhode, P. R.; Cai, W.; Wong, H. C. A Novel Fusion of ALT-803 (Interleukin (IL)-15 Superagonist) with an Antibody Demonstrates Antigen-Specific Antitumor Responses. *J. Biol. Chem.* **2016**, *291*, 23869–23881.

136. Vincent, M.; Teppaz, G.; Lajoie, L.; Solé, V.; Bessard, A.; Maillasson, M.; Loisel, S.; Béchard, D.; Clémenceau, B.; Thibault, G.; Garrigue-Antar, L.; Jacques, Y.; Quéméner, A. Highly Potent Anti-CD20-RLI Immunocytokine Targeting Established Human B Lymphoma in SCID Mouse. *MAbs* **2014**, *6*, 1026–1037.

137. Kawalkowska, J. Z.; Hemmerle, T.; Pretto, F.; Matasci, M.; Neri, D.; Williams, R. O. Targeted IL-4 Therapy Synergizes with Dexamethasone to Induce a State of Tolerance by Promoting Treg Cells and Macrophages in Mice with Arthritis. *Eur. J. Immunol.* **2016**, *46*, 1246–1257.

138. Fallon, J. K.; Vandeveer, A. J.; Schlom, J.; Greiner, J. W. Enhanced Antitumor Effects by Combining an IL-12/anti-DNA Fusion Protein with Avelumab, an Anti-PD-L1 Antibody. *Oncotarget* **2017**, *8*, 20558–20571.

139. Chen, X.; Xu, J.; Guo, Q.; Wang, L.; Yang, Y.; Guo, H.; Gu, N.; Zhang, D.; Qian, W.; Hou, S.; Li, J.; Dai, J.; Guo, Y.; Wang, H. Therapeutic Efficacy of an Anti-PD-L1 Antibody Based Immunocytokine in a Metastatic Mouse Model of Colorectal Cancer. *Biochem. Biophys. Res. Commun.* **2016**, *480*, 160–165.

140. Kamath, A. V. Translational Pharmacokinetics and Pharmacodynamics of Monoclonal Antibodies. *Drug Discov. Today Technol.* **2016**, *21-22*, 75–83.

141. Beers, S. A.; Glennie, M. J.; White, A. L. Influence of Immunoglobulin Isotype on Therapeutic Antibody Function. *Blood* **2016**, *127*, 1097–1101.

142. Wang, W.; Erbe, A. K.; Hank, J. A.; Morris, Z. S.; Sondel, P. M. NK Cell-Mediated Antibody-Dependent Cellular Cytotoxicity in Cancer Immunotherapy. *Front. Immunol.* **2015**, *6*.

143. Taylor, R. P.; Lindorfer, M. A. Cytotoxic Mechanisms of Immunotherapy: Harnessing Complement in the Action of Anti-Tumor Monoclonal Antibodies. *Semin. Immunol.* **2016**, *28*, 309–316.

144. Gong, Q.; Hazen, M.; Marshall, B.; Crowell, S. R.; Ou, Q.; Wong, A. W.; Phung, W.; Vernes, J. M.; Meng, Y. G.; Tejada, M.; Andersen, D.; Kelley, R. F. Increased in Vivo Effector Function of Human IgG4 Isotype Antibodies through Afucosylation. *MAbs* **2016**, *8*, 1098–1106.

145. Harding, F. A.; Stickler, M. M.; Razo, J.; DuBridge, R. B. The Immunogenicity of Humanized and Fully Human Antibodies: Residual Immunogenicity Resides in the CDR Regions. *MAbs* **2010**, *2*, 256–265.

146. Hamid, O.; Robert, C.; Daud, A.; Hodi, F. S.; Hwu, W.-J.; Kefford, R.; Wolchok, J. D.; Hersey, P.; Joseph, R. W.; Weber, J. S.; Dronca, R.; Gangadhar, T. C.; Patnaik, A.; Zarour, H.; Joshua, A. M.; Gergich, K.; Elassaiss-Schaap, J.; Algazi, A.; Mateus, C.; *et al.* Safety and Tumor Responses with Lambrolizumab (Anti-PD-1) in Melanoma. *N. Engl. J. Med.* **2013**, *369*, 134–144.

147. Chen, L.; Han, X. Anti – PD-1 / PD-L1 Therapy of Human Cancer : Past , Present , and Future. *J. Clin. Invest.* **2015**, *125*.

148. Larkin, J.; Chiarion-Sileni, V.; Gonzalez, R.; Grob, J. J.; Cowey, C. L.; Lao, C. D.; Schadendorf, D.; Dummer, R.; Smylie, M.; Rutkowski, P.; Ferrucci, P. F.; Hill, A.; Wagstaff, J.; Carlino, M. S.; Haanen, J. B.; Maio, M.; Marquez-Rodas, I.; McArthur, G. A.; Ascierto, P. A.; *et al.* Combined Nivolumab and Ipilimumab or Monotherapy in Untreated Melanoma. *N. Engl. J. Med.* **2015**, *373*, 23–34.

149. Pedicord, V. a; Montalvo, W.; Leiner, I. M.; Allison, J. P. Single Dose of Anti – CTLA-4 Enhances CD8 + T-Cell Memory Formation , Function , and Maintenance. *PNAS* **2011**, *108*, 266–271.

150. Hugo, W.; Zaretsky, J. M.; Sun, L.; Song, C.; Moreno, B. H.; Hu-Lieskovan, S.; Berent-Maoz, B.; Pang, J.; Chmielowski, B.; Cherry, G.; Seja, E.; Lomeli, S.; Kong, X.; Kelley, M. C.; Sosman, J. A.; Johnson, D. B.; Ribas, A.; Lo, R. S. Genomic and Transcriptomic Features of Response to Anti-PD-1 Therapy in Metastatic Melanoma. *Cell* **2016**, *165*, 35–44.

151. Van Allen, E. M.; Miao, D.; Schilling, B.; Shukla, S. A.; Blank, C.; Zimmer, L.; Sucker, A.; Hillen, U.; Geukes Foppen, M. H.; Goldinger, S. M.; Utikal, J.; Hassel, J. C.; Weide, B.; Kaehler, K. C.; Loquai, C.; Mohr, P.; Gutzmer, R.; Dummer, R.; Gabriel, S.; *et al.* Genomic Correlates of Response to CTLA-4 Blockade in Metastatic Melanoma. *Science* **2015**, *350*, 207–211.

152. Tyrsin, D.; Chuvpilo, S.; Matskevich, A.; Nemenov, D.; Römer, P. S.; Tabares, P.; Hünig, T. From TGN1412 to TAB08: The Return of CD28 Superagonist Therapy to Clinical Development for the Treatment of Rheumatoid Arthritis. *Clin. Exp. Rheumatol.* **2016**, *34*, 45–48.

153. Polu, K. R.; Lowman, H. B. Probody Therapeutics for Targeting Antibodies to Diseased Tissue. *Expert Opin. Biol. Ther.* **2014**, *14*, 1049–1053.

154. Kermer, V.; Hornig, N.; Harder, M.; Bondarieva, A.; Kontermann, R. E.; Muller, D. Combining Antibody-Directed Presentation of IL-15 and 4-1BBL in a Trifunctional Fusion Protein for Cancer Immunotherapy. *Mol. Cancer Ther.* **2014**, *13*, 112–121.

155. Yasunaga, M.; Manabe, S.; Matsumura, Y. Immunoregulation by IL-7R-Targeting Antibody-Drug Conjugates: Overcoming Steroid-Resistance in Cancer and Autoimmune Disease. *Sci. Rep.* **2017**, *7*, 1–14.

156. Strohl, W. R. Current Progress in Innovative Engineered Antibodies. *Protein Cell* **2017**, *9*, 1–35.

157. Chelius, D.; Ruf, P.; Gruber, P.; Plöscher, M.; Liedtke, R.; Gansberger, E.; Hess, J.; Wasiliu, M.; Lindhofer, H.; Chelius, D.; Ruf, P.; Gruber, P.; Plöscher, M.; Liedtke, R.; Gansberger, E.; Hess, J.; Wasiliu, M.; Structural, H. L.; Chelius, D.; *et al.* Structural and Functional Characterization of the Trifunctional Antibody Catumaxomab Structural and Functional Characterization of the Trifunctional Antibody Catumaxomab. **2016**, *0862*, 309–319.

158. Huehls, A. M.; Coupet, T. A.; Sentman, C. L. Bispecific T Cell Engagers for Cancer Immunotherapy. *Immunol. Cell Biol.* **2015**, *93*, 290–296.

159. Klinger, M.; Brandl, C.; Zugmaier, G.; Hijazi, Y.; Bargou, R. C.; Topp, M. S.; Gökbuget, N.; Neumann, S.; Goebeler, M.; Viardot, A.; Stelljes, M.; Hoelzer, D.; Degenhard, E.; Nagorsen, D.; Baeuerle, P. a; Wolf, A.; Kufer, P.; Dc, W.; Go, N. Immunopharmacologic Response of Patients with B-Lineage Acute Lymphoblastic Leukemia to Continuous Infusion of T Cell − Engaging Immunopharmacologic Response of Patients with B-Lineage Acute Lymphoblastic Leukemia to

Continuous Infusion of T Cell – Engagi. **2013**, *119*, 6226–6233.

160. Yuraszeck, T.; Kasichayanula, S.; Benjamin, J. E. Translation and Clinical Development of Bispecific T-Cell Engaging Antibodies for Cancer Treatment. *Clin. Pharmacol. Ther.* **2017**, *101*, 634–645.

161. Lee, K. J.; Chow, V.; Weissman, A.; Tulpule, S.; Aldoss, I.; Akhtari, M. Clinical Use of Blinatumomab for B-Cell Acute Lymphoblastic Leukemia in Adults. *Ther. Clin. Risk Manag.* **2016**, *12*, 1301–1310.

162. Kantarjian, H.; Stein, A.; Gökbuget, N.; Fielding, A. K.; Schuh, A. C.; Ribera, J.-M.; Wei, A.; Dombret, H.; Foà, R.; Bassan, R.; Arslan, Ö.; Sanz, M. A.; Bergeron, J.; Demirkan, F.; Lech-Maranda, E.; Rambaldi, A.; Thomas, X.; Horst, H.-A.; Brüggemann, M.; *et al.* Blinatumomab versus Chemotherapy for Advanced Acute Lymphoblastic Leukemia. *N. Engl. J. Med.* **2017**, *376*, 836–847.

163. Mack, M.; Riethmuller, G.; Kufer, P. A Small Bispecific Antibody Construct Expressed as a Functional Single-Chain Molecule with High Tumor Cell Cytotoxicity. *Proc. Natl. Acad. Sci.* **1995**, *92*, 7021–7025.

164. Hipp, S.; Tai, Y. T.; Blanset, D.; Deegen, P.; Wahl, J.; Thomas, O.; Rattel, B.; Adam, P. J.; Anderson, K. C.; Friedrich, M. A Novel BCMA/CD3 Bispecific T-Cell Engager for the Treatment of Multiple Myeloma Induces Selective Lysis in Vitro and in Vivo. *Leukemia* **2017**, *31*, 1743–1751.

165. Iwahori, K.; Kakarla, S.; Velasquez, M. P.; Yu, F.; Yi, Z.; Gerken, C.; Song, X.-T.; Gottschalk, S. Engager T Cells: A New Class of Antigen-Specific T Cells That Redirect Bystander T Cells. *Mol. Ther.* **2014**.

166. Ross, S. L.; Sherman, M.; McElroy, P. L.; Lofgren, J. A.; Moody, G.; Baeuerle, P. A.; Coxon, A.; Arvedson, T. Bispecific T Cell Engager (BiTE®) Antibody Constructs Can Mediate Bystander Tumor Cell Killing. *PLoS One* **2017**, *12*, 1–24.

167. Ryan, J. M.; Mittal, P.; Menoret, A.; Svedova, J.; Wasser, J. S.; Adler, A. J.; Vella, A. T. A Novel Biologic Platform Elicits Profound T Cell Costimulatory Activity and Antitumor Immunity in Mice. *Cancer Immunol. Immunother.* **2018**, *0*, 0.

168. Pilon-Thomas, S.; Mackay, A.; Vohra, N.; Mulé, J. J. Blockade of Programmed Death Ligand 1 Enhances the Therapeutic Efficacy of Combination Immunotherapy against Melanoma. *J. Immunol.* **2010**, *184*, 3442–3449.

169. Li, B.; Vanroey, M.; Wang, C.; Chen, T. H. T.; Korman, A.; Jooss, K. Anti-Programmed Death-1 Synergizes with Granulocyte Macrophage Colony-Stimulating Factor-Secreting Tumor Cell Immunotherapy Providing Therapeutic Benefit to Mice with Established Tumors. *Clin. Cancer Res.* **2009**, *15*, 1623–1634.

170. Vilgelm, A. E.; Johnson, D. B.; Richmond, A. Combinatorial Approach to Cancer Immunotherapy: Strength in Numbers. *J. Leukoc. Biol.* **2016**, *100*.

171. Chandra, R. A.; Wilhite, T. J.; Balboni, T. A.; Alexander, B. M.; Spektor, A.; Ott, P. A.; Ng, A. K.; Hodi, F. S.; Schoenfeld, J. D. A Systematic Evaluation of Abscopal Responses Following Radiotherapy in Patients with Metastatic Melanoma Treated with Ipilimumab. *Oncoimmunology* **2015**, *4*, 1–7.

172. Victor, C. T.-S.; Rech, A. J.; Maity, A.; Rengan, R.; Pauken, K. E.; Stelekati, E.; Benci, J. L.; Xu, B.; Dada, H.; Odorizzi, P. M.; Herati, R. S.; Mansfield, K. D.; Patsch, D.; Amaravadi, R. K.; Schuchter, L. M.; Ishwaran, H.; Mick, R.; Pryma, D. a.; Xu, X.; *et al.* Radiation and Dual Checkpoint Blockade Activate Non-Redundant Immune Mechanisms in Cancer. *Nature* **2015**, *520*, 373–377.

173. Zamarin, D.; Holmgaard, R. B.; Subudhi, S. K.; Park, J. S.; Mansour, M.; Palese, P.; Merghoub, T.; Wolchok, J. D.; Allison, J. P. Localized Oncolytic Virotherapy Overcomes Systemic Tumor Resistance to Immune Checkpoint Blockade Immunotherapy. *Sci Transl Med* **2014**, *6*, 226ra32.

174. Butte, M. J.; Keir, M. E.; Phamduy, T. B.; Sharpe, A. H.; Freeman, G. J.; Sharpe, H. PD-L1 Interacts Specifically with B7-1 to Inhibit T Cell Proliferation. *Immunity* **2009**, *27*, 111–122.

175. Rollins, M. R.; Gibbons Johnson, R. M. CD80 Expressed by CD8 + T Cells Contributes to PD-L1-Induced Apoptosis of Activated CD8 + T Cells. *J. Immunol. Res.* **2017**, *2017*, 1–6.

176. Ostrand-Rosenberg, S.; Horn, L. A.; Alvarez, J. A. Novel Strategies for Inhibiting PD-1 Pathway-Mediated Immune Suppression While Simultaneously Delivering Activating Signals to Tumor-Reactive T Cells. *Cancer Immunol. Immunother.* **2015**, *64*, 1287–1293.

177. Messenheimer, D. J.; Jensen, S. M.; Afentoulis, M. E.; Wegmann, K. W.; Feng, Z.; Friedman, D. J.; Gough, M. J.; Urba, W. J.; Fox, B. A. Timing of PD-1 Blockade Is Critical to Effective Combination Immunotherapy with Anti-OX40. *Clin. Cancer Res.* **2017**, *23*, 6165–6177.

178. Schreiber, R. D.; Old, L. J.; Smyth, M. J. Cancer Immunoediting: Integrating Immunity's Roles in Cancer Suppression and Promotion. *Science* **2011**, *331*, 1565–1570.

179. Barrett, D. M.; Singh, N.; Porter, D. L.; Grupp, S. A.; June, C. H. Chimeric Antigen Receptor Therapy for Cancer. *Annu Rev Med* **2014**, *65*, 333–347.

180. Peggs, K. S.; Quezada, S. a. PD-1 Blockade: Promoting Endogenous Anti-Tumor Immunity. *Expert Rev. Anticancer Ther.* **2012**, *12*, 1279–1282.

181. June, C. H.; Riddell, S. R.; Schumacher, T. N. Adoptive Cellular Therapy: A Race to the Finish Line. *Sci. Transl. Med.* **2015**, *7*, 280ps7–ps280ps7.

182. Freeman, G. J.; Sharpe, A. H.; Kuchroo, V. K. Protect the Killer: CTLs Need Defenses against the Tumor. *Nat. Med.* **2002**, *8*, 787–789.

183. Ahmad, M.; Rees, R. C.; Ali, S. a. Escape from Immunotherapy: Possible Mechanisms That Influence Tumor Regression/progression. *Cancer Immunol. Immunother.* **2004**, *53*, 844–854.

184. Bono, M. R.; Fernández, D.; Flores-Santibáñez, F.; Rosemblatt, M.; Sauma, D. CD73 and CD39 Ectonucleotidases in T Cell Differentiation: Beyond Immunosuppression. *FEBS Lett.* **2015**, *589*, 3454–3460.

185. Zhou, Q.; Xiao, H.; Liu, Y.; Peng, Y.; Hong, Y.; Yagita, H.; Chandler, P.; Munn, D. H.; Mellor, A.; Fu, N.; He, Y. Blockade of Programmed Death-1 Pathway Rescues the Effector Function of Tumor-Infiltrating T Cells and Enhances the Antitumor Efficacy of Lentivector Immunization. *J. Immunol.* **2010**, *185*, 5082–5092.

186. Kamphorst, A. O.; Ahmed, R. Manipulating the PD-1 Pathway to Improve Immunity. *Curr. Opin. Immunol.* **2013**, *25*, 1–8.

187. Iwai, Y.; Ishida, M.; Tanaka, Y.; Okazaki, T.; Honjo, T.; Minato, N. Involvement of PD-L1 on Tumor Cells in the Escape from Host Immune System and Tumor Immunotherapy by PD-L1 Blockade. *Proc Natl Acad Sci* **2002**, *99*, 12293–12297.

188. Karwacz, K.; Bricogne, C.; MacDonald, D.; Arce, F.; Bennett, C. L.; Collins, M.; Escors, D. PD-L1

Co-Stimulation Contributes to Ligand-Induced T Cell Receptor down-Modulation on CD8+ T Cells. *EMBO Mol. Med.* **2011**, *3*, 581–592.

189. Ascierto, P. a.; Marincola, F. M. 2015: The Year of Anti-PD-1/PD-L1s Against Melanoma and Beyond. *EBioMedicine* **2015**, *2*, 92–93.

190. Robert, C.; Long, G. V.; Brady, B.; Dutriaux, C.; Maio, M.; Mortier, L.; Hassel, J. C.; Rutkowski, P.; McNeil, C.; Kalinka-Warzocha, E.; Savage, K. J.; Hernberg, M. M.; Lebbé, C.; Charles, J.; Mihalcioiu, C.; Chiarion-Sileni, V.; Mauch, C.; Cognetti, F.; Arance, A.; *et al.* Nivolumab in Previously Untreated Melanoma without BRAF Mutation. *N. Engl. J. Med.* **2015**, *372*, 320–330.

191. Robert, C.; Ribas, A.; Wolchok, J. D.; Hodi, F. S.; Hamid, O.; Kefford, R.; Weber, J. S.; Joshua, A. M.; Hwu, W.-J.; Gangadhar, T. C.; Patnaik, A.; Dronca, R.; Zarour, H.; Joseph, R. W.; Boasberg, P.; Chmielowski, B.; Mateus, C.; Postow, M. a; Gergich, K.; *et al.* Anti-Programmed-Death-Receptor-1 Treatment with Pembrolizumab in Ipilimumab-Refractory Advanced Melanoma: A Randomised Dose-Comparison Cohort of a Phase 1 Trial. *Lancet* **2014**, *384*, 1109–1117.

192. Topalian, S. L.; Hodi, F. S.; Brahmer, J. R.; Gettinger, S. N.; Smith, D. C.; McDermott, D. F.; Powderly, J. D.; Carvajal, R. D.; Sosman, J. A.; Atkins, M. B.; Leming, P. D.; Spigel, D. R.; Antonia, S. J.; Horn, L.; Drake, C. G.; Pardoll, D. .; Chen, L.; Sharfman, W. .; Anders, R. A.; *et al.* Safety, Activity, and Immune Correlates of Anti-PD-1 Antibody in Cancer. *New Engl. J. Med.* **2012**, *366*, 2187–2198.

193. Brahmer, J. R.; Tykodi, S. S.; Chow, L. Q. .; Hwu, W. J.; Topalian, S. L.; Hwu, P.; Drake, C. G.; Camacho, L. H.; Wigginton, J. . Safety and Activity of Anti-PD-L1 Antibody in Patients with Advanced Cancer. *N. Engl. J. Med.* **2012**, *366*, 2148–2149.

194. Perica, K.; Bieler, J. G.; Schutz, C.; Varela, J. C.; Douglass, J.; Skora, A.; Chiu, Y. L.; Oelke, M.; Kinzler, K.; Zhou, S.; Vogelstein, B.; Schneck, J. P. Enrichment and Expansion with Nanoscale Artificial Antigen Presenting Cells for Adoptive Immunotherapy. *ACS Nano* **2015**, *9*, 6861–6871.

195. Blank, C.; Brown, I.; Peterson, A. C.; Transgenic, T. C. R.; Cells, C. D. T.; Spiotto, M.; Iwai, Y.; Honjo, T.; Gajewski, T. F. PD-L1 / B7H-1 Inhibits the Effector Phase of Tumor Rejection by T Cell Receptor (TCR) Transgenic CD8 + T Cells PD-L1 / B7H-1 Inhibits the Effector Phase of Tumor Rejection by T Cell Receptor. *Cancer Res.* **2004**, *64*, 1140–1145.

196. Kwong, B.; Liu, H.; Irvine, D. J. Induction of Potent Anti-Tumor Responses While Eliminating Systemic Side Effects via Liposome-Anchored Combinatorial Immunotherapy. *Biomaterials* **2011**, *32*, 5134–5147.

197. Khong, H. T.; Restifo, N. P. Natural Selection of Tumor Variants in the Generation Of "tumor Escape" phenotypes. *Nat Immunol* **2002**, *3*, 999–1005.

198. Carreno, B. M.; Magrini, V.; Becker-Hapak, M.; Kaabinejadian, S.; Hundal, J.; Petti, A. A.; Ly, A.; Lie, W.; Hildebrand, W. H.; Mardis, E. R.; Linette, G. P. A Dendritic Cell Vaccine Increases the Breadth and Diversity of Melanoma Neoantigen-Specific T Cells. *Science* **2015**, *348*, 1–9.

199. Toy, R.; Peiris, P. M.; Ghaghada, K. B.; Karathanasis, E. Shaping Cancer Nanomedicine: The Effect of Particle Shape on the in Vivo Journey of Nanoparticles. *Nanomedicine (Lond)* **2014**, *9*, 121–134.

200. Shen, C.; Cheng, K.; Miao, S.; Wang, W.; He, Y.; Meng, F.; Zhang, J. Latex Bead-Based Artificial Antigen-Presenting Cells Induce Tumor-Specific CTL Responses in the Native T-Cell Repertoires and Inhibit Tumor Growth. *Immunol. Lett.* **2013**, *150*, 1–11.

201. Turtle, C. J.; Riddell, S. R. Artificial Antigen Presenting Cells for Use in Adoptive Immunotherapy. *Cancer J.* **2010**, *16*, 374–381.

202. Oelke, M.; Schneck, J. P. HLA-Ig-Based Artificial Antigen-Presenting Cells: Setting the Terms of Engagement. *Clin. Immunol.* **2004**, *110*, 243–251.

203. Ugel, S.; Zoso, A.; Santo, C. De; Li, Y.; Marigo, I.; Zanovello, P.; Scarselli, E.; Cipriani, B.; Oelke, M.; Schneck, J. P.; Bronte, V. In Vivo Administration of Artificial Antigen-Presenting Cells Activates Low-Avidity T Cells for Treatment of Cancer. *Cancer Res.* **2009**, *69*, 9376–9385.

204. Walter, S.; Herrgen, L.; Schoor, O.; Wernet, D.; Bühring, H.; Stevanovic, S. Cutting Edge: Predetermined Avidity of Human CD8 T Cells Expanded on Calibrated MHC/Anti-CD28-Coated Microspheres. *J. Immunol.* **2003**, *171*, 4974–4978.

205. Durai, M.; Krueger, C.; Ye, Z.; Cheng, L.; Mackensen, A.; Oelke, M.; Schneck, J. P. In Vivo Functional Efficacy of Tumor-Specific T Cells Expanded Using HLA-Ig Based Artificial Antigen Presenting Cells (aAPC). *Cancer Immunol. Immunother.* **2009**, *58*, 209–220.

206. Fuertes Marraco, S. a; Baumgaertner, P.; Legat, A.; Rufer, N.; Speiser, D. E. A Stepwise Protocol

to Coat aAPC Beads Prevents out-Competition of Anti-CD3 mAb and Consequent Experimental Artefacts. *J. Immunol. Methods* **2012**, *385*, 90–95.

207. Casati, A.; Varghaei-Nahvi, A.; Feldman, S. A.; Assenmacher, M.; Rosenberg, S. A.; Dudley, M. E.; Scheffold, A. Clinical-Scale Selection and Viral Transduction of Human Naïve and Central Memory CD8+ T Cells for Adoptive Cell Therapy of Cancer Patients. *Cancer Immunol. Immunother.* **2013**, *62*, 1563–1573.

208. Schneck, J. P.; Slansky, J. E.; O'Herrin, S. M.; Greten, T. F. Monitoring Antigen-Specific T Cells Using MHC-Ig Dimers. *Curr. Protoc. Immunol.* **2001**, *Chapter 17*, Unit 17.2.

209. Pollizzi, K. N.; Powell, J. D. Integrating Canonical and Metabolic Signalling Programmes in the Regulation of T Cell Responses. *Nat. Rev. Immunol.* **2014**, *14*, 435–446.

210. Yamamoto, T.; Hattori, M.; Yoshida, T. Induction of T-Cell Activation or Anergy Determined by the Combination of Intensity and Duration of T-Cell Receptor Stimulation, and Sequential Induction in an Individual Cell. *Immunology* **2007**, *121*, 383–391.

211. Luxembourg, a T.; Brunmark, a; Kong, Y.; Jackson, M. R.; Peterson, P. A.; Sprent, J.; Cai, Z. Requirements for Stimulating Naive CD8+ T Cells via Signal 1 Alone. *J. Immunol.* **1998**, *161*, 5226–5235.

212. Andres, P. G.; Howland, K. C.; Dresnek, D.; Edmondson, S.; Abbas, A. K.; Krummel, M. F. CD28 Signals in the Immature Immunological Synapse. *J. Immunol.* **2004**, *172*, 5880–5886.

213. Saito, T.; Yokosuka, T.; Hashimoto-Tane, A. Dynamic Regulation of T Cell Activation and Co-Stimulation through TCR-Microclusters. *FEBS Lett.* **2010**, *584*, 4865–4871.

214. Jenkins, M. K.; Moon, J. J. The Role of Naïve T Cell Precursor Frequency and Recruitment in Dictating Immune Response Magnitude. *J. Immunol.* **2012**, *188*, 4135–4140.

215. Zhou, A. C.; Wagar, L. E.; Wortzman, M. E.; Watts, T. H. Intrinsic 4-1BB Signals Are Indispensable for the Establishment of an Influenza-Specific Tissue-Resident Memory CD8 T-Cell Population in the Lung. *Mucosal Immunol.* **2017**, *10*, 1294–1309.

216. Gao, H.; Shi, W.; Freund, L. B. Mechanics of Receptor-Mediated Endocytosis. *Proc. Natl. Acad. Sci.* **2005**, *102*, 9469–9474.

217. Nam, K.-O.; Kang, H.; Shin, S.-M.; Cho, K.-H.; Kwon, B. S.; Kwon, B. S.; Kim, S.-J.; Lee, H.-W.

Cross-Linking of 4-1BB Activates TCR-Signaling Pathways in CD8+ T Lymphocytes. *J. Immunol.* **2005**, *174*, 1898–1905.

218. Purwada, A.; Roy, K.; Singh, A. Engineering Vaccines and Niches for Immune Modulation. *Acta Biomater.* **2014**, *10*, 1728–1740.

219. Jhunjhunwala, S.; Raimondi, G.; Glowacki, A. J.; Hall, S. J.; Maskarinec, D.; Thorne, S. H.; Thomson, A. W.; Little, S. R. Bioinspired Controlled Release of CCL22 Recruits Regulatory T Cells in Vivo. *Adv. Mater.* **2012**, *24*, 4735–4738.

220. Sasawatari, S.; Tadaki, T.; Isogai, M.; Takahara, M.; Nieda, M.; Kakimi, K. Efficient Priming and Expansion of Antigen-Specific CD8+ T Cells by a Novel Cell-Based Artificial APC. *Immunol. Cell Biol.* **2006**, *84*, 512–521.

221. Maus, M. V; Thomas, A. K.; Leonard, D. G. B.; Allman, D.; Addya, K.; Schlienger, K.; Riley, J. L.; June, C. H. Ex Vivo Expansion of Polyclonal and Antigen-Specific Cytotoxic T Lymphocytes by Artificial APCs Expressing Ligands for the T-Cell Receptor, CD28 and 4-1BB. *Nat. Biotechnol.* **2002**, *20*, 143–148.

222. Butler, M. O.; Lee, J.-S.; Ansén, S.; Neuberg, D.; Hodi, F. S.; Murray, A. P.; Drury, L.; Berezovskaya, A.; Mulligan, R. C.; Nadler, L. M.; Hirano, N. Long-Lived Antitumor CD8+ Lymphocytes for Adoptive Therapy Generated Using an Artificial Antigen-Presenting Cell. *Clin. Cancer Res.* **2007**, *13*, 1857–1867.

223. Ugel, S.; Zoso, A.; De Santo, C.; Li, Y.; Marigo, I.; Zanovello, P.; Scarselli, E.; Cipriani, B.; Oelke, M.; Schneck, J. P.; Bronte, V. In Vivo Administration of Artificial Antigen-Presenting Cells Activates Low-Avidity T Cells for Treatment of Cancer. *Cancer Res.* **2009**, *69*, 9376–9384.

224. Sunshine, J. C.; Green, J. J. Nanoengineering Approaches to the Design of Artificial Antigen-Presenting Cells. *Nanomedicine* **2013**, *8*, 1173–1189.

225. Wrzesinski, C.; Paulos, C. M.; Kaiser, A.; Muranski, P.; Palmer, D. C.; Gattinoni, L.; Rosenberg, S. a; Restifo, N. P. Increased Intensity Lymphodepletion Enhances Tumor Treatment Efficacy of Adoptively Transferred Tumor-Specific T Cells. *J Immunother* **2010**, *33*, 1–7.

226. Kozielski, K. L.; Tzeng, S. Y.; Hurtado De Mendoza, B. A.; Green, J. J. Bioreducible Cationic Polymer-Based Environmentally Triggered Cytoplasmic siRNA Delivery to. *ACS Nano* **2014**, *8*,

3232–3241.

227. Fields, R. J.; Cheng, C. J.; Quijano, E.; Weller, C.; Kristofik, N.; Duong, N.; Hoimes, C.; Egan, M. E.; Saltzman, W. M. Surface Modified Poly(beta Amino Ester)-Containing Nanoparticles for Plasmid DNA Delivery. *J. Control. Release* **2012**, *164*, 41–48.

Curriculum Vitae

Alyssa K. Kosmides was born in 1990 in Princeton, NJ, USA.

Alyssa did her undergraduate work at Rutgers University School of Engineering in New Brunswick, NJ in Biomedical Engineering with a minor in Computer Science. At Rutgers, she conducted research in systems biology in the lab of Dr. Ioannis P. Androulakis and presented this work in Sao Paulo, Brazil during an undergraduate exchange program. Alyssa was awarded a National Science Foundation Graduate Research Fellowship for graduate school during her senior year.

Alyssa began her Ph.D. in biomedical engineering at Johns Hopkins School of Medicine in 2012 and joined Dr. Jonathan Schneck's lab in 2013. During her Ph.D., she co-developed and taught a new Immunoengineering course for undergraduates and served as Co-Director of Internships and Co-Chair of the JHU BME Extramural Development in Graduate Education program. Alyssa was also awarded an NIH F31 Fellowship, French-American Doctoral Exchange Seminar Scholarship, and was named a 2018 Siebel Scholar. She has authored or co-authored seven peer reviewed manuscripts and reviews and her work has been presented at over a dozen national and international conferences.